Regulation of iron homeostasis by the sulfur assimilation pathway

By

Andrew T. Hale

Dissertation

Submitted to the Faculty of the

Graduate School of Vanderbilt University

in partial fulfillment of the requirements

for the degree of

DOCTOR OF PHILOSOPHY

in

Biochemistry

February 29th, 2020

Nashville, Tennessee

Approved:

Charles Sanders Ph.D.

John York Ph.D.

Scott Hiebert Ph.D.

Emily Hodges Ph.D.

Dan Roden M.D

ACKNOWLEDGEMENTS

I would like to thank my advisor, Dr. John York for his support and mentorship throughout my thesis research. He provided a scientific environment that enabled me to pursue my own ideas, satisfy my intellectual curiosity and carve my own path. John not only taught me how to rigorously test a scientific hypothesis, but also how to think critically and be confident in pursuing independent ideas. This support was mirrored by my thesis committee, who provided instrumental feedback and thought-provoking suggestions to improve the quality and rigor of my work. I would also like to thank the Vanderbilt Medical Scientist Training Program for their endless guidance through this critical portion of physician-scientist training. I am lucky, fortunate, and privileged to have been afforded this opportunity available to so few.

Thank you to the members of the York laboratory, past and present, for their scientific insights, thoughtful conversations, and support through my doctoral research. Their fresh perspective often times sparked new directions and important ideas to consider. In particular, I would like to thank these members of the York lab: Ben Hudson, Ryan Irving, Bradley Clarke, Zigmund Luka, Brynna Eisele, and Pranathi Matta who have played instrumental roles in the work described herein and in my doctoral training. I would also like to thank our collaborators on the work presented here and other projects beyond the scope of this dissertation including Rachel Brown, Chris Williams, Cole Dovey (Stanford), Jan Carette (Stanford), Tudor Moldoveanu (St. Jude), Dan McNamara (St. Jude), Kevin Bersell, Andrew Glazer, and Dan Roden. Interacting with such a talented, enthusiastic, and capable group of scientists was a major highlight of my PhD training and experience.

Thank you to my family for encouraging and fostering my goal of becoming a physician-scientist through my college coursework/applications, MD/PhD applications/matriculation, and through the next stages of my research and clinical training. Thank you to the Thomas family for welcoming me with open arms into your family, for taking a genuine interest in the scientific/medical world, and for your understanding of this unconventional path. Finally, and most of all, thank you to my wife, Halley. Without your love, wisdom, and support, none of this would have been possible. You have always pushed me to be better, encouraged me to pursue my dreams, and been understanding and fully supportive of my passion for both science and medicine. Thank you for your patience through the nights and weekends, ups and downs, and often times unpredictable path you have chosen to walk alongside me. You have taught me what is most valuable in life, and I will love you always.

TABLE OF CONTENTS

Page

ACKNOWLEDGMENTS ii

LIST OF TABLES ix

LIST OF FIGURES x

LIST OF ABBREVIATIONS xii

Chapter

1 Sulfur assimilation metabolism 1

1.1 Introduction 1

1.2 Sulfate import 4

1.3 Phosphoadenosine phosphosulfate synthases (PAPSS) 5

1.4 Cytosolic sulfotransferases 8

1.5 Golgi-localized sulfotransferases 9

1.6 3'-nucleotidases 11

1.6.1 Golgi-localized phosphoadenosine phosphate phosphatase (gPAPP) 11

1.6.2 Bisphosphate nucleotidase 1 (Bpnt1) 15

1.7 Summary and research aims 22

2 Overview of mammalian iron metabolism and homeostasis 24

2.1 Introduction 24

2.2 Intestinal iron import 28

2.3 Iron sensing in the intestinal epithelium 30

2.4 Intestinal iron export to the blood 32

2.5 Iron transport in the blood 34

2.6 Iron storage 35

2.7 Summary and research aims 35

3 Modulation of intestinal sulfur assimilation metabolism regulates iron homeostasis 37

3.1 Introduction 37

3.2 Methods 39

3.2.1 Mouse model and diets 39

3.2.2 Western blot analysis 41

3.2.3 RNA and qRT-PCR 41

3.2.4 Tissue and serum iron quantification 42

3.2.5 Hematological analysis 43

3.2.6 Immunohistochemistry 43

3.2.7 PAP quantification 44

3.2.8 RNA sequencing and analysis 44

3.3 Results.....45

3.3.1 Bpnt1 global knockout mice develop iron deficiency anemia.....45

3.3.2 Intestinal-epithelium specific Bpnt1 knockout mice develop iron deficiency anemia.....50

3.3.3 Intestinal-epithelium specific Bpnt1 knockout mice displayed defects in apical iron import.....54

3.3.4 PAP accumulation induces transcriptional changes in iron metabolism associated genes, the HIF-2α pathway, and sulfur assimilation related genes.....56

3.3.5 Intestinal-epithelium specific Bpnt1 knockout mice displayed decreased HIF-2α levels but no difference in HIF-2α subcellular localization.....60

3.4 Discussion.....63

4 Modulation of sulfur assimilation metabolic toxicity overcomes anemia and hemochromatosis in mice…….....68

4.1 Introduction.....68

4.2 Methods.....70

4.2.1 Animals and diets.....70

4.2.2 Enteroid culture.....71

4.2.3 Quantification of PAP/PAPS levels.....73

4.2.4 Immunohistochemistry and electron microscopy.....73

4.2.5 Enterocyte isolation and quantitative RT-PCR.....74

4.2.6 Hematological analyses.....75

4.2.7 Statistics.....75

4.3 Results 75

4.3.1 Dietary methionine restriction reverses anemia in BPNT1 deficient mice 75

4.3.2 Catalytic activity of BPNT1 regulates iron import, sensing, and export 77

4.3.3 Restoration of Hif-2α normalizes iron homeostatic gene expression in BPNT1 deficient enteroids 80

4.3.4 Hif-2α is epistatic to Bpnt1 in the intestinal epithelium 84

4.3.5 Intestinal-epithelium specific loss of Bpnt1 attenuates hepatic iron-overload in Hfe^{C282Y} mice 86

4.4 Discussion 88

5 Identification of targets of PAP metabolic toxicity 93

5.1 Introduction 93

5.2 Methods 94

5.2.1 PAP affinity chromatography 94

5.2.2 Histone isolation & post-translational modification analysis 95

5.3 Results 95

5.3.1 PAP affinity chromatography identifies PAP binding proteins 95

5.3.2 Histones isolated from $Bpnt1^{-/int}$ enterocytes interact with PAP agarose 100

5.3.3 $Bpnt1^{-/int}$ enterocytes display histone post-translational modifications consistent with increased chromosomal accessibility 101

5.4 Discussion 103

6 Summary and Future Directions 108

6.1 Summary 108

6.2 Future directions.....111

6.2.1 PAP accumulation and histones as targets of metabolic toxicity 111

6.2.2 Additional targets of PAP toxicity.....113

6.2.3 Phase separation as a potential mechanistic consequence of PAP toxicity .115

6.2.4 rRNA processing and modifications as a mechanism for PAP metabolic toxicity 116

BIBLIOGRAPHY 119

LIST OF TABLES

Table Page

5.1 Protein species identified in eluent from Bpnt1$^{-/fl}$ and Bpnt1$^{-/int}$ enterocytes after competitive elution with PAP from PAP-agarose binding experiments.....98

5.2 Hallmark pathways identified by Gene Set Enrichment Analysis (false discovery rate $q<0.05$) using proteins identified in Bpnt1$^{-/int}$ enterocytes eluted from PAP-agarose.....99

LIST OF FIGURES

Figure Page

1.1 Overview of sulfur assimilation across species....2

1.2 Evolutionary dendrogram of taxonomic relationships between lithium-sensitive phosphatases....13

1.3 Loss of gPAPP in mice causes defects in endochondral ossification, long bone formation, and perinatal lethality....14

1.4 Loss of Bpnt1 in mice causes anasarca and liver failure....20

2.1 Abbreviated overview of iron absorption in the duodenal enterocyte and coordination of iron metabolism in mammals....27

3.1 Bpnt1 global knockout mice develop PAP-dependent iron deficiency anemia....47

3.2 Bpnt1 deficient intestine displays abnormal architecture....49

3.3 Generation and confirmation of intestine-specific Bpnt1 knockout mice....51

3.4 Body weight and intestinal morphology analysis of Bpnt1$^{-/int}$ mice....53

3.5 Inactivation of Bpnt1 s in the small intestine results in iron deficiency anemia....55

3.6 Bpnt1$^{-/int}$ enterocytes display defects in apical iron transport....55

3.7 Bpnt1$^{-/int}$ enterocytes display broad changes in transcriptional activity....57

3.8 PAP accumulation induces transcriptional changes in iron-metabolism related genes, the HIF-2α pathway and sulfur-assimilation related genes....59

3.9 Bpnt1$^{-/int}$ enterocytes and small intestine display decreased HIF-2α and no difference in HIF-2α subcellular localization....61

3.10 Accumulation of PAP in Bpnt1$^{-/int}$ enterocytes demonstrates broad changes in HIF-2α-associated gene targets....62

4.1 Dietary methionine restriction reduces metabolic toxicity and reverses iron deficiency anemia in Bpnt1$^{-/int}$ mice 77

4.2 Primary enteroids recapitulate PAP toxicity and Bpnt1 catalytic activity is required for iron homeostatic gene expression 79

4.3 Bpnt1$^{-/int}$ mice display decreased heterochromatin, abnormal brush border architecture, and nucleolar condensation 80

4.4 Restoration of Hif-2α, but not Xrn1, normalizes iron-regulatory gene expression perturbations in Bpnt1$^{-/int}$ enteroids.....82

4.5 Restoration of Hif-2α or Xrn1 does not ameliorate nucleolar condensation or chromatin defects in Bpnt1$^{-/int}$ enteroids.....83

4.6 Bpnt1 is epistatic to Hif-2α in the intestine.....85

4.7 Intestinal-specific deletion of Bpnt1 attenuates hepatic iron-overload in Hfe^{C282Y} homozygous mice.....87

5.1 Identification of PAP-binding proteins by affinity chromatography in Bpnt1$^{-/fl}$ and Bpnt1$^{-/int}$ enterocyte lysates.....96

5.2 Histones isolated from Bpnt1$^{-/int}$ enterocytes interact with PAP agarose.....101

5.3 Bpnt1$^{-/int}$ enterocytes display enrichment of histone post-translational modifications consistent with increased chromosome accessibility 102

LIST OF ABBREVIATIONS

ADP: Adenosine diphosphate

AMP: Adenosine monophosphate

APS: 5'-adenosinephosphosulfate

ARNT: Aryl hydrocarbon receptor nuclear translocator

ATP: Adenosine triphosphate

bHLH-PAS: Basic helix-loop-helix Per-Arnt-Sim

C. Elegans: Caenorhabditis Elegans

C4S: Chondroitin-4 sulfate

C4ST: Chondroitin-4 sulfotransferase

C6S: Chondroitin-6 sulfate

C6ST: Chondroitin-6 sulfotransferase

CBC: Complete blood count

cDNA: complementary deoxyribonucleic acid

CHST3: Carbohydrate sulfotransferase 3

CHST14: Carbohydrate sulfotransferase 14

CP: Choroid plexus

CSF: Cerebrospinal fluid

CYBRD1: Cytochrome reductase b

DAVID: Database for Annotation, Visualization, and Integrated Discovery

DKO: Double knockout

DMT1: Divalent metal transporter 1

EDS: Ehlers-Danlos syndrome

ELISA: Enzyme-linked immunosorbent assay

EPCAM: Epithelial cell adhesion molecule

EV: Empty vector

Fe^{2+}: ferrous iron

Fe^{3+}: ferric iron

FPN: Ferroportin

FWER: Family-wise error rate

GAG: Glycosaminoglycan

GO: Gene ontology

GPAPP: Golgi-localized phosphoadenosine phosphate phosphatase

GSEA: Gene set enrichment analysis

GSK3β: Glycogen synthase kinase 3β

Hb: Hemoglobin

HECT: Homologous to the E6-AP carboxyl terminus

HFE: Homeostatic iron regulator

HIF-2α: Hypoxia inducible factor 2α

HifRE: Hypoxia inducible factor response element

HFE: Hypoxia response element

HS: Heparan sulfate

IDA: Iron deficiency anemia

IRE: Iron response element

IRP1: Iron response protein 1

IRP2: Iron response protein 2

MCD: Macular corneal dystrophy

MCH: Mean corpuscular hemoglobin

MCV: Mean corpuscular volume

Met: Methionine

Met22: Methionine requiring gene 22

mRNA: messenger ribonucleic acid

MYO9: Myosin 9

NDFIP: Neural precursor cell expressed developmentally down-regulated protein 4 interacting protein 1

NDK: Nucleoside diphosphate kinase

NEDD4: Neural precursor cell expressed developmentally down-regulated protein 4

NEO: Neomycin resistant cassette

NES: Normalized enrichment score

PAP: 3'-phosphoadenosine 5'-phosphate

PAPS: 3'-phosphoadenosine 5'-phosphosulfate

PAPSS1: Phosphoadenosine phosphosulfate synthase 1

PAPSS2: Phosphoadenosine phosphosulfate synthase 2

PAPST1: 3'-phosphoadenosine 5'-phosphosulfate transporter 1

PAPST2: 3'-phosphoadenosine 5'-phosphosulfate transporter 2

PARP1: Poly (ADP-ribose) polymerase 1

PAXT1: Partner of exoribonuclease 1

PBS: Phosphate buffered saline

PCR: Polymerase chain reaction

PHD: Prolyl hydroxylase domain

PTM: Post translational modification

RBC: Red blood cell

RES: Reticuloendothelial system

RNASeq: Ribonucleic acid sequencing

rRNA: ribosomal ribonucleic acid

SAL1: Orthologue of bisphosphate nucleotidase1 in *Arabidopsis thaliana*

SO_{4}^{2-}: Inorganic sulfate

SSU-1: Cytosolic sulfotransferase ortholog in *Caenorhabditis Elegans*

SULT: Sulfotransferase

SULT1A1: Sulfotransferase 1A1

SULT1A3: Sulfotransferase 1A3

SULT1B1: Sulfotransferase 1B1

SULT1E1: Sulfotransferase 1E1

SULT2A1: Sulfotransferase 2A1

TF: Transferrin

TFR1: Transferrin receptor 1

TFR2: Transferrin receptor 2

TK: Thymidine kinase

UDN: Undiagnosed disease network

UTR: Untranslated region

VHL: von Hippel-Lindau

WWP2: WW domain containing E3 ubiquitin protein ligase 2

XRN1: 5’-3’ exoribonuclease 1

XRN2: 5’-3’ exoribonuclease

Chapter 1 Overview of sulfur assimilation metabolism

1.1 Introduction

This chapter will focus on the role of sulfur assimilation and metabolism in metazoans. The components of this pathway will be discussed in detail, with particular emphasis on reported roles of sulfur assimilation and metabolism in disease. Finally, in-depth discussion on the initial characterization and role of Bpnt1 across metazoans will be performed. Due to our unexpected discovery of Bpnt1 regulating iron absorption which is described in later chapters, an introduction to iron metabolism and homeostasis will be provided in Chapter 2. The discovery and initial characterization of mice lacking Bpnt1, a key regulator of sulfur assimilation metabolism, in the regulation of iron homeostasis will be discussed in Chapter 3. Genetic and dietary strategies to modulate sulfur assimilation metabolic toxicity due to loss of Bpnt1 will be discussed in Chapter 4. Mechanistic insights into targets of metabolic toxicity (i.e. phosphoadenosine phosphate accumulation) in Bpnt1 deficient animals will be presented in Chapter 5. Finally, a summary of this dissertation and future directions will be presented in Chapter 6.

Sulfur assimilation is the process of incorporating inorganic sulfate from the environment into sulfur-containing amino acids and sulfate-containing metabolites. Sulfur assimilation is an evolutionarily-conserved process shared across bacteria, yeast, plants and mammals (Gunal et al., 2019; Hudson and York, 2012; Kopriva et al., 2015; Takahashi et al., 2011). In metazoans, sulfur assimilation is initiated through the uptake of extracellular

inorganic sulfate (SO_4^{2-}) which is predominantly obtained through the catabolism of sulfur-containing amino acids methionine and cysteine. Inorganic sulfate, along with ATP, then

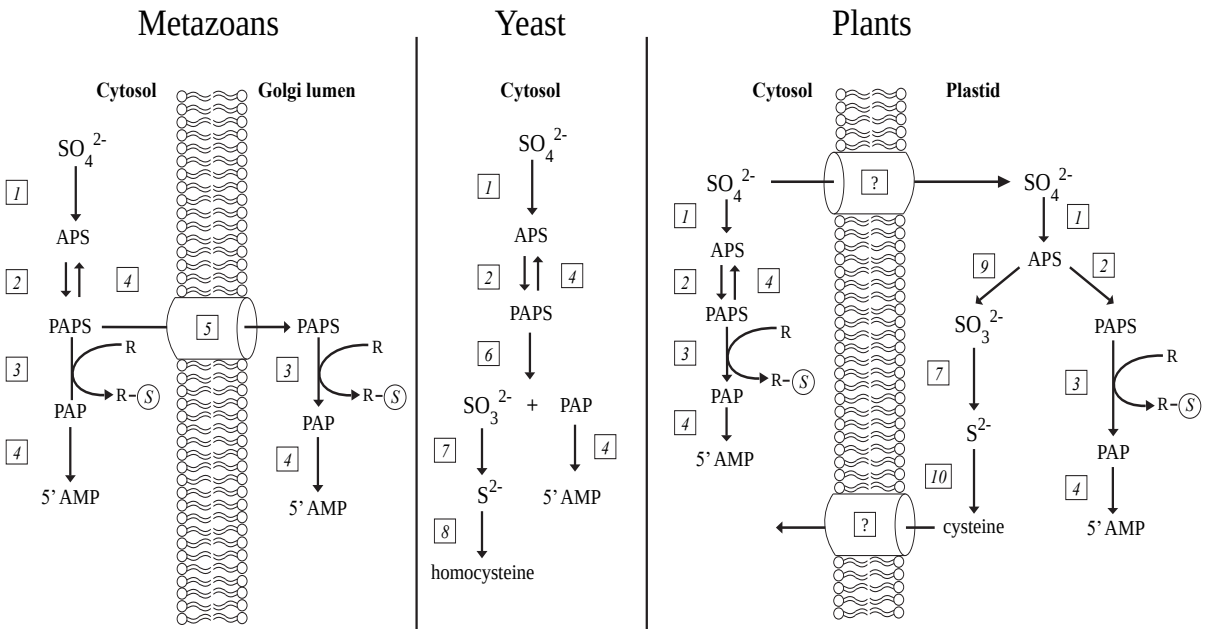

	Enzymatic activity	EC/TCDB number	*M. Musculus*	*S. Cerevisiae*	*A. Thaliana*
1	ATP sulfurylase	2.7.7.4	Papss1, Papss2	*MET3*	APS1, APS2, APS3, APS4
2	APS kinase	2.7.1.25	Papss1, Papss2	*MET14*	APK1, APK2, APK3, APK4
3	Sulfotransferase	2.8.2.X	SULT family	-	SOT family
4	3' nucleotidase	3.1.3.7	Bpnt1, gPAPP	*MET22*	SAL1, SAL2, AHL
5	PAPS transporter	2.A.7.11.3 (TCDB)	Slc35b1, Slc35b2	-	-
6	PAPS reductase	1.8.4.8	-	*MET16*	-
7	Sulfite reductase (yeast)	1.8.1.2	-	*MET5, MET10*	-
7	Sulfite reductase (plants)	1.8.7.1	-	-	SIR
8	Homocysteine synthase	2.5.1.49	-	*MET17*	-
9	APS reductase	1.8.4.8	-	-	APR1, APR2, APR3
10	O-acetylserine thiollyase	2.5.1.47	-	-	OASA1, OASA2, OASB, OASC

Figure 1.1. Summary of the sulfur assimilation pathway across species. Adapted from (Hudson and York, 2012).

serves as the substrate for the bifunctional enzyme phosphoadenosine phosphosulfate synthase (PAPSS) (Masselot and De Robichon-Szulmajster, 1975b; Patron et al., 2008), which harbors both ATP sulfurylase and 5'-adenosinephosphosulfate (APS) kinase activities in mammals (Harjes et al., 2005) (Figure 1.1). Bacteria, yeast and plants, in contrast, contain two independent gene products that perform APS kinase and ATP sulfurylase functions (Mountain et al., 1991).

Both isoforms of PAPSS in mammals use ATP to convert inorganic sulfate into a high-energy intermediate, 3'-phosphoadenosine 5'-phosphosulfate (PAPS). In the cytosol, PAPS serves as a substrate for a number of cytosolic sulfotransferases, which are predominantly involved in metabolizing xenobiotics by increasing solubility and excretion (Chen et al., 2015b; James and Ambadapadi, 2013; Leyh et al., 2013). Sulfotransferases (SULT) catalyze the removal of sulfate from PAPS and transfer that sulfate group to an alcohol or amine acceptor molecule. There are 13 cytosolic SULT isoforms in mammals, which differ in copy number and tissue expression distribution (Langford et al., 2017). After the sulfate group is removed by sulfotransferases, the byproduct 3'-phosphoadenosine 5'-phosphate (PAP) serves as the substrate for bisphosphate 3'-nucleotidase 1 (Bpnt1) to catalyze the production of 5'-AMP in the cytosol. Discussion of the discovery and characterization of Bpnt1 will be described later in this chapter. The unexpected role of Bpnt1 in regulating iron metabolism in mice is the topic of this dissertation and will be discussed in great detail in subsequent chapters.

Alternatively, the sulfate donor PAPS can be transported to the Golgi lumen by the PAPS transporter (PAPST1/2) (Figure 1.1). However, very little is known about the mechanism by which PAPST transports PAPS (Goda et al., 2006; Kamiyama et al., 2006; Kamiyama et al., 2003). It is hypothesized that PAPST acts as a PAPS-5'-AMP anti-porter, however detailed characterization of this mechanism has yet to be performed (Gigolashvili et al., 2012; Kamiyama et al., 2003). In the Golgi lumen, PAPS serves as the substrate for a wide variety of Golgi-localized sulfotransferases, which are predominantly involved in extracellular matrix formation (Cortes et al., 2009; Kirn-Safran et al., 2004; Pomin and Mulloy, 2018). Analogous to the function of Bpnt1 in the cytosol, Golgi-localized phosphoadenosine phosphate phosphatase (gPAPP) catalyzes the conversion of PAP to 5'-AMP exclusively in the Golgi (Frederick et al., 2008).

1.3 Sulfate import

Extracellular inorganic sulfate is imported into mammalian cells by Slc26a2 (Hastbacka et al., 1994). Loss of Slc26a2 function causes diastrophic dysplasia, a Mendelian disorder characterized by decreased sulfate of proteoglycans in the cartilage matrix (Hastbacka et al., 1994; Hastbacka et al., 1996; Superti-Furga et al., 1996).

Functional validation of disease-associated Slc26a2 mutations in *Xenopus* oocytes and HEK cells confirmed that defects in sulfate transport and were associated with the degree of clinical impairment in these patients (Karniski, 2001, 2004). Furthermore, validation of Slc26a2 disease associated mutations in mice recapitulated skeletal defects observed in humans (Forlino et al., 2005).

Slc26a2 has been shown to function as a electroneutral sulfate/hydroxyl/ or hydroxyl, chloride exchanger depending on extracellular chloride and hydroxyl concentration gradients (Ohana et al., 2012). Not surprisingly, Slc26a2 is highly-expressed in bone, but also present in lung, placenta, kidney, pancreas, colon and testis (Haila et al., 2001). Thus, in the absence of Slc26a2 expression, the ability of other tissues that utilize sulfur assimilation metabolism to import sulfate is not well understood because of the confounding issue of increased mortality associated with skeletal dysplasia.

1.4 Phosphoadenosine phosphosulfate synthases (PAPSS)

PAPSS catalyzes the incorporation of inorganic sulfate, obtained from dietary turnover of sulfur-containing amino acids methionine and cysteine in the high-energy intermediate PAPS. Mammals encode two independent PAPSS isoforms (Xu et al., 2000), PAPSS1 and PAPSS2, that differ in tissue expression distribution but catalyze the same enzymatic reaction. A detailed discussion of PAPSS1/2 will be discussed below.

The mouse isoforms of the APS kinase and ATP sulfurylase domains of PAPSS were initial cloned and characterized from a fetal brain cDNA library (Adams et al., 1993; Venkatachalam et al., 1998). Subsequently, the human isoforms were cloned (Yanagisawa et al., 1998). The N-terminal domain contains the APS kinase as well as 3 conserved nucleotide binding motifs. On the other hand, the C-terminus contains the ATP sulfurylase and is less conserved and more divergent across evolution (i.e. ~57% homology with plant isoform). Two isoforms of PAPSS exist in mammals (PAPSS1 & PAPSS2) (Kurima et al., 1998; Li et al., 1995) and share ~76% sequence similarity (Faiyaz ul Haque et al., 1998). Intriguingly, PAPSS1 and PAPSS2 exhibit similar expression patterns across human tissues (Girard et al., 1998; Xu et al., 2000), with a few notable exceptions. PAPSS1 is highly expressed in human brain and bone, where PAPSS2 expression is undetectable or substantially reduced; PAPSS2 is highly expressed in liver, wherein PAPSS1 expression is not observed (Girard et al., 1998; Xu et al., 2000). These tissue expression distribution patterns may reflect to degree to which individual tissues utilize sulfur assimilation metabolism.

Intriguingly, there is some evidence to suggest that PAPSS1 is expressed in both the nucleus and cytosol (Besset et al., 2000). Additional studies suggest that both isoforms contain nuclear-targeting motifs, and PAPSS1 is predominantly localized in the nucleus whereas PAPSS2 is predominantly cytosolic (Schroder et al., 2012). Both isoforms also form homodimers. In addition, there are mammalian-specific splice variants of PAPSS2, but not PAPSS1 (van den Boom et al., 2012). Many have hypothesized that this evolutionary

divergence of PAPSS genes may be due to expanded sulfation requirements among mammals and tissue-specific control mechanisms including transcriptional regulation and protein-protein interactions (Foster and Mueller, 2018; Mueller et al., 2018). The extent to which PAPSS1/2 are co-expressed with certain SULT isoforms is one mechanism by which tissue-specific sulfur assimilation utilization may have evolved (Kim et al., 2004; Sonoda et al., 2002). These remain important questions that have not yet been fully elucidated in sulfur assimilation biology.

Intriguingly, a brachymorphic phenotype in both mice and humans has been attributed to mutations in PAPSS2 (Faiyaz ul Haque et al., 1998; Kurima et al., 1998; Schwartz et al., 1978; Sugahara and Schwartz, 1979). Brachymorphism is characterized by defects in skeletal development and formation of cartilage, leading to a dwarfism phenotype. While there are many unique phenotypic variations among brachymorphism traits, alterations in cartilage and bone formation are central features of this disease class. PAPSS2 hypomorphic mutations have been observed in the APS kinase domain of PAPSS2 (Faiyaz ul Haque et al., 1998). However, complete loss of PAPSS1/2 function is predicted to be incompatible with life, underlying the importance of sulfation in development. Mutations in PAPSS2 leading to the brachymorphic phenotype were spontaneous and first observed and reported among inborn strains of laboratory mice (Lane and Dickie, 1968). However, the human disorder spondyloepimetaphyseal dysplasia attributed to mutations in PAPSS2 were observed in a consanguineous family and displayed an autosomal recessive pattern of inheritance (Faiyaz ul Haque et al., 1998). Mechanistically, loss of PAPSS function is

predicted to impair production of chondroitin sulfate and proteoglycan synthesis largely due to accumulation of APS and decreased production of PAPS (Sugahara and Schwartz, 1979). There have been no human or mouse pathologies definitively associated with defects in PAPSS1, although a putative disease-associated mutation in PAPSS1 has been identified in the Undiagnosed Disease Network (UDN) (undiagnosed.hms.harvard.edu/genes/papss1/). These patients feature both skeletal defects as well as a number of developmental abnormalities and profound medically-refractory epilepsy. While the cartilage and bone phenotypes of PAPSS mutant mice are best characterized because they cause early lethality, other defects associated with inborn errors of sulfur assimilation in these mice have not been extensively described. However, given the importance of sulfur assimilation, it is likely that additional tissue-specific roles for PAPS synthesis exist throughout mammalian life and disease.

1.4 Cytosolic sulfotransferases

The predominant role of cytosolic sulfotransferases (SULT) is to sulfate xenobiotics, catecholamines, thyroid hormones, and sex hormones. Sulfation of drugs mediates pharmacologic response by converting prodrugs into active compounds or by facilitating drug excretion by enhancing metabolite polarity and water solubility, among other functions (Chen et al., 2015b; Marto et al., 2017; Suiko et al., 2017). The five best-characterized cytosolic SULTS include SULT1A1, SULT1A3, SULT1B1, SULT1E1, and SULT2A1

(Riches et al., 2009), however there are at least thirteen members of the cytosolic SULT family (Blanchard et al., 2004; Freimuth et al., 2004). Tissue expression varies widely among these SULT family members (Langford et al., 2017). SULT1A1 is most highly expressed in the liver, whereas SULT1A3 is completely absent (Riches et al., 2009). Relevant to the role of sulfur assimilation metabolism in the intestine described in later Chapters, the expression distribution of SULT isoforms are as follows: SULT1B1 > SULT1A3 >> SULT1A1, SULT1E1, and SULT2A1 (Riches et al., 2009). Importantly, allele frequencies of SULT1A1 and SULT2A1 (and presumably other isoforms) vary among ancestral populations and may be clinically relevant for pharmacological efficacy and drug-drug interactions (Carlini et al., 2001). While frank disease phenotypes have not been observed with loss of cytosolic SULTs, there importance in human health (i.e. drug metabolism, drug-drug interactions, etc.) cannot be understated due to their roles in detoxification and homeostasis.

1.5 Golgi-localized sulfotransferases

Golgi-localized sulfotransferases are largely involved in sulfating carbohydrate moieties of glycosaminoglycans (GAG), which catalyze the formation, deposition and function of extracellular matrix. GAGs consist of chains of disaccharides that arrange around protein cores to form proteoglycans, the major component of the extracellular matrix. Sulfation of GAGs causes these molecules to be highly polar, which is important because in the extracellular matrix these molecules can diffuse freely. In particular, sulfation of GAGs

in cartilage enables joints to attract water and keep joints lubricated, enabling full range of motion and proper development. However, GAGs vary in disaccharide composition (and thus function) based on the position of sulfation on the sugar chain. One major GAG relevant to this dissertation is chondroitin sulfate, comprised of N-acetylgalactosamine and glucuronic acid, which play major roles in skeletal growth/development and nervous system plasticity (Cortes et al., 2009; Kirn-Safran et al., 2004; Mikami and Kitagawa, 2013). A number of human diseases have been attributed to the inborn errors of Golgi-localized sulfation (Soares da Costa et al., 2017), highlighting its importance in human pathobiology. Subtle alterations in GAG formation are also thought to underly neuronal plasticity and cognition (Alonge et al., 2019). Thus, phenotypic consequences of altered regulation of Golgi-mediated sulfation include skeletal, cardiac, and neurological defects, among others, highlighting the importance of maintaining sulfation homeostasis across varying tissue types.

Disorders of glycosaminoglycan sulfation are extremely rare and affect many organ systems including skeletal, connective tissue, cardiac, and nervous, largely due to differences in expression patterns of each sulfotransferase and reliance of each tissue type on specific carbohydrate moieties. Here, I will focus on the disorders associated with Golgi-localized sulfotransferases. Spondyloepiphyseal dysplasia Omani type is an autosomal recessive disorder caused by loss-of-function mutations in carbohydrate sulfotransferase 3 (CHST3). Features of this disorder include chondrodysplasia, joint abnormalities, and abnormal spinal curvature (Hermanns et al., 2008; Thiele et al., 2004). The CHST3 gene encodes the chondroitin-6-sulfotransferase (C6ST), leading to reduction in 6-O-sulfated disaccharides

and a corresponding increase in non- or under-sulfated disaccharides (Hermanns et al., 2008; Thiele et al., 2004). However, mutations in the CHST6 gene (encodes GlcNAc6ST5) cause macular corneal dystrophy (MCD), which causes corneal opacity defects in collagen fibril organization (Lewis et al., 2000). One of the most common and well-known disorders of GAG synthesis is Ehlers-Danlos syndrome (EDS) kosho type (Malfait et al., 2010; Miyake et al., 2010). EDS kosho type is characterized by abnormal connective tissue, joint abnormalities, and highly elastic skin. Patients with EDS kosho type are also at risk for a number of cardiovascular disorders (Yoshizawa et al., 2018). EDS kosho type is associated with mutations in carbohydrate sulfotransferase 14 (CHST14) (Kosho et al., 2010; Shimizu et al., 2011). However, EDS kosho type is a rare form of EDS, where the majority of EDS cases are associated with deleterious mutations in collagen genes.

1.6 3'-nucleotidases

1.6.1 Golgi-localized phosphoadenosine phosphate phosphatase (gPAPP)

Prior work from our laboratory identified a family of lithium-sensitive phosphatases (Figure 1.2) based on a conserved structural motif (D-X_n-EE-X_n-DP(i/l)D(s/g/a)T-X_n-WDX_{n-11}GG) which directly coordinates the binding of lithium leading to inhibition of phosphatase activity (York et al., 1995). One member of this family is gPAPP, later cloned and characterized by our laboratory and others (Frederick et al., 2008; Nizon et al., 2012; Sohaskey et al., 2008; Vissers et al., 2011).

gPAPP catalyzes the conversion of PAP to 5'-AMP in the Golgi-lumen (Figure 1.1). Loss of gPAPP in mice causes perinatal lethality, severely shortened long bones, pulmonary insufficiency, and defects in chondroitin sulfation (Figure 1.3) (Frederick et al., 2008; Sohaskey et al., 2008). Intriguingly, gPAPP knockout mice phenocopy loss of chrondroitin-4 sulfotransferase (C4ST) (Kluppel et al., 2005). Indeed, gPAPP-knockout mice display markedly decreased levels of chondroitin-4 sulfate (C4S) and relatively minor differences in chondroitin-6 sulfate (C6S) and heparan sulfate (HS) (Frederick et al., 2008). Defective production of C4S is associated with defects in endochondral ossification (an essential step in cartilage and long bone formation), which is hypothesized to underlie the phenotype seen in gPAPP-knockout mice (Frederick et al., 2008). Dwarfism and chondrodysplasia phenotypes are also mimicked in humans carrying putative loss of function mutations in gPAPP (Nizon et al., 2012; Vissers et al., 2011). Patients harboring frameshift mutations in gPAPP also display cleft palate, mental retardation, and brachydactyly, while homozygous missense mutations at D177 (predicted to be in the catalytic pocket and impair PAP catalysis) also display some of these features (Vissers et al., 2011).

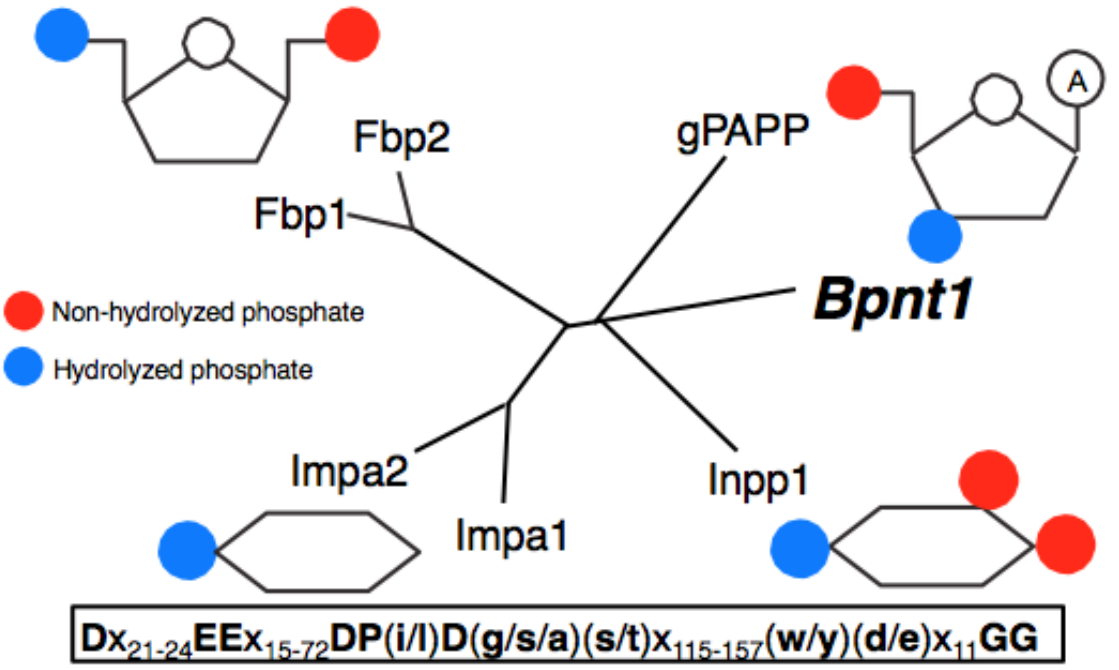

Figure 1.2. Dendrogram demonstrating taxonomic relationships among lithium-sensitive phosphatases initially described in (York et al., 1995) and adapted from (Spiegelberg et al., 2005). The sequence motif, Asp-Pro(Ile or Leu)-Asp-(Gly or Ser)-(Thr or Ser) binds to metal ions required for catalysis. The total conserved structural motif contains 5 alpha-helices and 11 beta-strands. All phosphatases are inhibited by lithium via an uncompetitive mode of inhibition.

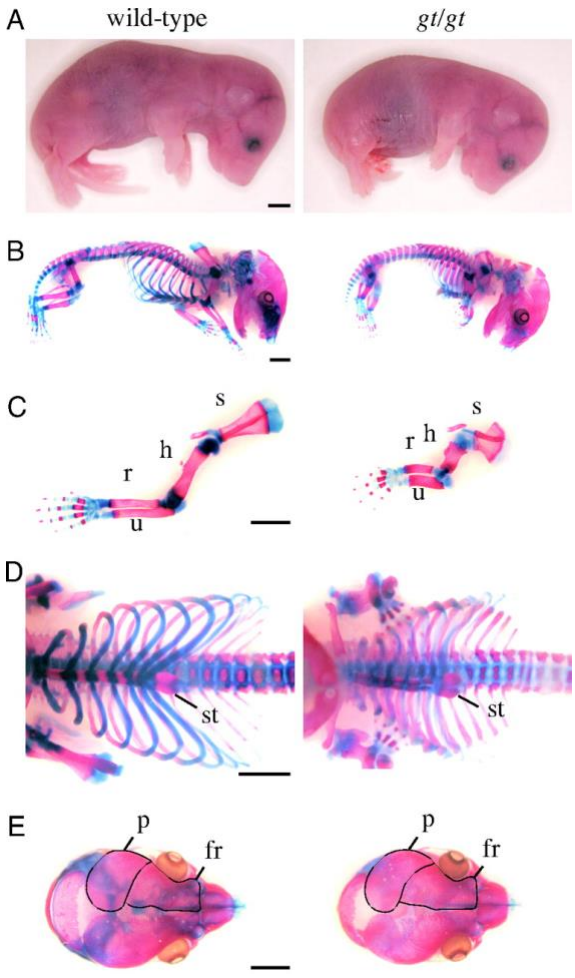

Figure 1.3. Loss of gPAPP in mice causes defects in endochondral ossification, long bone formation, and perinatal lethality. Copyright Frederick et al. PNAS 2008.

However, the mechanism by which loss of gPAPP causes these phenotypes is not known, but currently being investigated by our laboratory. There are many possibilities, including accumulation of PAP substrate, decreased production of 5'-AMP, PAP-mediated feedback inhibition of chondroitin sulfotransferases, impaired import of PAPS through

PAPST1 due to decreased 5'-AMP and impairment of the proposed anti-port mechanism of PAPST1 (Dick et al., 2015; Goda et al., 2006; Kamiyama et al., 2006; Sasaki et al., 2009), among others. Knockdown of PAPST1 in mouse embryonic stem cells leads to decreased chondroitin-4 sulfate and heparan sulfate production, similar to loss of gPAPP (Sasaki et al., 2009). Amplification of 8p11p-12, the genomic region encoding the gPAPP gene, is also frequently observed in breast cancer (Parris et al., 2014) and increased expression of gPAPP is observed in hepatocellular carcinoma (Hindupur et al., 2018), suggesting sulfation may play a role in tumorigenesis. Intriguingly, gPAPP and Bpnt1 are downregulated in glioma, while SULTs are upregulated (Li et al., 2018; Silver et al., 2013). Additional mechanistic insights underlying loss of gPAPP may lead to identification of strategies to overcome this severe inborn error of sulfur assimilation and reveal insights into the function of gPAPP.

1.6.2 Bisphosphate nucleotidase 1 (Bpnt1)

First, a thorough background on the discovery, cloning, and initial characterization of Bpnt1 will be presented. Second, the reported roles of Bpnt1 in regulating lithium toxicity will be described. Lastly, the known roles of Bpnt1 in higher eukaryotic organisms will be discussed. Our studies investigating the role of Bpnt1 in iron metabolism are the focus of this dissertation.

Analogous to the enzymatic function of gPAPP in the Golgi-Lumen, Bpnt1 catalyzes the conversion of PAP to 5'-AMP in the cytosol. However, the yeast ortholog of Bpnt1,

methionine requiring gene 22 (*MET22*), was initially identified by a screen to identify genes associated with methionine auxotrophy (i.e. the inability to grow in the absence of methionine) (Masselot and De Robichon-Szulmajster, 1975a). The mammalian homologue was subsequently cloned and characterized by two groups independently (Lopez-Coronado et al., 1999; Spiegelberg et al., 1999a). Bpnt1 has also been shown to utilize PAPS as a substrate, albeit with indeterminate efficiency (Spiegelberg et al., 1999a). Importantly, loss of Bpnt1 in mice leads to PAP accumulation nearly ~40-200 fold in select tissues (Hudson et al., 2013). However, there is also a modest (~5 fold) increase in PAPS levels as well. The implications of these results will be discussed extensively in this and remaining chapters of this dissertation.

Bpnt1 has also been shown to modulate lithium toxicity in yeast through accumulation of PAP substrate (Spiegelberg et al., 2005). Intriguingly, the inhibition constant of Bpnt1 for lithium is 157 μM (well below the therapeutic range of lithium, 0.6-1.2 mM), suggesting that PAP accumulation may mediate the physiological effects of lithium (Spiegelberg et al., 2005). Molecular modulators of lithium's therapeutic and toxicity effects has profound clinical implications as lithium has remained the first-line treatment for bipolar disorder since the 1940's (Cade, 1949). Bipolar disorder is characterized by periods of mania and depression and a markedly increase risk of suicide (Rybakowski, 2014). Thus, understanding the molecular actions of lithium has profound implications for designing drugs that can effectively treat bipolar disorder. While many hypothesize that lithium acts through inhibition of glycogen synthase kinase 3β (GSK3β) (Freland and Beaulieu, 2012),

direct biochemical evidence is lacking for this claim. Furthermore, the effective dose at which GSK3β activity is inhibited far exceeds the narrow therapeutic window for lithium. However, inhibitors of GSK3β are still being developed for the treatment of both bipolar disorder and cancer (Wagner et al., 2016).

Prior studies in yeast have shown that lithium toxicity causes PAP accumulation which modulates ribosomal RNA (rRNA) processing through inhibition of 5'-3' exoribonuclease (XRN1) (Dichtl et al., 1997a). Loss of 3'-nucleotidase activity in plants (SAL1) have also been shown to increase levels of PAP and inhibit rRNA processing enzymes (Gy et al., 2007). In mice lacking Bpnt1 (described in greater detail below), accumulation of 5.8S "long" rRNA was observed, consistent with inhibition of XRN1 (Hudson et al., 2013). However, global changes in rRNA processing were not observed. Intriguingly, XRN2 in *Caenorhabditis Elegans* requires XRN-binding protein partner of Xrn (Paxt-1) for activity and loss of Bpnt1 suppresses Paxt-1 lethality (Miki et al., 2016). XRN2 regulates polycistronic gene expression in *Caenorhabditis Elegans* suggesting a role for this pathway in transcriptional regulation. These data suggest that Bpnt1 and XRN function are genetically linked in yeast and *Caenorhabditis Elegans*. However, the mechanism by which PAP accumulation impairs cellular function and cellular toxicity requires additional study, which is discussed in later chapters.

Recent work on the homologue of Bpnt1 in *Caenorhabditis Elegans*, shows that Bpnt1 can modulate phenotypes associated with lithium (Meisel and Kim, 2016).

Intriguingly, phenotypes in *Caenorhabditis Elegans* associated with loss of Bpnt1 are phenocopied in *Caenorhabditis Elegans* treated with lithium. This group showed that loss of Bpnt1 function causes defects in ASJ sensory neuron function (dauer exit and pathogen avoidance) which can be partially overcome by expressing the cytosolic sulfotransferase SSU-1 in Bpnt1 mutant worms (Meisel and Kim, 2016). A detailed description of the *Caenorhabditis Elegans* nervous system and their role as model organisms can is described elsewhere (Sengupta and Samuel, 2009). These results are in contrast to mechanisms to overcome loss of Bpnt1 in mice (i.e. concomitant downregulation of PAP synthesis, ameliorating PAP metabolic toxicity), which are described in detail below and in subsequent chapters.

While gPAPP and Bpnt1 catalyze the same enzymatic conversion of PAP to 5'-AMP, Bpnt1 is expressed across a broader range of tissues. Bpnt1 transcript (identified by northern blot) has been observed across human and rat organs including intestine, liver, kidney, pancreas, skeletal muscle, and heart, among others (Lopez-Coronado et al., 1999; Spiegelberg et al., 1999a). Furthermore, Bpnt1 is localized exclusively in the cytosol, as evidenced by subcellular fractionation by ultra-centrifugation experiments (Spiegelberg et al., 1999b), whereas gPAPP localizes to the Golgi-lumen (Frederick et al., 2008).

While loss of gPAPP causes perinatal lethality and chondrodysplasia (Frederick et al., 2008), global loss of Bpnt1 in mice causes anasarca (Figure 1.4), liver failure, and iron deficiency anemia (Hudson et al., 2013; Hudson et al., 2018). Furthermore, loss of Bpnt1

causes defects in ribosome biogenesis, condensation of the nucleolus, accumulation of unprocessed rRNA, and decreased heterochromatin (Hudson et al., 2013; Hudson et al., 2018; Hudson and York, 2014). Mechanistically, phenotypes associated with loss of Bpnt1 can be completely suppressed with concomitant downregulation of PAP synthesis through introduction of a hypomorphic mutation in PAPSS2 (Hudson et al., 2013; Hudson et al., 2018).

Although we did not observe suppression of lethality with concomitant downregulation of PAP synthesis in gPAPP knockout mice, PAPSS2 is not highly expressed in brain and bone. Perhaps amelioration of PAPS synthesis via introduction of a hypomorphic mutation in PAPSS1 (expressed in both brain and bone) could overcome loss of gPAPP. Ongoing studies in the York laboratory by Brynna Eisele are aimed at further understanding the role of gPAPP in the brain and mechanisms underlying gPAPP deficiency.

Nonetheless, these data strongly suggest that accumulation of PAP substrate causes the phenotypes observed in the Bpnt1 deficient mouse. The discovery of Bpnt1 as a regulator of iron metabolism, strategies to overcome metabolic toxicity caused by loss of Bpnt1, and potential mechanistic insights into targets of PAP metabolic toxicity are discussed in detail in subsequent chapters.

WT Bpnt1 -/-

Figure 1.4. Loss of Bpnt1 in mice (Bpnt1 -/-) causes anasarca (whole-body edema) and liver failure at ~45 days of life. Adapted from (Hudson et al., 2013). Copyright PNAS 2013.

The initial motivation of generating mice lacking gPAPP or Bpnt1 was to determine if mice lacking 3'-nucleotidase function recapitulate the toxic or therapeutic effects of lithium. Given that both gPAPP and Bpnt1 are inhibited by lithium at sub-therapeutic levels (Frederick et al., 2008; Spiegelberg et al., 2005), the biochemical and structural rationale for these enzymes being direct targets of lithium is very strong (York et al., 1995). These data are in stark contrast to a widely-hypothesized "target" of lithium, glycogen synthase kinase 3β, which is only inhibited at toxic levels of lithium (Zhang et al., 2003).

To our knowledge, phenotypes our group has observed with loss of either gPAPP or Bpnt1 have not been classically associated with lithium toxicity observed in humans (i.e. nephrogenic diabetes insipidus or hypothyroidism, among others) (Grunfeld and Rossier, 2009; McKnight et al., 2012). Anecdotally, we have observed histopathologic features of lithium toxicity in Bpnt1 deficient kidney (personal communication with Roy Zent), but have never observed nephrogenic diabetes insipidus in Bpnt1 deficient mice (conventional and kidney-specific deletion) at any age. Neurobehavioral analysis of gPAPP cannot be performed due to early lethality, although brain-tissue specific analyses are on-going. Neurobehavioral analysis of Bpnt1 mutant mice are complicated by anasarca, greatly impairing normal motor and behavioral function. However, brain-specific Bpnt1 mutant mice have not been extensively characterized. Further characterization of these mouse models may reveal insights into the role of sulfur assimilation metabolism through 3'-nucleotidases in the therapeutic and toxic effects of lithium.

Loss of Bpnt1 predominantly affects tissues involved in regulating fluid homeostasis (liver, intestine, and kidney). Bpnt1 is also robustly expressed in the choroid plexus (CP), the epithelial layer in the brain responsible for production of cerebrospinal fluid (CSF), although loss of Bpnt1 does not appear to cause overt defects in CSF homeostasis (i.e. hydrocephalus) in mice. However, as knowledge of choroid plexus function improves (Lun et al., 2015), it is worth considering the role of Bpnt1 and sulfur assimilation metabolism in these processes.

1.7 Summary and Research Aims

This chapter summarized our current understanding of the major components of sulfur assimilation and their relationship to disease biology. In particular, the role of lithium-sensitive 3'-nucleotidases gPAPP and Bpnt1 (the focus of this dissertation) have been discussed. Both 3'-nucleotidases play essential roles in sulfur assimilation metabolism and despite catalyzing the same enzymatic reaction (although in different subcellular compartments), play highly divergent roles in metazoan biology. The mechanisms by which loss of 3'-nucleotidase activity alters organismal development and function also appear to occur via unique processes. Intriguingly, despite very convincing biochemical and structural evidence that therapeutic concentrations of lithium potently inhibits the activity of both enzymes, deletion of either Bpnt1 or gPAPP in mice does not appear to recapitulate the therapeutic or toxic effects of lithium *in vivo*. Furthermore, while the mechanism by which loss of Bpnt1 impairs cellular function points to an evolutionarily conserved role of PAP substrate accumulation, the mechanism by which loss of gPAPP causes disease remains largely unknown. While the role of both 3'-nucleotidases in metazoans continues to be explored, both genes have been shown to regulate fundamental pathways essential for homeostasis of numerous organ systems (bone, liver, intestine, nervous system, etc.).

Unexpectedly, our laboratory discovered a role for Bpnt1 in modulating iron metabolism, which is reviewed in Chapter 2. Future chapters will highlight recent studies of

Bpnt1 in regulating iron homeostasis in mice (Chapter 3), strategies to overcome metabolic toxicity in Bpnt1 deficient mice (Chapter 4), and identification of potential targets of sulfur assimilation PAP metabolic toxicity (Chapter 5). Finally, a discussion of the implications of this work and future directions are included in Chapter 6.

Chapter 2 Overview of mammalian iron metabolism and homeostasis

2.1 Introduction

Iron is an essential dietary nutrient that plays diverse roles in biology including oxygen transport, DNA repair, electron transport, and neurotransmitter synthesis among others (Gulec et al., 2014). Iron can exist bound to heme, a protein contained within red blood cells, or non-heme bound. Absorption of non-heme iron occurs in the proximal portion of the duodenum and is the critical checkpoint for regulating systemic iron levels since mammals do not possess a regulated iron excretory system, highlighting the importance of regulating apical iron import in the intestinal epithelium. Excess iron storage is maintained in the liver (and to a lesser extent the spleen) that can be mobilized under increased metabolic demand. Thus, understanding mechanisms regulating iron absorption have critical implications for elucidating strategies to maintain iron homeostasis and potentially augment disease pathophysiology.

Disorders of iron homeostasis comprise some of the most prevalent acquired and hereditary diseases across human pathobiology (Ganz, 2011).There are many human diseases associated with alterations in iron levels, including iron deficiency anemia (IDA, i.e. insufficient iron levels), which afflicts nearly 1 billion people world-wide (Camaschella, 2015; Camaschella, 2019) and is treated with exogenous iron supplementation and/or dietary modification to increase iron consumption. However, a minority of cases of IDA are refractory to iron treatment, suggesting the presence of unmapped genetic forms of IDA in the population (De Falco et al., 2013). On the other hand, hereditary hemochromatosis is a disorder of excess iron accumulation (Brissot et al., 2018; Camaschella, 2015) which is most commonly caused by biallelic mutations in homeostatic iron

regulator (Hfe_{C282Y}) (Levy et al., 2000). Hereditary hemochromatosis causes end-organ iron accumulation and can cause liver failure, cardiomyopathy, and Parkinsonism, among other features (Powell et al., 2016). Unfortunately, the treatment for hereditary hemochromatosis includes phlebotomy (i.e. blood-letting) which is associated with considerable morbidity or iron chelation (i.e. deferoxamine) and necessitates frequent interaction with the healthcare system for treatment. Although outside the scope of this review, accumulation of neuronal iron plays a major role in neurodegenerative disorders such as Parkinson's disease (Matak et al., 2016; Ward et al., 2014) and many have investigated the regulation of various iron homeostatic mechanisms in the central nervous system (Singh et al., 2014). Thus, while many genes regulating iron metabolism have been identified and characterized, understanding fundamental mechanisms controlling iron metabolism may lead to insights for therapeutic development for a wide range of human pathologies.

Sensing of iron levels occurs through the integration of the intestinal, hepatic, kidney, and bone marrow organ systems through the local production and hetero-tissue communication via the coordinated release, destruction, and cell signaling events triggered by hormones (Figure 2.1) (Hentze et al., 2010). When hepatic iron levels are high, hepcidin is released from the liver and decreases iron absorption from the intestine via a hepcidin-mediated internalization and degradation of intestinal-epithelium basolateral transporter ferroportin (Fpn, Figure. 2.1). Fpn is the only known mammalian iron exporter to the blood in the intestinal epithelium (Ganz, 2011), and deletion of Fpn in mice is lethal (Donovan et al., 2005). During low-iron states, transcriptional (ex. hypoxia inducible factor 2α) and post-transcriptional mechanisms (ex. iron response element system) lead to an increase in iron absorption through upregulation of the only known apical iron importer divalent metal transporter 1 (Dmt1, Figure 2.1). However, before iron is absorbed, iron

must be reduced from the Fe^{3+} to Fe^{2+} state by cytochrome reductase b (Cybrd1, Figure 2.1) or via alterations in the environment of the intestinal brush border. When intracellular levels of iron are high, iron is sequestered by ferritin granules (Sharp and Srai, 2007). Normally, apical iron import via Dmt1 is coupled with basolateral iron export by Fpn and iron-loading onto transferrin, the non-heme iron-carrying protein in the blood. Iron-bound transferrin is then deposited into the liver by receptor-mediated endocytosis and iron is released into the hepatocyte due to a decrease in endosomal pH (Harding et al., 1983). Collectively, these responses are coupled to production of erythropoietin by the kidney and increased production of red blood cells in the bone marrow to accommodate circulating iron storage (Haase, 2010), as free iron in the blood acts as a free radical eliciting cellular damage responses.

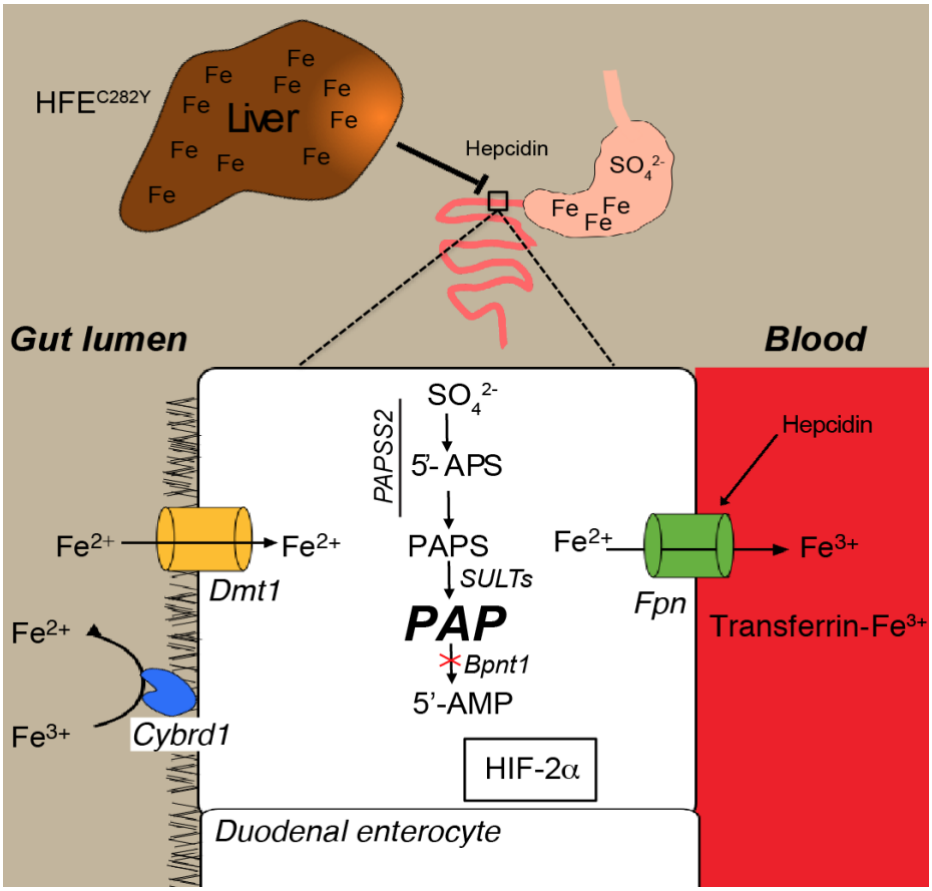

Figure 2.1. Abbreviated overview of iron absorption in the duodenal enterocyte and coordination of iron metabolism in mammals.

In the remainder of this chapter, the details of iron metabolism will be discussed, with a focus on the role of the intestinal-epithelium. This background information will be relevant for understanding the intersection of sulfur assimilation metabolism (discussed in Chapter 1) and iron absorption through regulation of Bpnt1, which be discussed in greater detail in Chapters 3, 4 and 5. Potential mechanisms of PAP metabolic toxicity and future directions are discussed in Chapter 6.

2.2 Intestinal iron import

Dietary non-heme iron primary exists in the oxidized Fe^{3+} (ferric) form, however Fe^{3+} must be reduced to Fe^{2+} (ferrous) iron before being transported into enterocytes by Dmt1 (Simpson and McKie, 2009). Enzymatic reduction of ferric to ferrous iron occurs by duodenal cytochrome reductase (Cybrd1) using ascorbate, providing a potential rationale for why vitamin C supplementation is recommended for patients taking exogenous iron for the treatment of iron deficiency anemia (He et al., 2018). When iron levels are low or cells sense a hypoxic environment, expression of Cybrd1 is increased substantially to improve iron absorption (Latunde-Dada et al., 2011). However, deletion of Cybrd1 in mice appears to be dispensable for iron regulation since mutant mice display no changes in hematological parameters (Gunshin et al., 2005b). These data suggest that other factors may act to reduce iron, especially since murine species can synthesize ascorbic acid, however humans do not possess this function.

Thus, at least in murine models, regulation of Dmt1 appears to be rate-limiting for iron absorption. One direct transcriptional regulator of Dmt1 is hypoxia inducible factor 2α (Hif-2α) (Mastrogiannaki et al., 2009; Mastrogiannaki et al., 2013; Shah et al., 2009), which has been the subject of intense study across disciplines (Frise et al., 2016; Gruber et al., 2007; Liu et al., 2012; Shah et al., 2009; Wallace et al., 2016). Proper function of Dmt1 is required for life, as complete genetic loss is lethal (Gunshin et al., 2005a; Gunshin et al., 1997). Consistent with this notion, mice harboring loss of function mutations in Dmt1 experience early-onset severe IDA and early death (Fleming et al., 1998; Fleming et al., 1997; Gunshin et al., 2005a; Levy et al., 2000). Dmt1 is highly conserved across mammals, and humans harboring both gain and loss of function Dmt1 alleles have also been identified (Blanco et al., 2009; Mims et al., 2005) and display iron-overload

and iron-deficiency phenotypes, respectively. Iron loading is dependent on Dmt1, evidenced by amelioration of hepatic iron accumulation in genetically-predisposed mice harboring loss of function mutations in Dmt1 (Levy et al., 2000). Finally, Dmt1 appears to be the only apical iron transporter in mammals (Mims and Prchal, 2005).

Dmt1 is a multipass transmembrane protein that mediates a proton-coupled uptake of ferrous iron (Gunshin et al., 1997). However, as its name suggests, Dmt1 can also transport other divalent metals including cobalt, manganese, and copper, but whether or not these actions are physiologically relevant and occur *in vivo* remain actively debated (Arredondo et al., 2014; Mackenzie et al., 2007; Shawki et al., 2012; Tennant et al., 2002). Regulation of Dmt1 occurs at multiple levels including transcription and through ubiquitination by the neural precursor cell expressed developmentally downregulated protein 4 (Nedd4) family of HECT-type ubiquitin ligases (Foot et al., 2008). Dmt1 undergoes ubiquitination by WW domain containing E3 ubiquitin ligase 2 (WWP2) and interacts with Nedd4 family member Nedd4 family interaction protein (Ndfip1) (Foot et al., 2008). Deletion of Ndfip1 leads to sustained expression of Dmt1 and an increase in hepatic iron deposition (Foot et al., 2008). In addition, Dmt1 is upregulated by hypoxia (Anderson et al., 2013a). Thus, many direct and indirect mechanisms regulate Dmt1 production and destruction. Regulation of Dmt1 appears to be a critical checkpoint for systemic iron regulation as mammals do not possess a regulated iron excretory system and excess iron deposition is detrimental to organismal function.

2.3 Iron sensing in the intestinal epithelium

Once ferrous iron is transported into the enterocyte, it is rapidly chelated by a variety of organic acids or binds to poly-r(C)-binding proteins (i.e. iron-chaperones) (Leidgens et al., 2013; Shi et al., 2008). Free intracellular iron causes release of free radicals leading to DNA and mitochondrial damage (Emerit et al., 2001). Indeed, disorders of excess iron (i.e. hemochromatosis) are treated with deferoxamine, an iron-chelator, that limits cellular damage due to iron-induced free radical generation (Brittenham, 2011).

Iron chaperone proteins are needed to load iron onto ferritin, the major storage center for intracellular iron (Boyd et al., 1984; Kwak et al., 1990). However, chaperones can also play direct signaling roles, such as activation of HIF prolyl hydroxylase (Nandal et al., 2011). While mechanisms regulating iron transport, trafficking, and localization of iron to intracellular compartments have been described, the overall coordination of these responses remains largely unknown (Asano et al., 2011; De Domenico et al., 2006; Philpott et al., 2017). When an organism's demand for iron is low, iron can be stored in ferritin granules (Linder, 2013). Ferritin consists of three heteropolymers of heavy and light chains (Ferreira et al., 2001), although not all intracellular iron is stored in ferritin as iron is a cofactor for many enzymes that differ in subcellular localization and function. However, excess free cellular iron is extremely toxic. The majority of intestinal-epithelial cells are rapidly turned over and sloughed off during normal intestinal-epithelial homeostasis, releasing ferritin into the extracellular space. Regulatory maintenance of iron levels in this context remain largely unknown, although intestinal ferritin expression has been shown to mediate iron absorption (Andrews, 2010; Darshan et al., 2009; Ferreira et al., 2001; Vanoaica et al., 2010). In addition, many distinct human pathologies have been associated with altered regulation of ferritin biology (Bowes et al., 2014; DeLoughery, 2014). When metabolic demand

for iron is high, intracellular ferritin and non-ferritin bound iron is transported across the basolateral membrane of the intestinal epithelium by ferroportin (Fpn) (Donovan et al., 2005; McKie et al., 2000) to be loaded onto transferrin, which will be discussed later in this chapter.

Studies aimed at understanding the regulation, function, and structure of the HIF family have been an area of intense focus over the last thirty years (Choudhry and Harris, 2018; Gleadle and Ratcliffe, 1998). In fact, discovery and characterization of mechanisms regulating the cellular response to oxygen levels, for which HIFs play a major role, was the subject of the 2019 Nobel Prize in Physiology or Medicine (Ledford and Callaway, 2019). Coordination of the intestinal-epithelial response to fluctuations in iron levels is coordinated, in part, by hypoxia inducible factor 2α (Hif-2α). In subsequent chapters we will explore the relationship between sulfur assimilation metabolism and Hif-2α-dependent signaling in regulating iron metabolism. Thus, the focus of this review will be centered on the role of Hif-2α in regulating iron metabolism in the intestine.

HIFs are a member of the basic helix-loop-helix Per-Arnt-Sim (bHLH-PAS) family of transcription factors (Bersten et al., 2013). HIFs and their core regulatory components are conserved across metazoans, although only mammals possess multiple isoforms of HIF (Kaelin and Ratcliffe, 2008). HIF heterodimerizes with the constitutively-active aryl hydrocarbon receptor nuclear translocator (ARNT) and binds to hypoxia response elements (HRE) present in the promoter regions of HIF target genes (Erbel et al., 2003; Kinoshita et al., 2004; Wang and Semenza, 1993). HIFs contain a DNA binding domain, PAS domain required for heterodimerization with ARNT, an oxygen-dependent degradation domain, and both N- and C-terminal activation domains (Wu et al., 2015; Wu et al., 2019a). At the post-translational level, HIF is regulated by hydroxylation by prolyl hydroxylase domain (PHD) containing enzymes (Ivan et al., 2001; Jaakkola et al., 2001). Once hydroxylated, HIF is recognized by von Hippel-Lindau

(VHL), a PHD-containing E3 ubiquitin ligase that targets HIFs to the proteasome for degradation (Kaelin, 2005, 2008). VHL also acts as a tumor suppressor, and VHL loss of function is associated with renal cell carcinoma (Kaelin, 2007). Under hypoxic conditions, HIF is not hydroxylated and therefore not recognized by VHL, and is stably expressed in the cell.

PHD enzymes including VHL are iron-dependent, such that under conditions of iron depletion, HIF-2α protein is not degraded (Kaelin, 2008). Hif-2α mRNA also contains an iron-response element (IRE) in the 5' untranslated region (UTR) that regulates transcript levels. The IRE consensus sequence is recognized by iron response proteins (IRP1/2) which regulate HIF-2α translation initiation (Anderson et al., 2013b; Ghosh et al., 2013; Wilkinson and Pantopoulos, 2013; Zimmer et al., 2008). In fact, inhibition of the IRP1-Hif-2α 5'-UTR interaction has been used as a proof-of-concept strategy to treat renal cell carcinoma caused by mutations in VHL (Zimmer et al., 2008). Repression of IRP1 in mice causes an increase in HIF-2α and HIF-2α target gene expression (Anderson et al., 2013b; Ghosh et al., 2013). Many have demonstrated through genetic and pharmacological studies that coordination of Hif-2α-dependent signaling events in the intestine are required for iron absorption and homeostasis (Mastrogiannaki et al., 2009; Wu et al., 2019b; Zimmer et al., 2008). Deletion of HIF-2α in mice leads to iron deficiency anemia (Taylor et al., 2011a), and will be discussed extensively in Chapters 3 and 4.

2.4 Intestinal iron export to the blood

Iron is exported to the blood via the basolateral transporter Fpn. Ferroportin was independently cloned across species by three groups (Abboud and Haile, 2000; Donovan et al., 2000; McKie et al., 2000). Fpn is expressed in the intestinal-epithelium, hepatocytes, placenta, and

macrophages, among other tissues and cell types. The function of Fpn *in vivo* was first clarified by the observation that homozygous deletion of Fpn was embryonic lethal due to defects in endodermal development, but intestinal-epithelium specific deletion revealed critical roles in modulating dietary iron absorption (Donovan et al., 2005). Intestinal-epithelium specific Fpn null mice reveal dramatic increases in intracellular iron accumulation (Donovan et al., 2005), which are also recapitulated in liver-specific and macrophage-specific Fpn mutant mice (Zhang et al., 2011; Zhang et al., 2012b). Deletion of Fpn precludes export into the blood, thereby causing systemic iron deficiency anemia despite cellular iron accumulation.

Regulation of Fpn expression in duodenal enterocytes occurs through multiple mechanisms and mRNA/protein levels are controlled by iron and oxygen demand, among other physiologic regulators. Hypoxia stabilizes protein expression of HIF-2α, which is a direct transcriptional regulator of Fpn through binding to the canonical hypoxia response element in the Fpn promoter (Taylor et al., 2011a). Fpn protein levels are also regulated by hepcidin, a hormone that is released from the liver when iron levels are sufficient. Hepcidin binds FPN causing its degradation and sequestration, thereby inhibiting iron uptake into the blood (Knutson, 2010). This feedback mechanism maintains systemic iron homeostasis such that excess iron is not absorbed since there is no regulated mechanism of iron excretion in humans. Deletion of hepcidin production in mice causes severe hemochromatosis and early lethality (Lesbordes-Brion et al., 2006). Detailed review of hepcidin function and regulation in hepatocytes is provided elsewhere (Zhao et al., 2013), as this is outside the scope of this review.

2.5 Iron transport in the blood

~70% of total iron in humans is transported via direct attachment to hemoglobin in red blood cells. Hemoglobin carries oxygen from the lungs, where hemoglobin's affinity for oxygen is high, to peripheral tissues where hemoglobin's affinity for oxygen is low to promote tissue oxygenation essential for life. Each heme group contains an iron atom which coordinates the binding of oxygen (Perutz et al., 1960). Here, iron plays a major role in electron transfer and oxidation-reduction reactions that mediates the interaction of oxygen and heme (Ogura et al., 2018). In the reticuloendothelial system (RES), comprised predominantly of circulating monocytes and resident tissue macrophages, senescent red blood cells release iron and this system serves as a storage depot of excess iron that can later be mobilized when metabolic demand for iron is high (Knutson and Wessling-Resnick, 2003). Since iron is not excreted in a regulated fashion, the amount of iron required for normal homeostasis is maintained by augmenting iron absorption in the intestinal epithelium.

Alternatively, the major non-heme transporter of iron is transferrin (Kuhn et al., 1984; Yang et al., 1984). Once iron is exported through FPN, iron is transferred onto transferrin at the basolateral surface of the intestinal-epithelium (Drakesmith et al., 2015). Transferrin saturation is often used clinically as a marker to determine whether or not iron is functionally available. For instance, if transferrin saturation is low, this is suggestive of iron deficiency anemia; however, if transferrin saturation is increased, this may suggest an iron overload state (either iatrogenic or underlying genetic predisposition to iron overload). Transferrin-bound iron is then taken up by target cells by receptor-mediated endocytosis via the transferrin receptor (Tfr) (Kawabata et al., 1999; Montemiglio et al., 2019). In mammals, there are two isoforms of Tfr, Tfr1 and Tfr2. Complete loss of Tfr1 is embryonic lethal, however conditional deletion of Tfr1 leads to alterations

in epithelial barrier function, lipid accumulation, compromised intestinal stem cell maintenance, and early lethality (Chen et al., 2015a). Thus, expression of Tfr1/2 on target cells requiring iron is a major regulatory step in delivering iron to tissues. Conversely, basolateral intestinal-epithelial Tfr1 expression may play an entirely different role altogether, such as regulation of intestinal cell differentiation (Chen et al., 2015a).

2.6 Iron storage

The major depot of iron storage in mammals is the liver and to a lesser extent the spleen. Hepatic iron levels are tightly controlled by hepcidin release and degradation of Fpn (discussed above) in addition to regulation of iron uptake via Tfr expression. Introduction of a premature stop codon in Tfr2 leads to hereditary hemochromatosis type 3 (Fleming et al., 2002). This is presumably due to the inability to sense that excess iron is present, leading to markedly increase absorption of iron through the intestinal epithelium. Indeed, these data are consistent with the requirement of homeostatic iron regulator (Hfe) to bind Tfr2 on the basolateral side of the intestine to impair iron absorption (Gao et al., 2009). Conversely, liver-specific deletion of Tfr1 leads to iron deficiency anemia (IDA) and decreased hepatic iron accumulation (Fillebeen et al., 2019). This summary collectively highlights the intricacy of iron homeostasis and control via communication of many organ systems and coordination of systemic iron levels.

2.7 Summary and Research Aims

This chapter summarizes the major components of intestinal iron biology and perturbations leading to various diseases. An overview of iron import, sensing, export, transport and storage is

provided. A framework of the core components and axis of iron absorption is essential for understanding subsequent chapters elucidating the role of sulfur assimilation metabolism (reviewed in Chapter 1) in iron regulation. Subsequent chapters will summarize our studies elucidating a role for nucleotide hydrolysis and sulfur assimilation in regulating disorders of iron deficiency and iron overload.

Chapter 3 Modulation of intestinal sulfur assimilation metabolism regulates iron homeostasis

This chapter was adapted from Hudson, Hale, et al. *PNAS*, 2018. Copyright by PNAS

3.1 Introduction

This chapter outlines our laboratory's initial studies characterizing the role of bisphosphate 3'-nucleotidase (Bpnt1) in regulating iron metabolism in mice. Here we revealed an unexpected function of Bpnt1 in regulating iron metabolism. Our studies discussed in detail below revealed an intestinal-epithelium specific role for Bpnt1 in mediating iron absorption. We demonstrated that mice lacking Bpnt1 (either whole-body or intestinal-epithelium specific) develop iron deficiency anemia (IDA). Mechanistically, we demonstrate that loss of Bpnt1 causes IDA through toxic accumulation of PAP substrate by restoring iron homeostasis in Bpnt1 null animals by forward-genetic suppression of PAP synthesis through introduction of a hypomorphic mutation in PAPSS2. Unbiased transcriptomic analysis of Bpnt1 null enterocytes reveal broad and extensive alterations in transcription that mimic, at least in part, deletion of Hif-2α. We confirm decreased HIF-2α protein expression and no difference in subcellular localization in Bpnt1 null intestinal epithelium. A detailed description of these results is provided in this chapter.

Regulation of iron homeostasis is perturbed in numerous pathologic states. Thus, identification of mechanisms responsible for iron metabolism have broad implication for disease modification. The sulfur assimilation pathway is an evolutionarily conserved pathway regulating nucleotide hydrolysis, sulfation, and organismal homeostasis. Deletion of Bpnt1, a key component of the sulfur assimilation pathway (reviewed in Chapter 1), leads to toxic accumulation of phosphoadenosine phosphate (PAP) substrate. IDA in Bpnt1 animals is due, at least in part, to

inhibition of hypoxia-inducible factor 2-α (Hif-2α), a key transcriptional regulator of iron homeostasis. Mechanistically, we demonstrate that reduction of PAP through introduction of a hypomorphic mutation in 3'-phosphoadenosine 5-phosphosulfate synthase 2 gene (Papss2, the enzyme responsible for PAP production) rescues IDA (and other phenotypes associated with loss of Bpnt1) (Hudson et al., 2013; Hudson et al., 2018). The studies outlined in this chapter define a new genetic basis for iron-deficiency anemia, a molecular approach for rescuing loss of 3'-nucleotidase function and an unanticipated link between nucleotide hydrolysis in the sulfur assimilation pathway and iron homeostasis.

Iron is a critical dietary micronutrient that serves as a cofactor for numerous metabolic reactions and is necessary for the production of red blood cells (RBCs) that transport oxygen throughout the body (Andrews, 2008; Hentze et al., 2010; Knutson, 2010). Disease states result from an imbalance in systemic iron homeostasis including hereditary hemochromatosis, neurodegenerative disease and anemia (Andrews, 2008; Hentze et al., 2010). Hereditary hemochromatosis, the most common genetic cause of iron dysregulation in humans, results in tissue iron overload and eventual organ failure (Siddique and Kowdley, 2012). In contrast, anemia due to chronic iron deficiency is a pervasive world-wide problem, affecting as many as 1 billion people (Cameron and Neufeld, 2011). Discovery of mechanisms affecting regulation of iron are paramount to understanding the molecular basis of numerous diseases.

Sulfur assimilation is the process of incorporating inorganic sulfate from the environment into sulfur-containing amino acids and sulfate-containing metabolites, and is a feature shared among bacteria, yeast, plants and mammals (Hudson and York, 2012; Kopriva et al., 2015; Takahashi et al., 2011). Key regulators of metabolic flow in the sulfur assimilation pathway are the enzymes phosphoadenosine phosphosulfate synthetase (Papss2) and bisphosphate 3'-

nucleotidase (Bpnt1); the latter is a member of a structurally-related family of phosphatases (York et al., 1995). Mice and humans encode two such 3'-nucleotidases: Golgi-resident 3'-phosphoadenosine 5'-phosphate phosphatase (gPAPP) and the cytoplasmic Bpnt1. Loss of gPAPP activity in mice results in impaired chondroitin sulfation that underlies chondrodysplasia, pulmonary insufficiency, and bone joint defects (Frederick et al., 2008), which are mimicked in human patients carrying recessive mutations (Vissers et al., 2011). In contrast, animals deficient for Bpnt1 develop anasarca, hepatic insufficiency, and impaired ribosomal biogenesis (Hudson et al., 2013), consistent with compartment specific roles for sulfur assimilation and nucleotide hydrolysis in mammalian physiology. Here, we uncover a tissue specific role for cytoplasmic nucleotidase Bpnt1 in iron homeostasis, define a new genetic basis for iron deficiency anemia and provide a molecular strategy that rescues the disease.

3.2 Methods

3.2.1 Mouse model and diets

Bpnt1 floxed mice were generated using a standard homologous recombination approach. Briefly, we recombined the 4^{th} and 5^{th} exons of the Bpnt1 locus in 129/SvEv ES cells with a construct containing flanking LoxP sites and a neomycin resistance cassette. Cells resistant to neomycin were confirmed by polymerase chain reaction (PCR) and Southern blotting, injected into blastocysts and implanted into pseudopregnant females by the University of North Carolina Animal Models Core. Chimeric founders were identified by Southern blotting and PCR and crossed with B6.Cg-Tg(ACTFLPe)9205Dym/J mice (The Jackson Laboratory) expressing FLP recombinase in order to remove the neomycin cassette. $Bpnt1^{+/fl}$ mice were then backcrossed four

generations into the C57BL/6J background, intercrossed and maintained as Bpnt1$^{fl/fl}$ animals. To obtain intestine-specific knockouts, we first crossed B6.SJL-Tg(Vil-cre)997Gum/J mice (The Jackson Laboratory) expressing Cre recombinase under the control of the villin promoter with Bpnt1$^{+/-}$ animals to obtain Bpnt1$^{+/-}$Vil-Cre^{+} double heterozygotes. These animals were then crossed to Bpnt1$^{fl/fl}$ mice to generate Bpnt1$^{+/fl}$, Bpnt1$^{-/fl}$, Bpnt1$^{+/int}$, and Bpnt1$^{-/int}$ mice. Wild-type and conventional knockout Bpnt1 alleles were genotyped by multiplex PCR using the following primers: (a) 5'-cctatagtcctagcacttgagagg-3'; (b) 5'-accaaagaacggagccggttggcg-3'; and (c) 5'-aggtcggaaccctgttctctagtc-3'. Floxed Bpnt1 alleles were genotypes by PCR using the following primers: (a) 5'-cttgtggtttgggttgacccttag-3' and (b) 5'-ctctagcccagtcagacatgtcag-3'. Villin-Cre expression was determined by PCR using the following primers: (a) 5'-gcggtctggcagtaaaaactatc-3' and (b) 5'-gtgaaacagcattgctgtcactt-3'. All animals unless otherwise noted were maintained on Purina 5058 natural products chow. Animals receiving supplemental iron were injected into the scruff of the neck weekly for a total of 3 weeks with 5 mg of sterile iron-dextran (Sigma). After 3 weeks, mice were sacrificed and analyzed as described above. Animals challenged with iron-deficient diets were maintained on normal Purina 5058 chow until the time of weaning (P23) at which point they were given either iron-deficient AIN-93G defined chow with 2-6 ppm total iron or an identical AIN-93G supplemented with 200 ppm iron(II) sulfate (Harlan-Teklad TD.120105 and TD.120106 respectively). Mice were sacrificed after 5 weeks of dietary treatment and analyzed for hematological parameters as described above. Animal care and experiments were performed in accordance with the National Institutes of Health guidelines and approved by the Duke University Institutional Animal Care and Use Committee.

3.2.2 Western blot analysis

Intestinal tissue for Western blotting was isolated from mice anesthetized with avertin and immediately transferred to ice-cold PBS with 1 mM PMSF. Whole intestines were dissected longitudinally and rinsed vigorously in ice-cold PBS to remove lumenal fecal contents. The tissue was then cut into desired segmental lengths (usually 3 cm) transferred to 15-mL conical tubes containing 5 mL of dissociation buffer (1x PBS, 3 mM EDTA, 1 mM PMSF, and 1x Roche Complete EDTA free protease inhibitor tablets) and mixed thoroughly. Tubes were mixed end-over-end in a 4^{o}C room for 45 minutes with vigorous shaking every 5 minutes. Mesenchyme was removed with forceps and intestinal epithelial cells were collected by centrifugation at 1,000 x g at 4^{o}C for 5 minutes followed by snap freezing in LN_2 and storage at -80^{o}C. Cells were lysed by resuspending in 250 mM sucrose, 30 mM Histidine pH 7.2, 1 mM PMSF, and 1x protease inhibitor tablet and passing through an 18G followed by a 22G syringe. Lysates were centrifuged at 6,000 x g for 5 minutes at 4^{o}C, supernatants collected, and added to 5x SDS buffer followed by incubation at room temperature for 1 hour (Dmt1 aggregates if heated to 95^{o}C). Primary antibodies detecting Dmt1 (a generous gift from P. Gros, McGill University), Bpnt1 (#2296, York lab), and Actin (Sigma) were incubated overnight at 4^{o}C and analyzed by Li-COR.

3.2.3 RNA and qRT-PCR

Total duodenal RNA was extracted from tissues isolated as described above in Western blot analysis from a 1-2 mm strip of intestine immediately distal to the pyloric sphincter. RNA was extracted using Trizol according to the manufacturer's recommendations (Life Technologies). Briefly, snap frozen tissue segments were added to 20 volumes of Trizol and rapidly homogenized

using a PowerGen 700 homogenizer (Fisher Scientific – power "4") and disposable hard tissue generators (Omni International). cDNA was synthesized with the Bio-Rad iScript reverse transcriptase kit using random hexamers. Control (-)RTase reactions were included for each sample. Quantitative PCR was performed on a Bio-Rad iQ5 using the SsoFast Evagreen PCR supermix. Primers were generated using the NCBI Primerblast software and were designed to cross an intronic boundary. Primers were tested for linearity over 3 logs of dilution and (-)RT reactions consistently yielded no amplified product. See Table S1 for primer sequences.

3.2.4 Tissue and serum iron quantification

Iron analysis was performed according to standard methodologies with minor modifications. Briefly, livers and spleens were isolated following PBS perfusion, blotted dry, and snap frozen in liquid nitrogen. The tissues were weighed while still frozen and added to 9 volumes of acid lysis buffer (3 M HCl, 0.61 M trichloroacetic acid). The samples were shaken vigorously and incubated at 95^{o}C overnight until completely dissociated. Samples were then centrifuged at 5,000 x g for 10 minutes. To quantify iron content, 5 volumes of saturated sodium acetate, 5 volumes of milliQ water, and 1 volume of chromogen stock solution (1.86 mM bathophenanthroline, 143 mM thioglycolic acid in milliQ water) were combined to generate the chromogen working solution. 100 µL of supernatant was then added to 1 mL of working chromogen buffer and incubated for 10 min at room temperature to allow for color development. Absorbencies were measured on a Beckman Coulter DU730 spectrophotometer and compared to a standard curve of iron(II) sulfate ranging from 0 to 4000 µg/dL Fe^{2+}. Samples above the linear range of the assay were diluted 1:10 with acid lysis buffer.

3.2.5 Hematological analysis

For hematological analysis, mice were sacrificed by CO_2 exposure and blood was collected by cardiac stick from the right ventricle. Blood was collected into K_2EDTA tubes (Becton Dickinson) and mixed gently to prevent clotting. Complete blood counts were performed by the Duke Veterinary Diagnostic Laboratory using an Abbot Cell Dyn 3700. For blood smears, whole blood was collected via cardiac stick, spread onto glass slides (Fisher Scientific), allowed to air-dry, and stained with Wright-Giemsa (Electron Microscopy Services, Duke University).

3.2.6 Immunohistochemistry

For histological analysis, mice were sacrificed using the above method and then perfused transcardially with 30 mL of phosphate-buffered saline pH 7.4. Tissues for histology were fixed in 10% formalin (VWR) for 2 days then embedded in paraffin by the Duke University Medical Center Immunohistology Research Laboratory. 5μm sections were stained for Perls' iron by the Duke University Medical Center Immunohistology Research Laboratory. A section of iron-loaded human liver serves as positive control for staining quality. For immunohistochemistry, sections were blocked, stained, and visualized with DAB according to standard procedures. Primary antibodies recognizing fibrillarin (Abcam), Bpnt1 (York lab-2296) or HIF-2α (Novus Biological) were incubated at 4°C overnight. Slides were imaged on a Nikon TE2000 inverted microscope. Quantification was performed using Image-J (NIH).

3.2.7 PAP quantification

Tissue PAPS and PAP levels were measured using a combination of two previously published protocols (Hazelton et al., 1985; Lin and Yang, 1998). Briefly, frozen intestine segments (~3 cm) were boiled for 3 minutes in 5 μL of PAP isolation buffer (50 mM glycine (pH 9.2)) per mg of tissue and disrupted using a PowerGen 700 homogenizer (Fisher Scientific – power "4") and disposable hard tissue generators (Omni International). This process was repeated once more before transferring the samples to ice. Homogenates were clarified by at 16,100 x g, 4$_{o}$C for 20 minutes. Following addition of 0.2 volumes of $CHCl_3$, mixtures were shaken vigorously and then centrifuged at 16,100 x g, 4$_{o}$C for 20 minutes. Finally, the upper aqueous phases were collected. The final extract was stable at -80$_{o}$C for at least 3 months. PAP quantification was performed as described previously (Hudson et al., 2013).

3.2.8 RNA sequencing and analysis

Poly-A selected mRNA libraries were prepared with KAPA Biosystems sample kits using indexed adaptors (Illumina), pooled (twelve libraries), and subjected to 75 bp paired-end sequencing according to the manufacturer's protocol (Illumina NextSeq500). Raw data and alignment quality control were performed using QC3 (Guo et al., 2014). Raw data were aligned with TopHat2 (Kim et al., 2013) against human transcript genome HG19, and read counts per gene were obtained using HTSeq (Anders et al., 2015). Differential expression analysis was performed using DESeq2 (Anders and Huber, 2010). We defined false discovery rate as FDR <0.05. Unsupervised cluster analysis was performed using Heatmap3 by selecting the top 5% of genes with the highest coefficient of variance (Zhao et al., 2014). We performed gene ontology analysis

using Database for Annotation, Visualization and Integrated Discovery (DAVID) as previously described (Huang da et al., 2009a, b). Gene set enrichment analysis (GSEA) was performed as previously described (Subramanian et al., 2005). GSEA enabled us to rank every transcript sequenced according to fold change and p-value in order to determine physiologically significant overlap in gene expression patterns of known biological pathways and functions.

The following Gene Ontology (GO) transcriptional signatures were used. 1. Iron metabolism: GO:0020037, heme binding; GO:0051536, iron-sulfur cluster binding- as well as genes involved in Bpnt1 biology (Frederick et al., 2008; Hudson et al., 2013; Hudson and York, 2012, 2014). 2. The HIF-2α target genes were derived as previously described (Schaefer et al., 2009). 3. Nucleolus, GO:0005730. 4. Sulfate assimilation: Transferase activity transferring sulfur containing groups, GO:0016782; Sulfur metabolic process, GO:0006790; Sulfur compound biosynthetic process, GO:0044272; Oxidoreductase activity acting on sulfur group of donors, GO:0016667; and KEGG Sulfur metabolism. In addition, we compared our RNAseq data with sequencing data from a HIF-2α intestine-specific knockout as previously described (Taylor et al., 2011a). In addition, we studied the Broad Institute Molecular Signatures Database C2 curated gene sets as well as manual input of genes known to be involved in Bpnt1 biology (Frederick et al., 2008; Hudson et al., 2013; Hudson and York, 2012).

3.3 Results

3.3.1 Bpnt1 global knockout mice develop iron deficiency anemia

Our phenotypic analysis of Bpnt1 deficient mice revealed an age-dependent hair-loss (alopecia), a clinical manifestation suggestive of iron deficiency anemia. Thus, we analyzed

complete blood counts (CBCs) from wild-type and conventional global Bpnt1 knockout (Bpnt1$^{-/-}$) mice. Bpnt1$^{-/-}$ animals had significantly lower hemoglobin (Hb), smaller mean corpuscular volumes (MCV), and reduced average cellular hemoglobin (MCH), indicative of microcytic hypochromic anemia (Figure 3.1B-D). Microcytic anemia is most frequently due to systemic iron deficiency. Thus, to probe whether the anemia observed in Bpnt1$^{-/-}$ animals was the result of inadequate iron stores or a primary defect in the hematopoietic system, we supplemented wild-type and Bpnt1$^{-/-}$ mice with subcutaneous Fe-dextran or saline once a week for three weeks and assessed CBCs at the end of the fourth week. Bpnt1$^{-/-}$ mice that received Fe-dextran displayed normalized Hb levels (Figure 3.1E), confirming that the anemia was due to a defect in iron homeostasis. Thus, global loss of Bpnt1 impairs the maintenance of sufficient bodily iron stores for normal hematopoiesis.

Our previous studies of 3'-nucleotidase mutant mice revealed two distinct mechanisms that contributed to observed phenotypes: the first involved the toxic accumulation of PAP substrate as depicted in -/- labeled pathway (Figure 3.1A) (Hudson et al., 2013); whereas the second was consistent with impaired sulfation through defective import of Golgi PAPS and/or failure to produce 5'AMP (Frederick et al., 2008). To further probe if either mechanism explained the observed microcytic anemia, we generated a double mutant mouse (Bpnt1$^{-/-}$ Papss2$^{bm/bm}$ – DKO) deficient for Bpnt1 and harboring a hypomorphic mutation in the phosphoadenosine phosphosulfate synthase, Papss2. We surmised according to the first model that a double mutant would rescue iron deficiency anemia because of concomitant downregulation of PAP synthesis depicted by DKO pathway (Figure 3.1A), whereas if the second model were true, an exacerbation of the anemia would be expected. Indeed, the double mutant mice exhibited dramatically reduced PAP accumulation relative to Bpnt1 deficiency alone, and indeed displayed no detectable

hematological abnormalities (Figure 3.1B-D). We conclude that Bpnt1 is a key regulator of PAP and aberrant accumulation of PAP results in toxic modulation of pathways relevant to the onset of microcytic anemia. Importantly, we also define a potential therapeutic strategy to overcome iron deficiency anemia caused by loss of 3'-nucleotidase through concomitant inhibition of PAPS synthase.

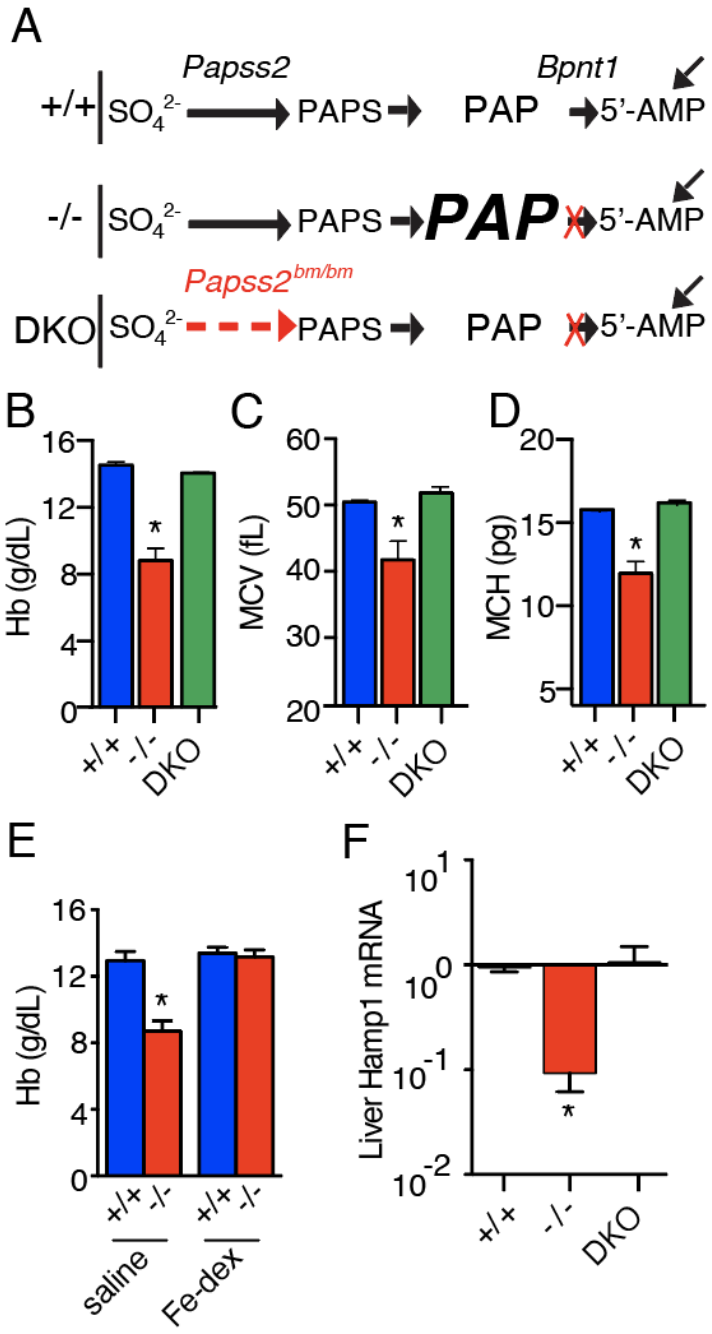

Figure 3.1. Bpnt1 global knockout mice develop PAP-dependent iron deficiency anemia. (A) Top schematic (+/+) shows abbreviated molecular components of the sulfur assimilation pathway and PAP metabolism by 3'-phosphoadenosine 5-phosphosulfate synthase 2 (Papss2) and Bpnt1 in normal cells. Horizontal arrows represent cellular reactions, while diagonal arrows represent contribution from the predominant sources of 5'-AMP independent of the sulfur assimilation pathway. Middle schematic (-/-) represents pathway in Bpnt1 deficient cells (red "X") with PAP, enlarged font and bolded, symbolizing up to 40-fold elevation of cellular concentrations, yet normal levels of other metabolites as reported in normal and mutant tissue (Hudson et al., 2013). Lower schematic (DKO) represents double mutant in which tissue possess both a partial loss of PAPSS2 activity (dashed red arrow) and Bpnt1 deletion (red "X") illustrating the metabolic reduction PAPS synthesis and PAP levels, even in the context of 3'-nucleotidase loss. (B-D) Hematological parameters of 8-week-old wild-type (+/+; blue), Bpnt1$^{-/-}$ knockouts (-/-; red), and Bpnt1$^{-/-}$Papss2$^{bm/bm}$ double mutants (DKO; green) fed standard grain-based chow. (E) Hemoglobin levels of 1-year-old wild-type and knockout mice that received subcutaneous saline or Fe-dextran once a week for three weeks prior to sacrifice at the end of the fourth week. (F) qRT-PCR of Hamp1 transcript relative to beta actin from total liver RNA of 8-week-old mice.

Iron homeostasis is exquisitely maintained by a series of complex physiological pathways including hepatic production of the small peptide hormone Hepcidin (encoded by the Hamp1 gene). Hepcidin executes its function at the duodenum through binding the basolateral iron transporter Fpn and regulating its availability, stability, and ability to mediate iron trafficking to the blood (Nemeth et al., 2004). Since impaired iron absorption can result from the pathological overproduction of hepcidin, as in anemia of inflammation (Nicolas et al., 2002), and because Bpnt1$^{-/-}$ mice display significant defects in hepatic function (Hudson et al., 2013), we postulated that aberrant overproduction of hepcidin might be responsible for the iron deficiency observed. Surprisingly, we found that relative to wild-type, Bpnt1$^{-/-}$ livers had ~10-fold lower levels of Hamp1 mRNA (Figure 3.1F). This data confirms that the hepatic hepcidin signaling axis responds normally to the iron deficient state, yet is insufficient to overcome systemic iron deficiency anemia. In addition, the Bpnt1$^{-/-}$ animals displayed heavier, pale, dilated, and abnormal nucleolar morphology in the intestinal-epithelium suggesting a marked effect of PAP accumulation in the

intestine (Figure 3.2A-D). Taken alongside the subcutaneous rescue by Iron-Dextran (Figure 3.1E), our data suggest the anemia may be a result of impaired iron absorption in the intestine.

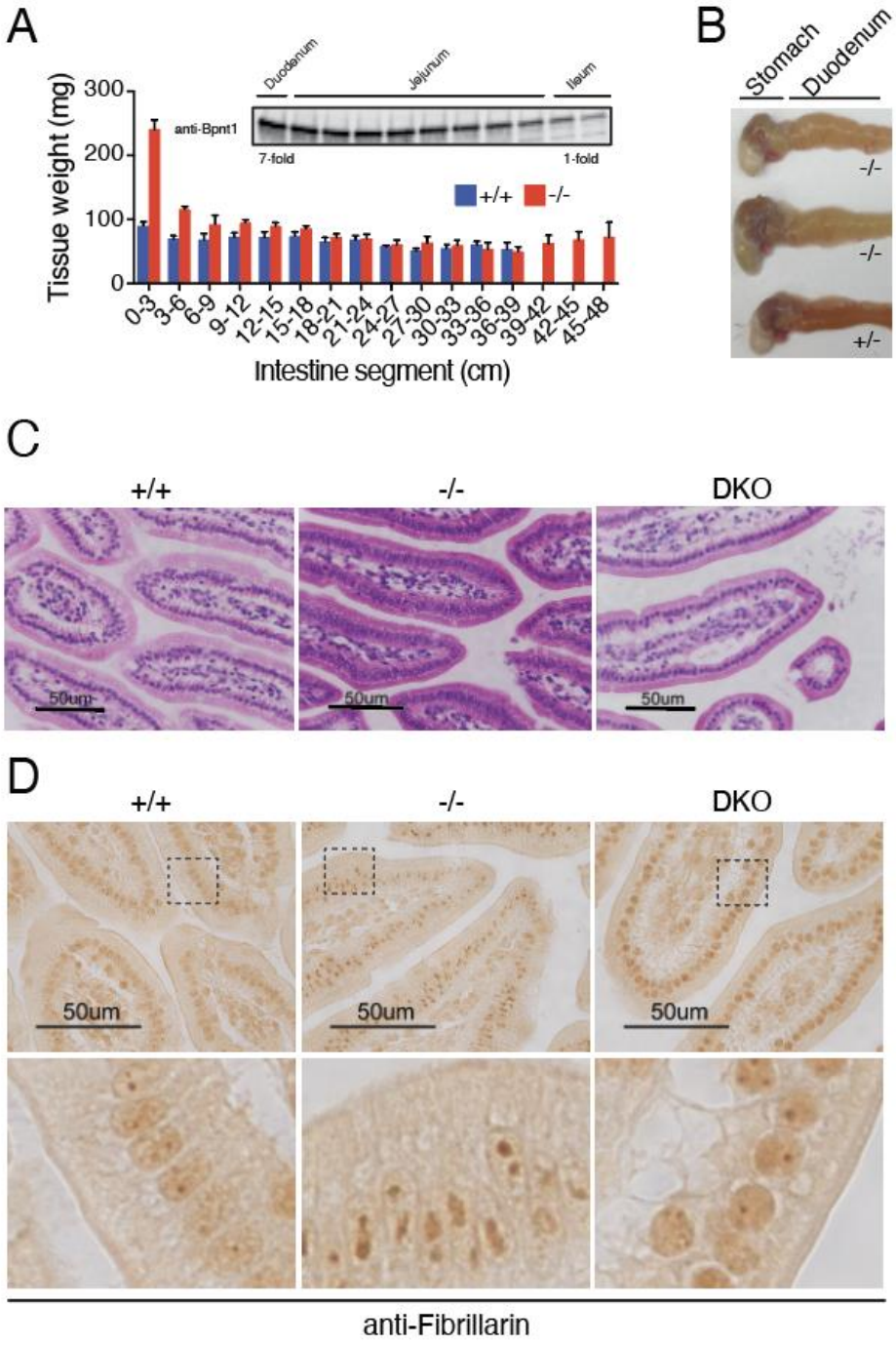

Figure 3.2. Bpnt1 deficient intestine displays abnormal architecture. (A) Dietary iron absorption occurs primarily in the duodenum, the proximal portion of the small intestine immediately distal to the stomach. Macroscopic comparison of wild-type and Bpnt1$^{-/-}$ intestinal architecture reveal that mutant intestines are heavier, longer (~48 cm versus ~39 cm), and pale in color. This effect is most obvious in the proximal duodenum, which weighs on average ~2-fold more than the matching segment of wild-type intestine. Average wet weights of 3-cm segments of wild-type (n=4) or Bpnt1$^{-/-}$ mice (n=4) demonstrating both heavier proximal sections and greater overall length in mutant animals. (A, inset) Western blot for Bpnt1 demonstrating increased Bpnt1 protein expression in the proximal duodenum that decreases gradually distally through the small intestinal tract. (B) Photograph of Bpnt1 knockout (top two) and Bpnt1 heterozygous (bottom) gastroduodenal segments showing pale color and dilated appearance, demonstrating marked alteration of the intestinal architecture in Bpnt1-/- mice. (C) H&E staining of wild-type and Bpnt1-/- mice demonstrating profound changes in intestinal morphology in Bpnt1-/- mice that are rescued in the DKO mice. (D) Immunohistochemistry analysis of nucleoloar-resident fibrillarin in duodenal villi. Here, we report perturbed nucleolar architecture in Bpnt1 deficient gut enterocytes, an indicator of tissue-specific elevation of cellular PAP levels (Hudson and York, 2014). (D, lower panels) Higher magnification of aberrant enterocyte nuclear and nucleolar architecture in global Bpnt1 deficient enterocytes that is rescued in the DKO animal.

3.3.2 Intestinal-epithelium specific Bpnt1 knockout mice develop iron deficiency anemia

The aberrant intestinal morphology coupled with the hypothesis that Bpnt1 may specifically regulate iron absorption in enterocytes prompted the generation of tissue-specific Bpnt1 deficiency by crossing mice harboring a floxed allele of Bpnt1 with animals expressing Cre recombinase driven by the intestinal-epithelium specific *villin* promoter (Figure 3.3A). Intestine-epithelium specific loss was confirmed by immunoblotting for Bpnt1 and analyzing PAP levels in the small intestine (Figure 3.3B-C).

Bpnt1$^{-/int}$ mice appeared normal at birth and display no detectable differences in weight gain following weaning (Figure 3.4A). By 8 weeks postnatal, Bpnt1$^{-/int}$ mice developed moderate alopecia similar to global knockouts (Figure 3.4B). Bpnt1$^{-/int}$ mice also displayed aberrant intestinal morphology and nucleolar condensation similar to Bpnt1$^{-/-}$ mice (Figure 3.4C), but no differences in intestinal iron content (Figure 3.4D).

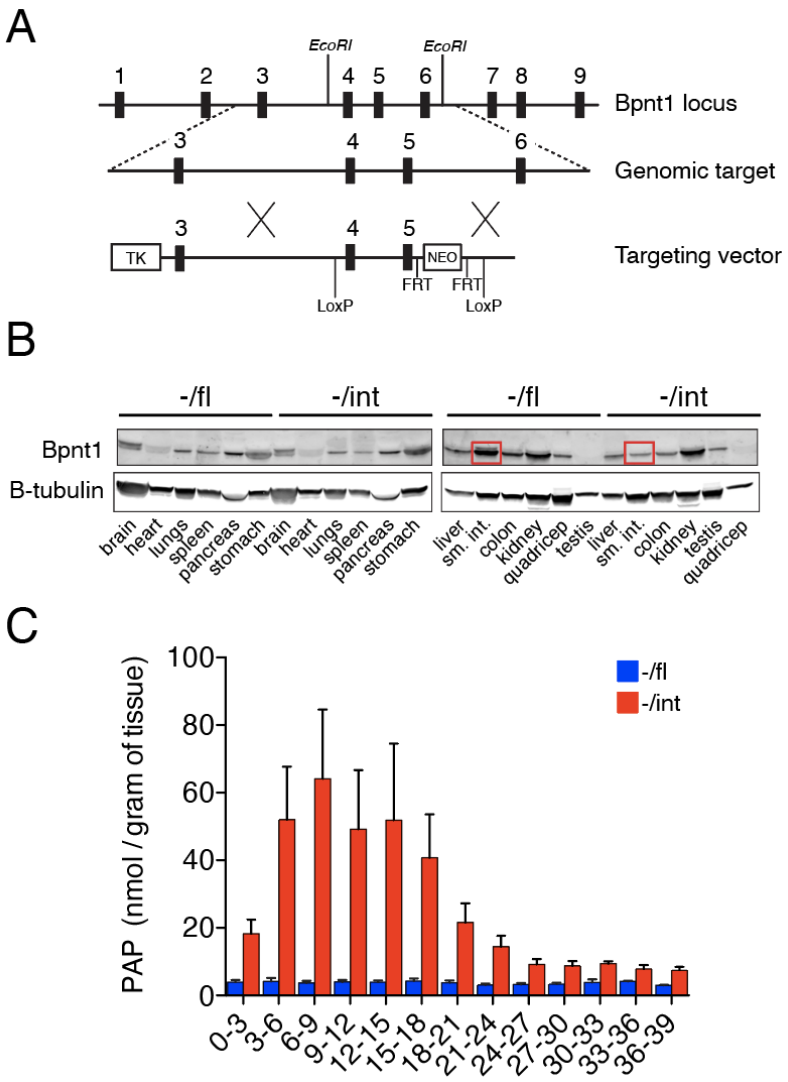

Figure 3.3 Generation and confirmation of intestine-specific Bpnt1 knockout mice. (A) Genomic targeting strategy to introduce LoxP sites flanking the 4th and 5th exons of the Bpnt1 locus. TK = thymidine kinase cassette for negative selection; NEO = neomycin resistance cassette for positive selection. Floxed mice were then crossed with mice expressing Cre recombinase under the control of the villin promoter to generate intestine-specific knockouts. (B) Representative western blot analysis of tissues from Bpnt1$^{-/fl}$ and Bpnt1$^{-/int}$ mice demonstrating significant decrease in expression of Bpnt1 in whole small intestine. Appearance of incomplete knockout is due to residual Bpnt1 protein in intestinal cell types that don't express villin. (C) PAP analysis in the small intestines of Bpnt1$^{-/fl}$ and Bpnt1$^{-/int}$ mice demonstrating robust elevation of PAP in the proximal small intestine (n=3).

CBCs and blood smears of Bpnt1$^{-/int}$ animals revealed lower Hb levels and mean corpuscular volume as well as small hypochromic RBCs (Figure 3.5A-C). We also analyzed bodily iron stores and found that Bpnt1$^{-/int}$ mice have roughly 50% and 30% lower hepatic and splenic iron content, respectively (Figure 3.5D). Consistent with the results from the global Bpnt1 mutant, we observed a marked down-regulation of Hamp1 transcript in livers derived from Bpnt1$^{-/int}$ animals (Figure 3.5E). While the intestinal-epithelium specific loss of Bpnt1 recapitulates the iron-deficiency anemia observed in the global Bpnt1 knockouts, we note that other phenotypes reported for the global Bpnt1 knockout, such as anasarca, have not been observed in the intestine-specific mutant at any age. Collectively, our data confirm that proper metabolic flow through the sulfur assimilation pathway in the small intestine is required for normal iron absorption and mice with impaired Bpnt1 function are predisposed to developing anemia despite maintaining an iron-sufficient diet, the latter of which has potential significance in identifying unmapped inherited forms of anemia.

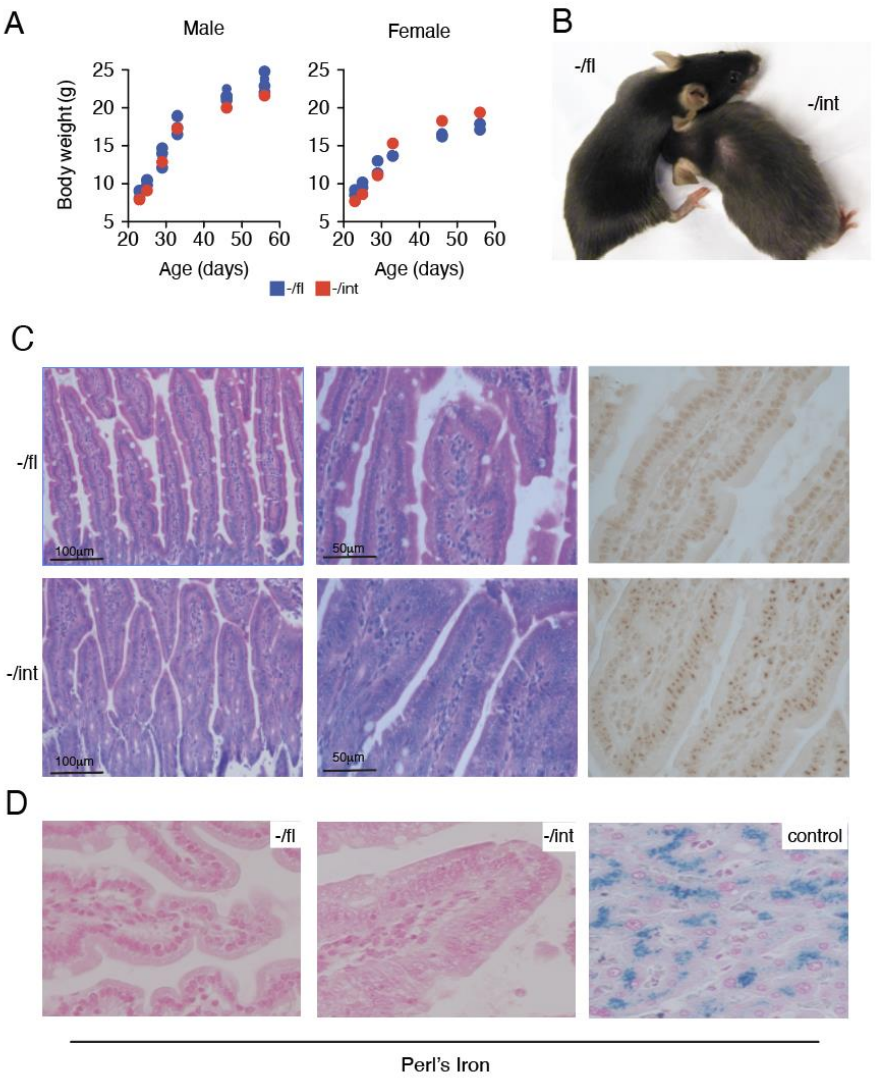

Figure 3.4. Body weight and intestinal morphology analysis of Bpnt1$^{-/int}$ mice. (A) Analysis of body weight after weaning in male and female intestine specific knockout mice. Bpnt1$^{-/int}$ mice have no obvious growth defects or abnormalities through 8 weeks postnatal. (B) Representative photograph of 8-week-old mice demonstrating alopecia in Bpnt1$^{-/int}$ mice. (C, left) H&E staining of wild type and Bpnt1$^{-/int}$ proximal duodenum demonstrating profound changes in cellular architecture and brush border changes. (C, right) Fibrillarin staining of wild type and Bpnt1$^{-/int}$ mice demonstrating aberrant nucleolar condensation in Bpnt1$^{-/int}$ mice. (D) Photograph of Perls' iron stained duodenal villi. Note the lack of detectable iron staining in Bpnt1$^{-/int}$ mice. The positive control section is iron-loaded, human liver. Donovan et al. (2005) reported that a defect in the basolateral iron transporter, ferroportin, leads to sequestration and accumulation of iron in the enterocyte (Donovan et al., 2005). Our RNA sequencing data showed that loss of Bpnt1 resulted in defects in apical iron transporter, Dmt1, as well as decreased ferroportin expression. Thus, we expected no accumulation of iron in the Bpnt1$^{-/int}$ mouse because iron was unable to be absorbed into the enterocyte.

3.3.3 Intestinal-epithelium specific Bpnt1 knockout mice displayed defects in apical iron import

Because Bpnt1$^{-/int}$ mice appear unable to adequately modulate iron stores, we wondered whether Bpnt1 deficient enterocytes might also be susceptible to diet-induced iron starvation. To test this, mice were fed iron-deficient (2-6 ppm) or control (200 ppm) diets *ad libitum* for 5 weeks from weaning after which we measured CBCs. Bpnt1$^{-/int}$ animals displayed average hemoglobin concentrations of 4.1 g/dL relative to 9.5 g/dL for Bpnt1$^{-/fl}$ controls (Figure 3.6A). To understand why Bpnt1$^{-/int}$ mice were unable to respond to the low iron stress, we looked for defects in apical and basolateral iron transport. When basolateral transport is impaired, either through up-regulated hepcidin or Fpn deficiency, intracellular iron accumulates in the duodenal enterocytes and is visible as ferritin granules by histological iron staining (Donovan et al., 2005). Bpnt1$^{-/int}$ animals displayed no detectable increase in enterocyte iron stores, suggesting that defective basolateral transport was not primarily responsible for the iron deficiency (Figure 3.4D). We next examined the functionality of iron import across the apical membrane by Dmt1. To test this, we analyzed the transcript and protein levels of Dmt1 from isolated duodenal enterocytes. Normally, when an organism is iron-starved, there is a profound compensatory response to induce Dmt1 expression, subsequently increasing iron absorption. Strikingly, while iron-depleted Bpnt1$^{-/fl}$ animals significantly up-regulated Dmt1, Bpnt1$^{-/int}$ enterocytes failed to increase Dmt1 transcript or protein levels (Figure 3.6B-C). Our data suggests that insufficient iron transport across the apical membrane by Dmt1 gives rise to the iron deficiency anemia in Bpnt1$^{-/int}$ mice.

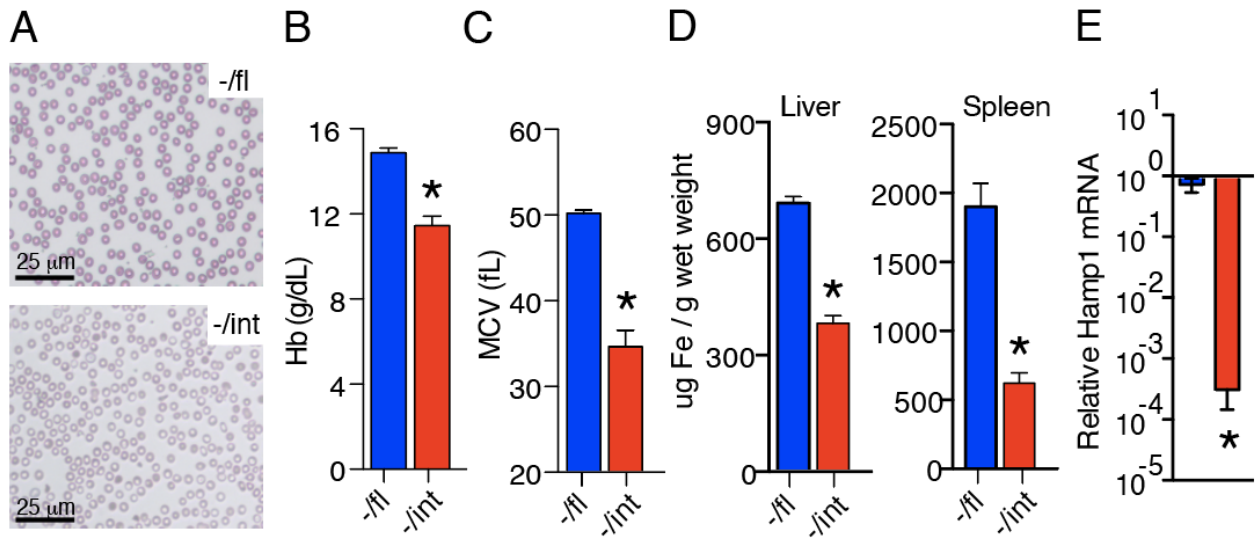

Figure 3.5. Inactivation of Bpnt1 s in the small intestine results in iron deficiency anemia. (A) Representative photograph of Wright stained whole blood smear from Bpnt1$^{-/fl}$ and Bpnt1$^{-/int}$ showing microcytic hypochromic RBCs. (B-C) Hematological parameters of Bpnt1$^{-/fl}$ and Bpnt1$^{-/int}$ 8-week-old mice demonstrating anemia (n=6-8 per group). (D) Quantification of tissue iron stores in livers and spleens of 8-week-old male Bpnt1$^{-/fl}$ and Bpnt1$^{-/int}$ mice. (E) qRT-PCR of Hamp1 mRNA relative to beta actin from total liver RNA in Bpnt1$^{-/fl}$ and Bpnt1$^{-/int}$ mice (n=4).

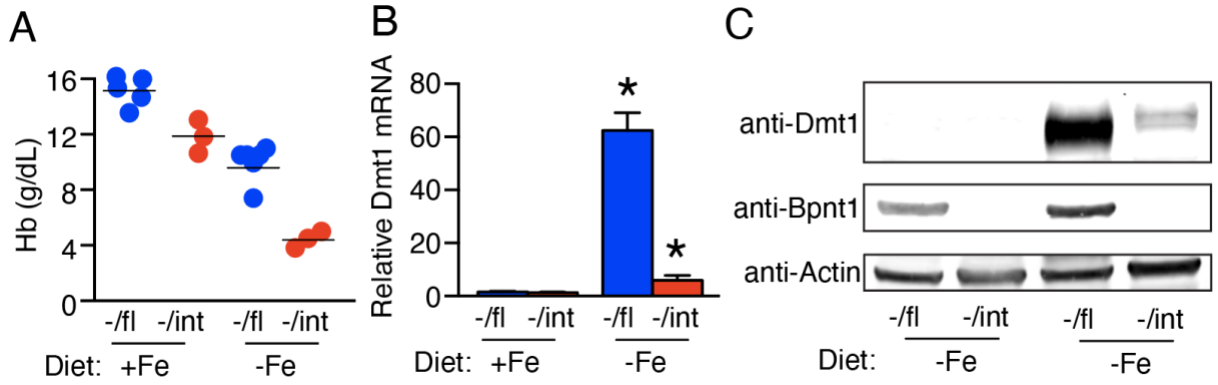

Figure 3.6. Bpnt1$^{-/int}$ enterocytes display defects in apical iron transport. (A) Hemoglobin levels of mice on control or iron deficient diets. Mice were fed a low iron (2 ppm) or control (200 ppm) diet for 5 weeks after weaning (n=3-5 per group). (B) qRT-PCR of Dmt1+IRE mRNA relative to actin in the duodena of control or iron starved mice (n=3-5 per group). (C) Western blot analysis of Dmt1, Bpnt1, and actin loading control from isolated enterocytes of the same mice as in panel B.

3.3.4 PAP accumulation induces transcriptional changes in iron metabolism associated genes, the HIF-2α pathway, and sulfur assimilation related genes

Recently, a number of studies have implicated transcription factor hypoxia-inducible factor 2 alpha (Hif-2α) as a key mediator of the intestine's response to iron deficiency (Anderson et al., 2013b; Mastrogiannaki et al., 2009; Taylor et al., 2011a). During iron starvation, degradation of HIF-2α is inhibited, leading to its accumulation and subsequent transcription of genes containing HIF response elements (HifREs). Mice lacking intestinal HIF-2α display blunted responses to iron deficiency, including an inability to upregulate Dmt1, and thus are unable to maintain sufficient serum iron and hemoglobin levels. Because Dmt1 expression in Bpnt1$^{-/int}$ mice is not stimulated following iron deficiency, we surmised that HIF-2α or other genes under the control of HIF-2α might also be perturbed.

Thus, we performed RNA sequencing (RNAseq) on polyA-selected RNA isolated from enterocytes of Bpnt1$^{-/fl}$ and Bpnt1$^{-/int}$ mice fed either iron-replete or iron-deficient chow (Figure 3.7A). Strikingly, the pathways and biological functions identified using gene set enrichment analysis (GSEA) pointed to iron-related and hematologic parameters as functionally pertinent (Figure 3.7B).

A

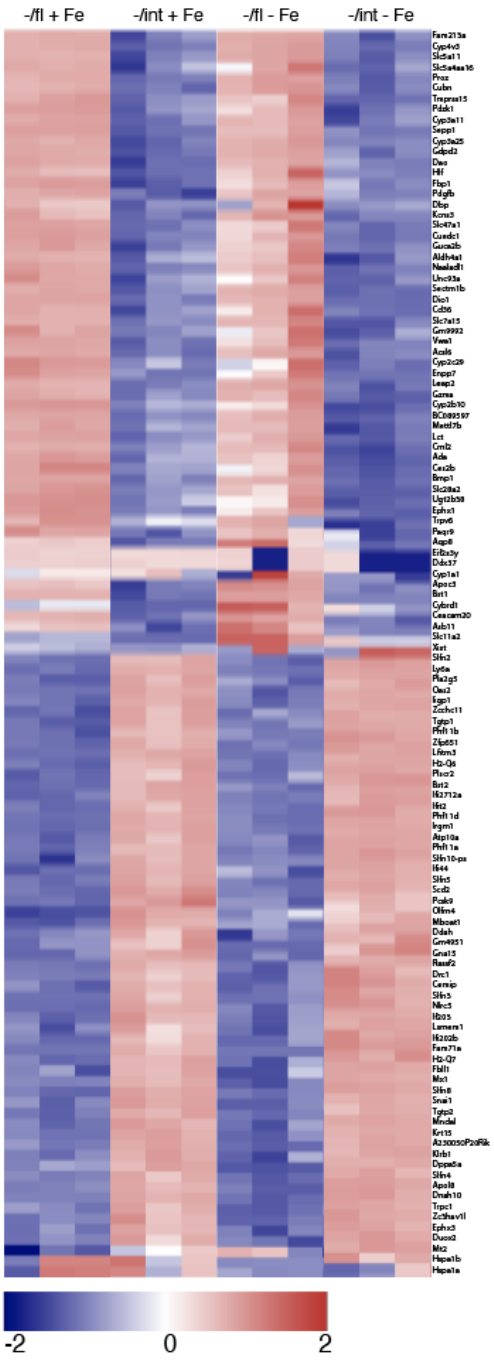

B

Category	Term	# Genes	p-value
GOTERM_MF_FAT	Porphyrin binding	8	9.50E-06
GOTERM_MF_FAT	Aromatase activity	5	2.30E-05
GOTERM_MF_FAT	Iron Ion Binding	10	4.60E-05
GOTERM_MF_FAT	Heme Binding	7	7.80E-05
GOTERM_BP_FAT	Oxidation Reduction	13	7.00E-05
GOTERM_BP_FAT	Response to Iron ion	2	1.40E-02
GOTERM_CC_FAT	Brush Border	5	1.80E-05
KEGG_PATHWAY	Metabolism of xenobiotics by cytochome P450	6	7.70E-06
KEGG_PATHWAY	Retinol Metabolism	5	1.90E-04
KEGG_PATHWAY	Linoleic Acid Metabolism	4	9.80E-04
KEGG_PATHWAY	Drug Metabolism	4	4.00E-03
KEGG_PATHWAY	PPAR signaling pathway	4	4.60E-03

C

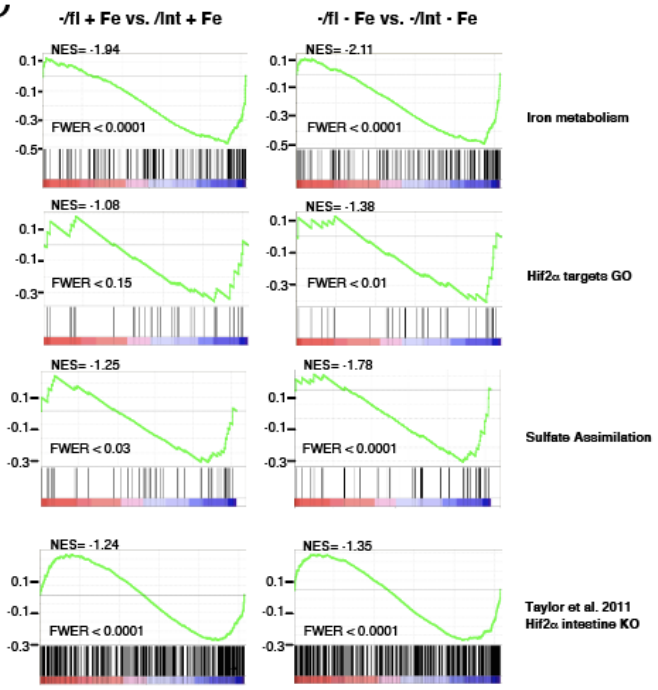

D

Category	Term	# Genes	p-value
UP_SEQ_FEATURE	Glycosylation site	29	8.0E-03
UP_SEQ_FEATURE	Signal peptide	24	2.9E-02
UP_SEQ_FEATURE	Disulfide bond	19	6.6E-02
UP_SEQ_FEATURE	Heme axial ligand	3	9.5E-02
GOTERM_MF_FAT	Iron ion binding	7	8.1E-03
GOTERM_MF_FAT	Iron ion transmembrane transporter activity	2	3.5E-02
GOTERM_BP_FAT	Response to iron ion	2	1.6E-02
GOTERM_BP_FAT	Iron ion transport	3	1.3E-02
SP_PIR_KEYWORDS	Iron transport	3	4.4E-03
SP_PIR_KEYWORDS	Iron	7	5.4E-03

Figure 3.7. Bpnt1$^{-/int}$ enterocytes display broad changes in transcriptional activity. (A) Heatmap displaying top five percent of genes that changed between enterocytes of Bpnt1$^{-/fl}$ vs. Bpnt1$^{-/int}$ mice fed either an iron-replete or iron-deficient diet for 5 weeks (n=3 per group). (B) Database for Annotation, Visualization and Integrated Discovery (DAVID) gene ontology analysis on the genes in (A) highlighting changes in biological processes related to iron metabolism between Bpnt1$^{-/fl}$ vs. Bpnt1$^{-/int}$ mice fed either an iron-replete or iron-deficient diet for 5 weeks. (C) Gene Set Enrichment Analysis (GSEA) was used to compare the transcriptional signature of Bpnt1$^{-/int}$ enterocytes to gene ontology signatures of iron metabolism, HIF-2α, sulfate assimilation and sequencing data from HIF-2α$^{-/int}$ animals published by (Donovan et al., 2005). Enrichment score is plotted on the y-axis and each vertical line along the x-axis represents an individual gene. These analyses were performed according to Subramanian et al. (2005)'s instructions. (D) Database for Annotation, Visualization and Integrated Discovery (DAVID) analysis of the shared subset of genes (92) described in (Fig. 4C). DAVID gene ontology analysis confirmed that the shared subset of genes in HIF-2α$^{-/int}$ and Bpnt$^{-/int}$ animals is intricately involved in iron metabolism.

GSEA was performed and revealed significant enrichment of iron-metabolism related genes, HIF-2α gene ontology signature and sulfate assimilation gene ontology signatures (Figure 3.8A). Of note, genes that are essential for proper iron homeostasis, import, and export including HIF-2α, transferrin receptor (Tfr1), ferroportin (Fpn), and iron reductase (Dcytb), and Dmt1 (Figure 3.6B-C and 3.8A) were altered in Bpnt1$^{-/int}$ enterocytes, supporting the role of PAP accumulation in mediating control of iron metabolism at each step. Furthermore, only under conditions of iron-deficiency does the HIF-2α dependent transcriptional signature (Schaefer et al., 2009) become enriched (Figure 3.8A and 3.7C). This suggests that an animal with a defect in the sulfur assimilation pathway may be genetically predisposed to develop iron deficiency anemia through aberrant HIF-2α signaling. However, the precise mechanism by which this occurs is not known.

Both Bpnt1$^{-/int}$ and HIF-2α$^{-/int}$ animals are unable to stimulate Dmt1 production when fed iron-deficient chow (Taylor et al., 2011a), indicating that loss of Bpnt1 or HIF-2α phenocopy one another, at least in part. Thus, we surmised that PAP accumulation may recapitulate the molecular

signature of a HIF-2α-deficient cell. We performed GSEA comparing the transcriptional signature of genes that changed more than three-fold when Bpnt$^{-/int}$ and HIF-2α$^{-/int}$ animals were fed iron-deficient chow (Figure 3.8A and 3.7C). We observed significant enrichment between the HIF-2α$^{-/int}$ genetic signature and Bpnt$^{-/int}$ mice that were fed either iron-rich or iron-deplete chow. We hypothesize this is likely due to repression of HIF-2α in Bpnt$^{-/int}$ enterocytes, independent of dietary iron content (Figure 3.8B).

A

	-/fl + Fe vs. /int + Fe		-/fl - Fe vs. -/int - Fe	
Gene Ontology	**NES**	**FWER**	**NES**	**FWER**
Iron Metabolism	-1.94	<0.0001	-2.11	<0.0001
HIF-2α targets	-1.08	<0.15	-1.38	<0.01
Sulfate Assimilation	-1.25	<0.03	-1.78	<0.0001
HIF-2α intestine KO (Taylor et al. 2011)	-1.24	<0.0001	-1.35	<0.0001

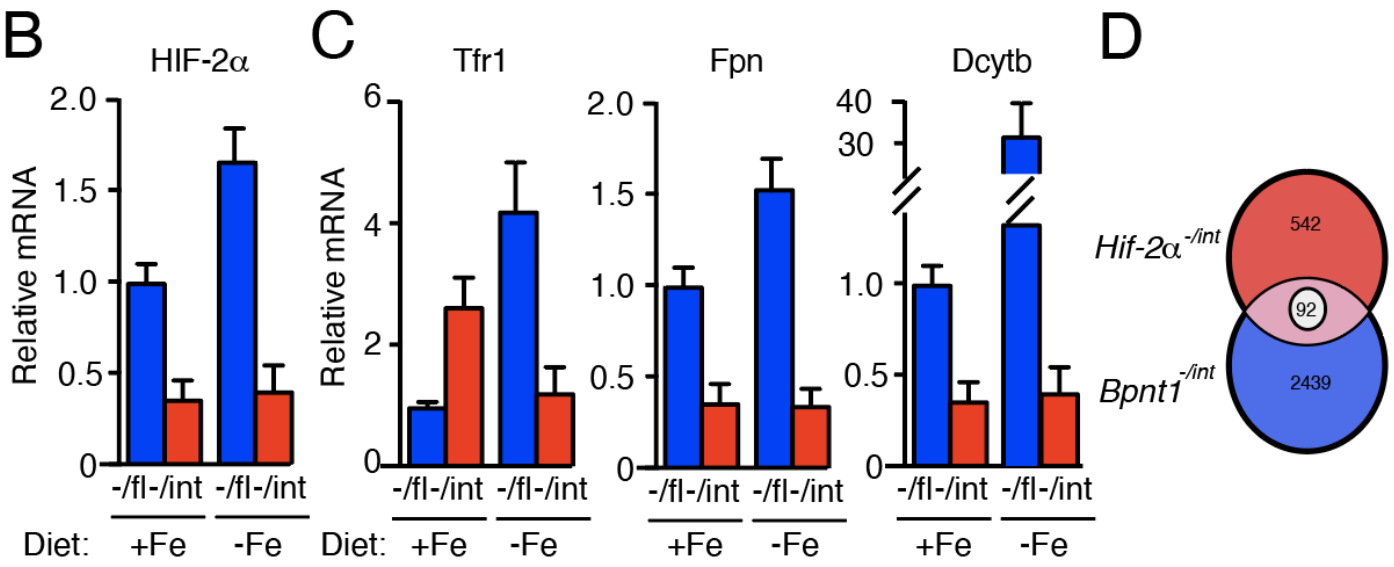

Figure 3.8. PAP accumulation induces transcriptional changes in iron-metabolism related genes, the HIF-2α pathway and sulfur-assimilation related genes. (A) Enterocytes of Bpnt1$^{-/fl}$ vs. Bpnt1$^{-/int}$ mice fed either an iron-replete or iron-deficient diet for 5 weeks (n=3 per group) were isolated and subjected to poly-A selected RNA sequencing. Gene Set Enrichment Analysis (GSEA) was performed on pertinent gene ontology signatures defined for targets of iron metabolism, the HIF-2α pathway, genes involved in sulfur assimilation, as well as sequencing data from HIF-2α$^{-/int}$ mice published by (Taylor et al., 2011a). GSEA analysis comparing the Bpnt$^{-/int}$ and HIF-2α$^{-/int}$ transcriptional signatures was performed as follows. Genes that changed greater than three-fold in HIF-2α$^{-/int}$ mice (542) and Bpnt1$^{-/int}$ mice (2439) were compared using GSEA. NES represents Normalized Enrichment Score. Family wise error rate (FWER) < 0.05 was considered statistically significant. (B) qRT-PCR of HIF-2α mRNA relative to actin in the duodena of control or iron starved mice (n=3 per group). (C) RNA-seq reveals expression changes of key iron-regulatory genes. (D) Venn-diagram showing unique and shared transcriptional signature of genes described in (A). There were 92 genes whose expression was altered analogously in. HIF-2α$^{-/int}$ and Bpnt1$^{-/int}$ mice.

3.3.5 Intestinal-epithelium specific Bpnt1 knockout mice displayed decreased HIF-2α levels but no difference in HIF-2α subcellular localization

Of the total number of transcripts that were altered in HIF-2α$^{-/int}$ (542) and Bpnt$^{-/int}$ (2439) animals, 92 genes were similarly altered between genotypes (Figure 3.8D). Assessment of HIF-2α by immunohistochemistry in normal and mutant intestinal tissue confirmed that loss of *Bpnt1* results in decreased HIF-2α protein levels (Figure 3.9A-B). We did not observe an appreciable difference in HIF-2α subcellular localization in Bpnt$^{-/int}$ intestine as compared to wild-type (Figure 3.9A). As a control, we confirmed the specificity of the antibody signal observed by staining intestinal tissue from HIF-2α knockout tissue (Figure 3.9A-B), which revealed very minimal signal as expected.

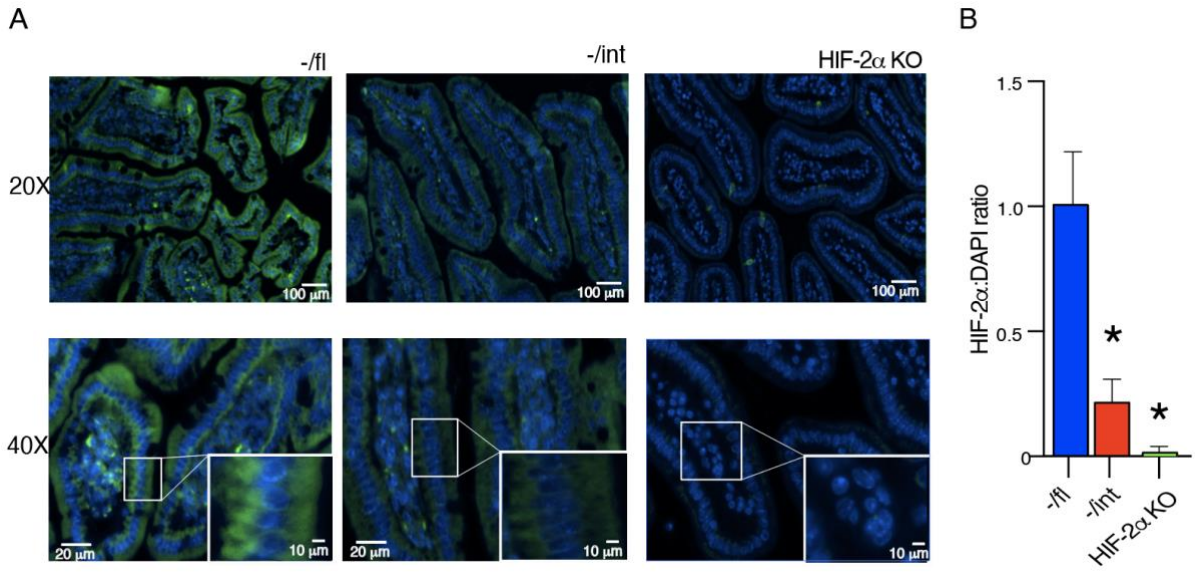

Figure 3.9. Bpnt1$^{-/int}$ enterocytes and small intestine display decreased HIF-2α and no difference in HIF-2α subcellular localization. (A) Representative images of immunofluorescence staining of proximal duodenum in -/fl WT control (left), Bpnt1$^{-/int}$ (-/int, center) and HIF-2α knockout (HIF-2α KO) for HIF-2α (green) and DAPI (blue) at 20x and 40x with magnified inset. (B) Quantification of HIF-2α fluorescent signal relative to DAPI signal in WT, Bpnt1$^{-/int}$ and HIF-2α KO (n=3, 5 sections per animal) proximal duodenum sections as seen in (B).

Furthermore, canonical targets of HIF-2α but no other HIF family members, were largely repressed in Bpnt$^{-/int}$ enterocytes (Figure 3.10). Intriguingly, Dmt1, Dcytb and Fpn were all repressed in both HIF-2α$^{-/int}$ and Bpnt$^{-/int}$ animals. We suspect that PAP's ability to impair Dmt1 transcription and translation (Figure 3.6B-C) is most important because there is no increase in iron stores in Bpnt$^{-/int}$ animals (Figure 3.4D). However, modulation of transcriptional control of iron bioavailability at the level of reduction, import, nuclear transcriptional activity, and export represents exquisite control of iron metabolism at every key step. Collectively, these data are consistent with a role for Bpnt1 in the control of transcriptional responses to iron deficiency through modulation of HIF-2α-dependent and independent mechanisms.

		Normal chow			Fe-deficient chow		
		Fold Change	log2 Fold Change	p value	Fold Change	log2 Fold Change	p value
Canonical HIF-2α targets	Alas2	1.324453827	0.40539755	0.66616449	0.916666668	-0.12553088	0.60118538
	Epas1	0.339088925	-1.56026443	0.00000000	0.234659137	-2.09136146	0.00000000
	Epo	0.425778719	-1.23182425	0.00458135	0.331341235	-1.59361034	0.00876784
	Epor	1.834727697	0.87556596	0.29531787	1.923738484	0.94391269	0.65842612
	Fech	0.616836837	-0.69703917	0.00000019	0.722448979	-0.46903239	0.00000000
	Hba-a1	0.426269953	-1.23016073	0.01619693	0.207920792	-2.26589406	0.00259314
	Hba-a2	0.177238918	-2.49623267	0.00862805	0.139534884	-2.84130225	0.00097100
	Slc25a37	2.304376372	1.20437637	0.00000000	4.387931032	2.13354085	0.00000000
	Slc25a38	0.995641286	-0.00630204	0.97004617	1.16372093	0.21874513	0.09624013
HIF family members	Hif1a	1.507448307	0.59210853	0.00089307	1.312894099	0.39275055	0.46749888
	Hif1an	0.826227114	-0.27538969	0.03950493	0.720817729	-0.47229360	0.00037678
	Hif3a	2.357207628	1.23707884	0.04147384	1.409666989	0.49535439	0.36573067
HIF-2α Gene Ontology targets	Apex1	5.124278901	2.35734900	0.00000000	2.967317146	1.56915913	0.00000000
	Arnt	0.80128187	-0.31961826	0.02209683	0.802797756	-0.31689151	0.04067043
	Abcg2	0.340669549	-1.55355510	0.00000000	0.340032557	-1.55625521	0.00000000
	Bhlhe40	0.557707783	-0.84241869	0.00041404	0.887722445	-0.17181942	0.23876492
	Cited2	0.541050289	-0.88616540	0.00001220	0.470758546	-1.08694081	0.00000000
	Crebbp	0.993532475	-0.00936097	0.94905788	1.024581914	0.03503533	0.81367677
	Cul2	1.530085127	0.61361192	0.00001720	1.211735669	0.27707502	0.07854539
	Eif3e	2.305999787	1.20539238	0.00000000	1.831931336	0.87336543	0.00000094
	Efna1	0.40003003	-1.32181979	0.00000000	0.299727587	-1.73827622	0.00133394
	Egln1	0.782078013	-0.35461557	0.01508751	0.551835812	-0.85768901	0.00000004
	Egln2	0.642650768	-0.63789314	0.00017454	0.725351043	-0.46324872	0.00016309
	Egln3	0.265367028	-1.91393897	0.00000000	0.330731178	-1.59626904	0.00413345
	Elk1	2.249496574	1.16960217	0.00009870	1.787045181	0.83757611	0.00555204
	Ep300	1.062673341	0.08769819	0.63782639	0.968912688	-0.04556143	0.85398371
	Ets1	0.212050803	-2.23751815	0.00000000	0.222723597	-2.16667368	0.00000050
	Flt1	1.148397759	0.19962242	0.82013774	0.710992231	-0.49209430	0.56947177
	Fxn	2.122804129	1.08597126	0.00000035	2.217511306	1.14894146	0.00000181
	Kdr	0.716878078	-0.48020032	0.47252928	1.285120081	0.36190317	0.56018222
	Mmp14	0.995794126	-0.00608059	0.97116155	1.145144781	0.19553001	0.16272921
	Pgk1	0.930595141	-0.10377444	0.45637573	0.833753576	-0.26230705	0.03782296
	Pou5f1	1.108710203	0.14888232	0.86371144	1.086546155	0.11974946	0.88773231
	Rbx1	1.707735378	0.77208444	0.00000006	1.606541537	0.683958282	0.88773231
	Rps27a	2.79820242	1.48450033	0.00000000	2.427872449	1.27969263	0.00000000
	Sirt1	0.843002725	-0.24639080	0.14553125	0.830613163	-0.26775136	0.13477989
	Slc11a2	0.399849215	-1.32247204	0.00000000	0.165060548	-2.59893276	0.00029955
	Slc2a1	2.056142495	1.03994025	0.00000000	1.99518978	0.99652598	0.00000000
	Sp1	1.165427331	0.22085905	0.17983662	0.974635934	-0.03706468	0.81272555
	Serpine1	0.551322884	-0.85903061	0.05256612	1.123490519	0.16798795	0.82254253
	Tceb1	1.319287773	0.39975929	0.00829574	1.119385636	0.16270714	0.34537547
	Tceb2	0.987850385	-0.01763554	0.92551412	1.087232524	0.12066052	0.41642491
	Uba52	1.370972554	0.45519969	0.00935380	1.459089985	0.54506886	0.00205065
	Ube2d1	1.258686817	0.33191936	0.05908987	1.241381318	0.31194634	0.06615203
	Ube2d2a	1.067525647	0.09427073	0.45827651	0.970015624	-0.04392011	0.71452840
	Ube2d3	0.98328059	-0.02432493	0.85058723	0.952966781	-0.06950217	0.57651479
	Vegfa	0.18065622	-2.46868117	0.00000000	0.262566628	-1.92924453	0.00000000
	Vhl	0.945537276	-0.08079376	0.62233202	0.853387888	-0.22872646	0.17489223

Figure 3.10. Accumulation of PAP in Bpnt1$^{-/int}$ enterocytes demonstrates broad changes in HIF-2α-associated gene targets. Summarized RNA sequencing data (Fig. S5) for canonical HIF-2α target genes, other members of the HIF family, additional HIF-2α ontology terms and manually curated genes associated with hypoxia signaling. Data are expressed as fold change and $\log_2$ fold change as analyzed by DESeq (n=3 per group).

3.4 Discussion

This work uncovers an unanticipated link between intestinal-epithelial specific nucleotide hydrolysis in the sulfur assimilation pathway and iron homeostasis. Our data point to a mechanism by which inactivation of the 3'-nucleotidase Bpnt1 in intestinal tissue leads to a dramatic accumulation of its substrate PAP, thereby preventing the physiological response to low iron levels. Remarkably, by reducing PAP synthesis in the context of Bpnt1 deficiency, we are able to completely rescue the pathophysiology of iron deficiency anemia. This has profound implications in two areas: the first being a new complementation group for iron deficiency anemia and the second being a potential therapeutic approach to overcome genetic defects that are caused by 3'-nucleotidase deficiency.

Mechanistically, we show that iron deficiency is likely due to a failure of Bpnt1 null mice to upregulate Dmt1 at the apical enterocyte surface in order to promote iron uptake. In addition, we observed a striking parallel between phenotypic characterization of Bpnt1 and Hif-2α intestine knockout mice in that both animals are incapable of mounting a transcriptional response to iron starvation. Furthermore, Bpnt1 and Hif-2α intestine knockout mice display common transcriptional signatures: most notably decreased expression of Dmt1, Dcytb, Tfr1, and Fpn- thereby broadly regulating iron metabolism at all three essential steps in the metabolism of iron in the small intestine. However, the primary role of PAP appears to hinge on impairment of apical iron transport through Dmt1. These data suggest multiple potential functions of PAP in mediating iron metabolism which are explored in later chapters.

Recent reports have demonstrated that Hif-2α is an important component of the transcriptional response to iron starvation (Taylor et al., 2011b). Since loss of Bpnt1 in intestine

tissue corresponds to decreased Hif-2α mRNA transcript and protein levels, independent of iron levels in the diet, it seems that accumulation of PAP directly or indirectly influences transcription. Quantification of Hif-2α levels in Bpnt1 mutant intestine tissue indicates about an 70% decrease, but not complete ablation. This partial reduction, rather than complete, may explain why only a subset of transcriptional targets are altered (92 out of 542 based on RNA-seq data). Comparisons of RNA-Seq data from our work and published Hif-2α intestinal-epithelium specific knockout tissue suggests about 20 percent of Hif-2α targets are decreased data indicate the elevated levels of PAP may inhibit Hif-2α. Perhaps more importantly, ~25% of transcripts sequenced displayed greater than three-fold changes in gene expression, providing evidence that PAP accumulation augments transcription. However, the mechanism by PAP accumulation and loss of Bpnt1 result in diminished Hif-2α is an important question and is explored in future chapters. Given that both transcript levels and protein are decreased relatively proportionally, it seems likely that accumulation of PAP may primarily augment transcription, a question that is explored in later chapters.

Thus, PAP may impair the ability of Hif-2α to sense that the enterocyte is iron starved at baseline, given that independent of dietary iron content, Bpnt1$^{-/int}$ mice develop iron deficiency anemia. It is also possible that there is an impairment Hif-2α's ability to bind HREs and activate downstream transcriptional programs in response to iron starvation. Given the broad differences observed in gene expression between Bpnt1$^{-/fl}$ and Bpnt$^{-/int}$ mice, this possible effect may reveal new genes involved in maintenance of iron homeostasis. It is also possible that DNA contains PAP-responsive elements that disrupt downstream transcriptional pathways, however there is currently no evidence for this claim. Furthermore, PAP may alter the conformation of HIF-2α and block nuclear import and stabilization of HIF-2α protein. Given that PAP has been shown to

directly bind upstream sulfotransferases (Rens-Domiano and Roth, 1987) it is conceivable that PAP acts as a broad, yet specific, inhibitor of other proteins involved in regulation of iron metabolism. However, further investigation is needed to address these possibilities. Studies probing these questions are performed in subsequent chapters using dietary, genetic, and biochemical approaches.

It is also plausible that PAP accumulation, or other metabolites such as PAPS, influences additional targets that contribute to the iron deficiency anemia observed in Bpnt1 mutant animals. Bpnt1 is kinetically most effective at hydrolyzing PAP to 5'AMP but also has weaker activity in converting PAPS to 5'APS and 1000-fold diminished activity as an inositol bisphosphate phosphatase (Rens-Domiano and Roth, 1987). Additionally, analysis of metabolites from Bpnt1 -/- hepatocytes shows that by far the highest fold accumulation occurs in PAP (40-fold) as compared to modest changes in PAPS (5-fold) and no significant changes in ATP, ADP or AMP (Hudson et al., 2013). Our forward genetics approach to concomitantly decrease PAP synthesis (Papss2$^{bm/bm}$) in the Bpnt1 knockout mouse (DKO) showed that the rescue of phenotypes was not due to inositol phosphatase activity or failure to produce 5'AMP, but rather due to toxic PAP accumulation. That said, the Papss2$^{bm/bm}$ approach does not definitively eliminate that PAPS accumulation may also be involved, such that PAPS accumulation could promote hyper-activation of sulfotransferase (SULTs) reactions. In this scenario, the DKO may act to restore a more normal SULT activity. Interestingly, PAP has been shown to inhibit SULTs, thus this model does not necessary hold as the DKO would also reduce the PAP inhibition.

Additionally, a number of studies have demonstrated that the 5'-3' exoribonucleases 1 and 2 (Xrn1/2) are targets of PAP toxicity and modulated by PAP accumulation in a variety of cell types and organisms (Hudson et al., 2013; Lopez-Coronado et al., 1999; Miki et al., 2016;

Spiegelberg et al., 2005; Spiegelberg et al., 1999a). Complementation of Bpnt1 null cells with Xrn1 in an attempt to suppress loss of Bpnt1 is explored in later chapters. Interestingly, in contrast to our previous study (Hudson et al., 2013), in which the production of highly abundant hepatic proteins is attenuated, Dmt1 protein is normally expressed at relatively low levels and is only robustly expressed upon iron starvation (Gunshin et al., 1997). Thus, while high levels of PAP directly inhibit nuclear Xrn2 (Dichtl et al., 1997b) and lead to ribosomal RNA processing defects in hepatocytes, it is unclear how this defect would impact protein levels in enterocytes. Furthermore, there does not appear to be gross defects in protein production in the intestinal-epithelium specific Bpnt1 mutant animal, as these mice do not display any diarrhea, weight loss, or nutrient (other than iron) deficiencies. Thus, delineation of the direct target(s) of PAP requires more extensive mechanistic inquiry, which is explored in Chapter 5.

These data also imply that leverage of pathways involved in sulfur assimilation may represent a new avenue for therapeutic development. Given that Bpnt1 is potently inhibited by lithium (Spiegelberg et al., 2005; Spiegelberg et al., 1999a), it is possible that lithium may be mediating its toxic and/or beneficial effects through accumulation of PAP. Because Bpnt1$^{-/int}$ animals display both microscopic and macroscopic defects in the small-intestinal architecture, this is certainly a possibility. In contrast, inhibition of Bpnt1 and accumulation of PAP may be useful in the treatment of diseases associated with Hif-2α such cancer, cardiovascular disease, or abnormalities in embryonic development (Patel and Simon, 2008). Given the diverse functions associated with Hif-2α, novel inhibitors may have broad implications in the treatment of many diseases. Thus, development of small-molecule inhibitors of Papps2 may represent an approach to ameliorate IDA, while inhibiting Bpnt1 and accumulating PAP may represent a strategy to inhibit a host of Hif-2α dependent diseases.

In summary, we define a new genetic basis and complementation group for iron-deficiency anemia and demonstrate a molecular genetic approach for overcoming the induced pathophysiology caused by loss of cytoplasmic 3'-nucleotidase activity. This work uncovers an unanticipated link between an intestinal-epithelium specific nucleotide hydrolysis in the sulfur assimilation pathway and iron homeostasis. Our data point to a mechanism by which loss of Bpnt1 leads to massive elevation in PAP substrate which prevents the physiological response to low iron levels by perturbing transcriptional upregulation of iron homeostasis factors, possibly through modulation of HIF-2α activity. Our work identifies a new complementation group for iron deficiency anemia and provides insights into strategies to overcome disease pathophysiology through concomitant down regulation of PAPSS2 metabolism. Future chapters will explore dietary, genetic, and biochemical approaches aimed at understanding a potential mechanistic basis for PAP metabolic toxicity caused by loss of Bpnt1.

Chapter 4 Modulation of sulfur assimilation metabolic toxicity overcomes anemia and hemochromatosis in mice

This chapter was adapted from Hale et al., *Advances in Biological Regulation* (2020), Copyright by Elsevier.

4.1 Introduction

In Chapter 3, our initial characterization of the role of Bpnt1 in regulating iron metabolism was discussed. We defined a new genetic complementation group for iron deficiency anemia and a mechanistic basis for loss of Bpnt1 through accumulation of PAP substrate impairing iron absorption and homeostasis. In this chapter, our data describing dietary and genetic approaches to overcome metabolic toxicity in Bpnt1 deficient animals is discussed. We establish an *in vitro* culture system using primary intestinal organoids, recapitulating metabolic and cellular phenotypes observed in Bpnt1 null tissue. Furthermore, we demonstrate that PAP metabolic toxicity in the intestinal-epithelium can be selectively leveraged to overcome systemic iron overload caused by mutations associated with hereditary hemochromatosis through inhibition of intestinal iron loading and absorption. The focus of this chapter is to summarize our studies aimed at delineating strategies to overcome metabolic toxicity caused by loss of Bpnt1.

Iron homeostasis is required for numerous cellular and organismal functions. Disorders of iron homeostasis include anemia, hemochromatosis, and Parkinson's disease, among others (Hentze et al., 2010). Iron deficiency anemia (IDA) affects up to 1 billion people worldwide (Camaschella, 2015), whereas hemochromatosis is one of the most common Mendelian disorders (~1 case per 500 persons of European ancestries) and can cause organ failure due to toxic iron

accumulation (Powell et al., 2016). In addition, iron accumulation in the central nervous system plays a role in neurodegenerative disease (Ward et al., 2014). Thus, identifying factors involved in iron homeostasis is essential to understanding a potential basis of a wide range of diseases.

Sulfur assimilation is a critical metabolic pathway in which inorganic sulfate is incorporated into sulfur-containing amino-acids or sulfated end-products (Hudson and York, 2012; Kopriva et al., 2015; Takahashi et al., 2011). Inorganic sulfate, found in the diet of metazoans, is metabolized to 3'-phosphoadenosine 5'-phosphosulfate (PAPS) by the bifunctional enzyme phosphoadenosine phosphosulfate synthetase (PAPSS2), which harbors both ATP sulfurylase and adenosine 5'-phophosulfate (APS) kinase activities. PAPS, a high-energy intermediate and sulfate donor, serves as the substrate for several cytosolic sulfotransferases (SULTs) leading to the production of 3'-phosphoadenosine 5'-phosphate (PAP) in the cytosol. Alternatively, PAPS can be translocated into the Golgi lumen via the PAPS transporter and act as a substrate for Golgi-localized sulfotransferases (Kamiyama et al., 2003). In the cytoplasm, bisphosphate 3'-nucleotidase (Bpnt1) uses PAP as a substrate to make 5'-AMP (Spiegelberg et al., 2005; Spiegelberg et al., 1999a); whereas in the Golgi, PAP is converted to 5'-AMP by the Golgi-resident PAP phosphatase (GPAPP) (Frederick et al., 2008). Loss of Gpapp in mice is perinatal-lethal and causes defects in chondroitin sulfation leading to chondrodysplasia (Frederick et al., 2008; Sohaskey et al., 2008). Based on studies of the Gpapp deficient mouse, human patients carrying loss-of-function mutations in GPAPP were identified, leading to characterization of a Mendelian disease recapitulating bone defects observed in mutant mice (Vissers et al., 2011). Conversely, mice lacking BPNT1 develop anasarca, liver failure, and iron deficiency anemia (IDA), which are rescued in Bpnt1 null mice harboring hypomorphic mutations in Papss2 causing decreased PAP metabolic toxicity (Hudson et al., 2013; Hudson et al., 2018). Collectively, these studies

demonstrate essential subcellular-compartment specific roles for 3'-nucleotidases in regulating sulfur assimilation and disease pathophysiology.

We extended our studies of Bpnt1 in mice through generation of an intestinal-epithelium specific mutant (Bpnt1$^{-/int}$) which recapitulated the profound dietary-iron independent IDA but not the other phenotypes observed in the conventional knockout (discussed in Chapter 3) (Hudson et al., 2018). We observed that Bpnt1$^{-/int}$ mice experienced tissue specific metabolic toxicity (elevated PAP levels in the duodenal epithelium) that cause reduced expression of key iron homeostatic genes involved in 1) dietary iron reduction via duodenal cytochrome reductase (Cybrd1), 2) apical iron import through divalent metal transporter 1 (Dmt1), 3) transcriptional coordination of iron regulatory genes by hypoxia inducible factor 2α (Hif-2a), and 4) iron export to the blood via ferroportin (Fpn).

Here we further our mechanistic studies underlying loss of Bpnt1 presenting two approaches to overcome metabolic toxicity resulting from Bpnt11 deficiency. Remarkably, we find that reducing methionine in the diet of mice is sufficient to downregulate metabolic toxicity and completely reverses IDA in Bpnt1$^{-/int}$ mice. Furthermore, capitalizing on the observation that loss of BPNT1 impairs expression of known genetic modifiers of hemochromatosis, the most common genetic form of iron-overload in humans, we identify inhibition of intestinal Bpnt1 as a strategy to overcome hemochromatosis in mice. Our study provides insights into the role of sulfur assimilation metabolism in mediating disorders of iron deficiency and overload in mice.

4.2 Methods

4.2.1 Animals and diets

Bpnt1 floxed mice (Bpnt1$^{-/fl}$) were generated as previously described (Hudson et al., 2018). Hif-2α floxed animals (Hif-2α$^{-/fl}$) were obtained from Jackson laboratories as previously described (Gruber et al., 2007). Animals expressing Cre recombinase under the control of an intestinal-epithelium specific *villin* promoter (B6.SJL-Tg(Vil-cre)997Gum/J) were obtained from Jackson laboratories (Madison et al., 2002). All animals were maintained on standard chow unless specified. Irradiated chow containing a minimal of methionine (5CC7, 0.12% methionine) and control diet (5CC7, 0.6% methionine & 0.4% cysteine) were obtained from TestDiet (Nashville, TN). All animal care and experiments were performed in accordance with the Vanderbilt University Institutional Animal Care and Use Committee.

4.2.2 Enteroid culture

Primary enteroids were established as described previously (Reddy et al., 2016; Sato et al., 2009). Briefly, the first 10 cm of duodenum was removed and thoroughly flushed with ice-cold phosphate-buffered saline without calcium or magnesium (PBS) to remove luminal contents. The duodenum was then splayed open with blunt-tip scissors and sequentially washed with PBS, PBS with 0.04% bleach, and finally with PBS alone. The duodenum was minced, transferred to a fresh tube containing ice-cold PBS, and rocked at 4°C for 15 min. The duodenal fragments were then briefly vortexed, washed twice in fresh PBS and gently inverted to detach villous components. After three washes, the minced duodenum was then incubated in dissociation buffer (2 mM EDTA in PBS) with gentle rocking at 4°C for 30 min. Fragments were then washed twice with fresh PBS without calcium or magnesium and placed in shaking buffer (43.3 mM sucrose and 54.9 mM sorbitol in PBS), followed by gentle shaking to manually disrupt crypts. Once the crypts were isolated, they were embedded in growth factor-reduced Matrigel (Corning, 356231) overlaid with

Mouse IntestiCult media (Stem Cell Technologies, 6005). For initial plating, IntestiCult was supplemented with 1% penicillin-streptomycin and 0.002% primocin. For subsequent passages, enteroids were collected in PBS, gently sheared using a 25-G needle, and plated in fresh growth factor-reduced Matrigel overlaid with Mouse IntestiCult supplemented with 1% penicillin-streptomycin.

Full-length Bpnt1 (*mus musculus*) was cloned into a pFUGW lentiviral mammalian expression vector containing GFP (Addgene plasmid #25870). Mutant Bpnt1 without catalytic activity (D51A) was made using a QuikChange site-directed mutagenesis kit (Agilent). Lentivirus was packaged by transfecting HEK293T cells (ATCC) at 50% confluency in 10 cm plates with 1 μg pMD2.G (Addgene plasmid #12259), 1 μg psPAX2 (Addgene plasmid #12260) vectors, and 2 μg of Bpnt1 or Bpnt1$_{D51A}$ vector and polyethyleneimine (MW 25,000, Polyscience Inc., #23966). Media were changed the following morning. Supernatant containing virus was harvested 48 hours later, filtered through a 0.45 μm filter, and centrifuged overnight at 4°C. Purified HIF-2α-CMV viral particles and empty-viral control were obtained from ABM (LVP479475). Viral pellets were resuspended in 250 μL L-WRN conditioned media (produced from an L-cell line engineered to secrete Wnt3a, R spondin 3, and Noggin) containing 10 μM Rock inhibitor (Y37632) and 8 μg/mL polybrene as described previously (Miyoshi and Stappenbeck, 2013). Freshly harvested crypts from Bpnt1$^{-/fl}$ and Bpnt1$^{-/int}$ mouse duodenum were resuspended in the L-WRN and viral particle solution, incubated for 6 hours, and plated in growth factor-reduced Matrigel overlaid with Intesticult supplemented with 1% penicillin-streptomycin, 0.002% primocin, and 10 μM Rock inhibitor (Y37632). Crypts were allowed to recover (and form enteroids) for 3 days before selection with 2 μg/mL puromycin to ensure positive selection of virally-transduced cells.

Enteroids were then routinely split into media containing 2 μg/mL puromycin to maintain positive selection.

4.2.3 Quantification of PAP/PAPS levels

Quantification of PAP/PAPS was performed as previously described (Hazelton et al., 1985; Hudson et al., 2013; Hudson et al., 2018; Lin and Yang, 1998). Isolated enteroids or intestinal segments were boiled in 5 μL 50 mM glycine (pH 9.2) buffer per mg of tissue and homogenized. Lysates were centrifuged at 16,100 g and 4°C for 20 minutes. The supernatant was then added to 0.2 volumes of chloroform, thoroughly mixed and centrifuged at 16,100 g and 4°C for 20 minutes. The upper aqueous phase was collected. Quantification was performed using a colorimetric absorbance assay where Sult1a1-GST uses PAP/PAPS as a catalytic cofactor to produce 2-naphthol from p-nitrophenyl sulfate. The byproduct of this reaction, 4-nitrophenol, was then observed over time as a marker of reaction velocity. Michaelis-Menten plots of reaction velocity vs. PAP concentration were used to determine the concentration of PAP/PAPS in the sample. PAP/PAPS concentration was then normalized to total protein content determined by a BSA assay.

4.2.4 Immunohistochemistry and electron microscopy

Histopathological analysis was performed on 10% formalin-fixed tissue embedded in paraffin by the Translational Pathology Shared Resource core at Vanderbilt University Medical Center. Thick sections (5 μM) were made and stained for nucleolar-resident fibrillarin (Abcam) and counterstained with DAB according to the manufacturer's suggested protocol. For transmission electron microscopy, cells and tissue fixed in buffer containing 4%

paraformaldehyde, 2.5% glutaraldehyde, 2 mM $CaCl_2$ in 0.1M cacodylate pH 7.4 overnight and post-fixed in 1% tannic acid in 0.1M cacodylate for 1 hour followed by 1% OsO_4 for 1 hour. The samples were stained in 1% uranyl acetate for 30 minutes then dehydration in a graded ethanol series. After dehydration, the samples were infiltrated with a Quetol 651 formulation of Spurr's Resin or Epon-812 using propylene oxide as a transitional solvent and polymerization at 60^oC for 48 hours. Samples were thin sectioned at 70 nm and collected on 300 mesh Copper grids. Imaging was performed on an FEI T-12 transmission electron microscope equipped with a LaB6 filament at 100kv, using a AMT CCD. All electron microscopy experiments were performed using three independent mice and three independent sample preparations.

4.2.5 Enterocyte isolation and quantitative RT-PCR

Enterocytes were isolated as previously described (Hudson et al., 2018). Briefly, proximal duodenum (~ first 10 cm from the pyloric junction) was harvested, dissected open, and washed of luminal contents in ice-cold PBS (without calcium and magnesium) with 1 mM PMSF. The tissue was then placed in dissociation buffer containing 1X PBS (without calcium or magnesium) containing 3 mM EDTA, 1 mM PMSF, and a protease inhibitor cocktail (Roche). Tissues were maintained on a rotating apparatus at 4°C and were manually-disrupted every 10 minutes for 1 hour to slough off enterocytes. Once enterocytes had been digested from the mesenchyme, the remaining tissue was discarded, and enterocytes were pelleted by centrifugation (1000g at 4°C for 5 minutes). Cell pellets were then frozen and remained at -80°C prior to RNA isolation. RNA was extracted using a RNAeasy mini kit (Qiagen) according to manufacturer's instructions. Reverse transcription (RT) was performed using BioRad iScript reverse transcription kit. Quantitative RT-

PCR was performed using SsoFast Evagreen PCR mastermix on a BioRad CFX96 machine. Primer sequences were designed using NCBI Primerblast as previously described (Hudson et al., 2018).

4.2.6 Hematological analysis

Hematological analysis was performed with the assistance of the Translational Pathology Shared Resource core at Vanderbilt University Medical Center. Briefly, mice were sacrificed by excess CO_2 exposure and blood was collected by cardiac puncture. Whole blood was deposited into collection tubes containing EDTA and gently mixed to avoid clot formation. Complete blood counts were performed using an Alfa Wasserman machine. Transferrin saturation was determined using a kit from Alfa Wasserman (ACl-35). Quantification of iron stores was performed as previously described (Hudson et al., 2018).

4.2.7 Statistics

All data are presented as mean ± SEM. Statistical significance was defined at $p< 0.05$ *a priori*. For comparisons of two groups an unpaired two-tailed student's t-test was used. For comparison of more than two groups a two-way ANOVA with Tukey's post-hoc test was used.

4.3 Results

4.3.1 Dietary methionine restriction reverses anemia in BPNT1 deficient mice

Bpnt1 is the mammalian orthologue of *met22*/*hal2*, and was first identified as a methionine auxotroph in budding yeast (Masselot and De Robichon-Szulmajster, 1975a). However, the role of BPNT1 in methionine metabolism *in vivo* is not known. Thus, we hypothesized that dietary reduction of methionine, a major source of dietary sulfate, could modulate iron homeostasis in BPNT1 deficient mice through one of two mechanisms: 1) improve IDA through decreased incorporation of inorganic sulfate through PAPSS2 and reduction of PAP metabolic toxicity or 2) exacerbate IDA due to a lack of substrate for the reverse reaction to make PAPS from PAP, further increasing PAP levels and exacerbate IDA. We placed mice lacking intestinal-epithelium specific Bpnt1 (Bpnt1$^{-/int}$), which develop IDA but none of the other phenotypes observed in the global Bpnt1 knockout mice, and floxed Bpnt1 (Bpnt1$^{-/fl}$) control mice on a methionine-restricted diet (met$_{min}$). After 4 weeks, we assessed duodenal PAP levels and hematological parameters. Bpnt1$^{-/int}$ mice fed met$_{min}$ diet displayed decreased accumulation of PAP in the duodenum (Figure 4.1A) and normalized hematological parameters (Figure 4.1B-F), consistent with our first hypothesis. Thus, reduction of dietary methionine reduces PAP levels, alleviates associated metabolic toxicity and reverses IDA/iron homeostasis in Bpnt1$^{-/int}$ mice. Importantly, these results phenocopy forward-genetic suppression via reduced PAPSS2 function (Hudson et al., 2018), further strengthening a mechanism involving PAP metabolic toxicity. Remarkably, these data provide a simple, iron-independent dietary strategy to overcome IDA caused by loss of Bpnt1 in mice.

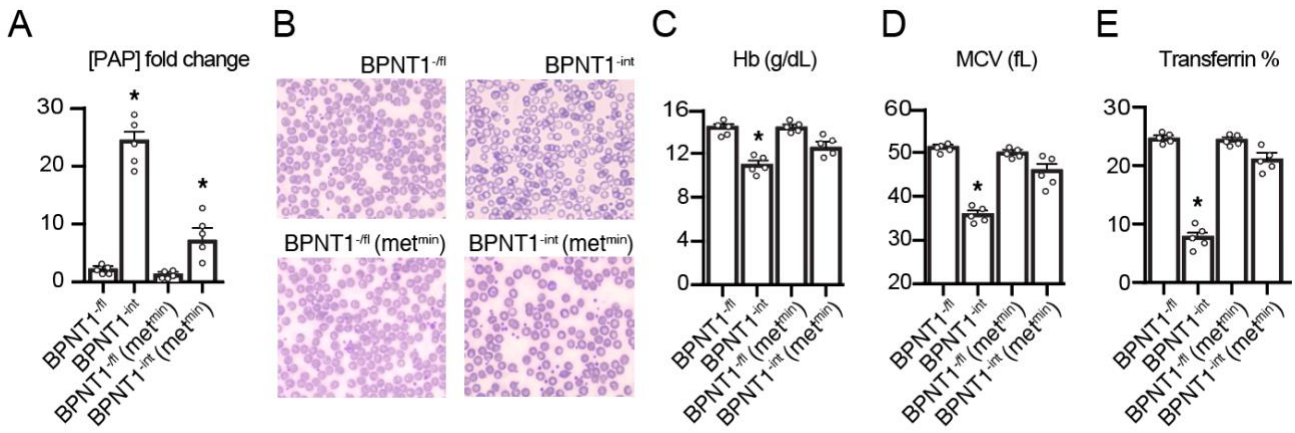

Figure 4.1. Dietary methionine restriction reduces metabolic toxicity and reverses iron deficiency anemia in Bpnt1$^{-/int}$ mice. (A) PAP levels in duodena isolated from Bpnt1$^{-/fl}$ and Bpnt1$^{-/int}$ mice fed standard chow (-/fl and -/int, respectively) or a minimal-methionine chow (met_{min}) for 4 weeks (n= 5). (B) Representative image of Wright-Giemsa stained blood-smear from Bpnt1$^{-/fl}$ fed standard chow (-/fl), Bpnt1$^{-/int}$ fed standard chow (-/int), Bpnt1$^{-/fl}$ fed minimal-methionine chow (-/fl met_{min}), and Bpnt1$^{-/int}$ fed minimal-methionine chow (-/int met_{min}). (C) Hemoglobin (Hb, g/dL), (D) mean corpuscular volume (MCV, fL), and (E) Transferrin saturation (transferrin %) (n= 5). *Represents $p < 0.05$ by two-way ANOVA with Tukey's post-hoc test. Data are represented as mean ± SEM.

4.3.2 Catalytic activity of BPNT1 regulates iron import, sensing, and export

To gain mechanistic insights into the role of intestinal BPNT1 in iron regulation, we established a primary mouse duodenal organoid (enteroid) culture system (Leushacke and Barker, 2014). Importantly, enteroids derived from Bpnt1$^{-/int}$ mice display elevated levels of PAP substrate (Figure 4.2A-B) and altered nuclear architecture, characterized by nucleolar condensation/enlargement and loss of heterochromatin as determined by immunohistochemical staining for nucleolar-resident fibrillarin and electron microscopy, respectively (Figure 4.2C-D). Importantly, these data recapitulate both metabolic and histological observations due to PAP accumulation *in vivo* (Hudson et al., 2013; Hudson et al., 2018; Hudson and York, 2014). Our prior studies demonstrated that reduction of PAP synthesis through introduction of a hypomorphic

mutation in PAPS synthase (Papss2) could suppress IDA and other phenotypes caused by a loss of BPNT1 (Hudson et al., 2013; Hudson et al., 2018). These data strongly suggested, but did not prove, that loss of BPNT1 catalytic activity, which normally converts PAP to 5'-AMP, is responsible for IDA in the BPNT1 deficient animal. To further these studies, we used lentiviral-mediated gene transfer to introduce a catalytic-dead BPNT1 mutant ($Bpnt1^{D51A}$) into enteroids isolated from $Bpnt1^{-/int}$ or Bpnt1 floxed ($Bpnt1^{-/fl}$) control mice. We then measured mRNA expression of key iron homeostatic genes: Cybrd1, Dmt1, Hif-2α, and Fpn by quantitative real-time polymerase chain reaction (qRT-PCR) (Figure 4.2E). While expression of Cybrd1, Dmt1, Hif-2α, and Fpn was repressed in $Bpnt1^{-/int}$ enteroids and $Bpnt1^{-/int}$ enteroids complemented with catalytic-dead BPNT1 (-/int + $Bpnt1^{D51A}$), $Bpnt1^{-/int}$ enteroids complemented with wild-type Bpnt1 (-/int + $Bpnt1^{WT}$) displayed normalized iron regulatory gene expression (Figure 4.2E). These data demonstrate that catalytic activity of BPNT1 is required for iron homeostatic gene expression.

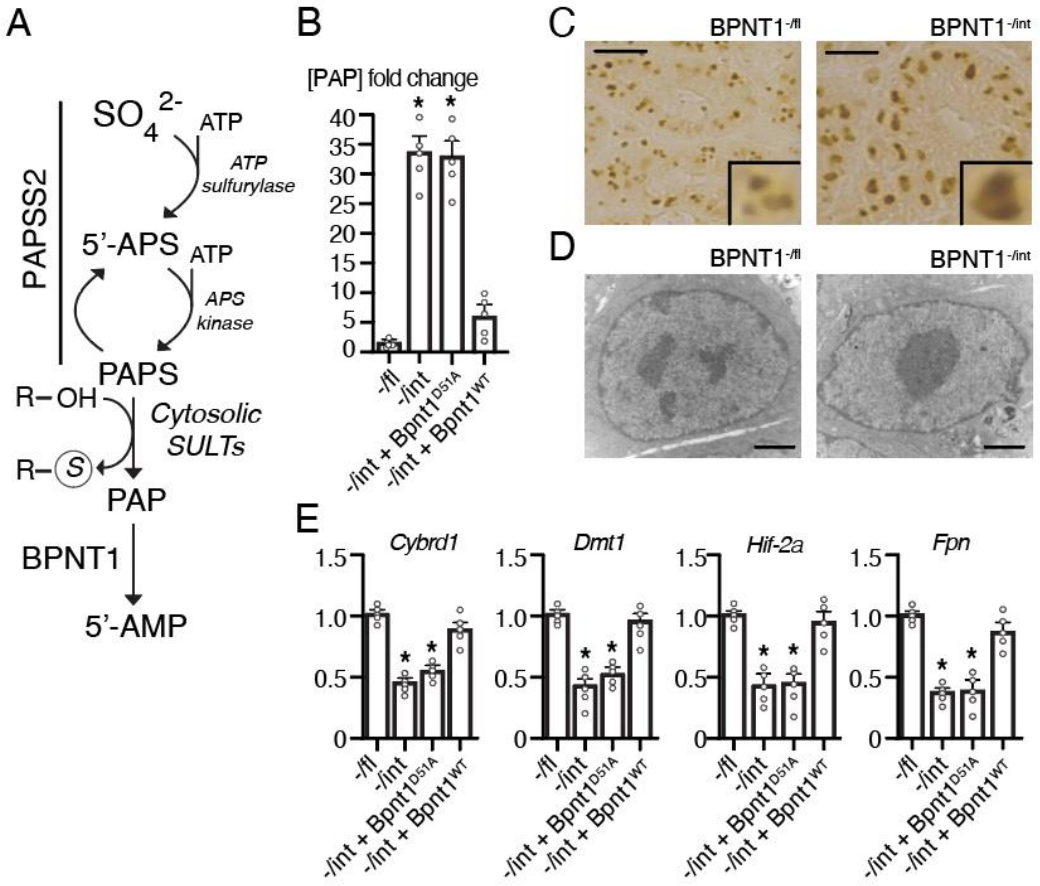

Figure 4.2. Primary enteroids recapitulate cellular phenotypes associated with PAP toxicity and Bpnt1 catalytic activity is required for iron homeostatic gene expression. (A) Abbreviated components of the evolutionarily-conserved cytosolic sulfur assimilation pathway. Inorganic sulfate (SO_4^{2-}) obtained from the diet or turnover of amino acids is incorporated by the action of the bifunctional enzyme 3'-phosphoadenosine 5-phosphosulfate synthase 2 (Papss2), a bifunctional enzyme, which acts as an ATP sulfurylase to generate adenosine 5'-phosphosulfate (5'-APS) and as an 5'-APS kinase to generate 3'-phosphoadenosine 5'-phosphosulfate (PAPS). A number of cytosolic sulfotransferases (SULTs) use PAPS as a sulfur-donor to sulfate target proteins, generating 3'-phosphoadenosine 5'-phosphate (PAP). Bisphosphate 3'-nucleotidase (Bpnt1) then catalyzes the terminal step of cytosolic sulfur assimilation to produce adenosine 5'-phosphate (5'-AMP) using PAP as a substrate. (B) Quantification of PAP levels in Bpnt1$^{-/fl}$ floxed control (-/fl), villin-cre driven knockout of Bpnt1 (-/int) and -/int duodenal enteroids (n=5). *Represents $p < 0.05$ by two-tailed student's t-test. (C) Representative image of nucleolar-resident fibrillarin staining demonstrating in Bpnt1^{-fl} (left) and Bpnt1$^{-/int}$ (right) enteroids. Scale bar represents 10 μm. Inset is representative enteroid. (D) Representative transmission electron microscopy image in Bpnt1$^{-/fl}$ and Bpnt1$^{-/int}$ enteroids taken at 11,000x magnification. Scale bar represents 2 microns. (E) qRT-PCR of Cybrd1, Dmt1, Hif-2α, or Fpn relative to β-actin from complemented enteroid lines (n=5) described in (B). *Represents $p < 0.05$ by two-way ANOVA with Tukey's post-hoc test. Data are represented as mean ± SEM.

4.3.3 Restoration of Hif-2α suppresses loss of Bpnt1 through normalization of iron homeostatic gene expression

Our prior studies and others indicated that PAP-mediated metabolic toxicity may act broadly to cause IDA in Bpnt1 null mice for the following reasons: 1) PAP has been shown to directly interact or modulate a number of targets (Dichtl et al., 1997a; Schneider et al., 1998), 2) BPNT1 deficient mice accumulate PAP to near-equivalent levels of ADP (Hudson et al., 2013), and 3) Bpnt1$^{-/int}$ enterocytes display broad changes in gene expression, with ~25% of the transcriptome differentially expressed more than three-fold (Hudson et al., 2018). Intriguingly, Bpnt1$^{-/int}$ duodena display abnormal nucleolar condensation/enlargement consistent with previous studies, but also display markedly decreased heterochromatin (Figure 4.3), consistent with massive transcriptional changes observed in Bpnt1$^{-/int}$ enterocytes (Hudson et al., 2018), through PAP-dependent metabolic toxicity.

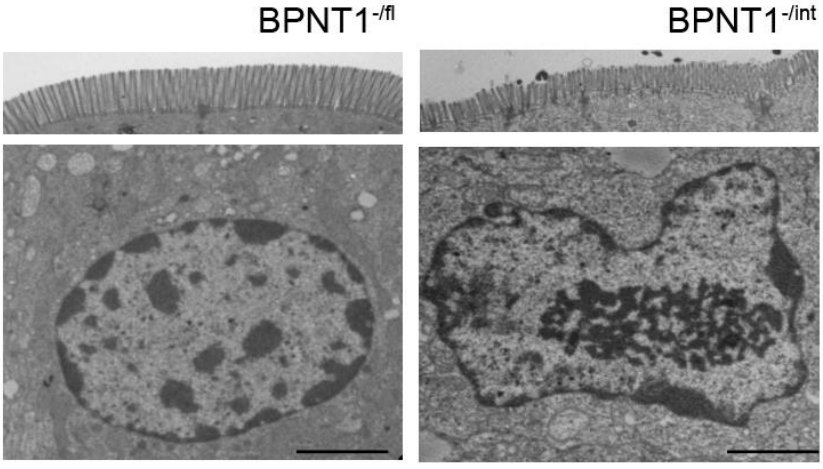

Figure 4.3. Bpnt1$^{-/int}$ mice display decreased heterochromatin, abnormal brush border architecture, and nucleolar condensation. Representative transmission electron micrograph of brush border (top) and enterocyte (bottom) from duodena isolated from Bpnt1$^{-/fl}$ (-/fl) and Bpnt1$^{-/int}$ (-/int) mice. Scale bars represent 2 μm. 3,200x magnification. All experiments were performed in triplicate.

While many genes were differentially expressed in Bpnt1$^{-/int}$ enterocytes, our analyses indicate that decreased Hif-2α transcription is a major contributing factor to IDA in Bpnt1$^{-/int}$ mice for the following reasons: 1) a statistically-significant reduction in Hif-2a expression in Bpnt1$^{-/int}$ enterocytes after a highly conservative Bonferroni correction for the total number of sequenced poly-A selected transcripts (Hudson et al., 2018), 2) decreased HIF-2α protein accumulation and no change in HIF-2α subcellular localization in Bpnt1$^{-/int}$ duodena (Hudson et al., 2018), 3) gene set enrichment analysis (GSEA) identified HIF-2α dependent transcription as the most significantly-enriched pathway in Bpnt1$^{-/int}$ enterocytes (Hudson et al., 2018), 4) an overlap of transcriptional signatures in enterocytes isolated from intestinal epithelium-specific Hif-2α knockout (Hif-2α$^{-/int}$) (Taylor et al., 2011a) and Bpnt1$^{-/int}$ mice including decreased Dmt1, Cybrd1, and Fpn expression, and 5) Hif-2α$^{-/int}$ mice phenocopy IDA in Bpnt1$^{-/int}$ mice (Gruber et al., 2007). Thus, we reasoned that over-expression of Hif-2α may represent a genetic strategy to suppress loss of BPNT1 through restoration of iron homeostatic gene expression.

To test this hypothesis, we virally over-expressed Hif-2α or an empty vector (EV) control in Bpnt1$^{-/fl}$ and Bpnt1$^{-/int}$ enteroids, and after positive selection of stably transduced enteroids, measured Dmt1 mRNA transcript levels by qRT-PCR. We observed Hif-2α overexpression elevated Dmt1 expression in Bpnt1$^{-/fl}$ enteroids and normalized Dmt1 expression in Bpnt1$^{-/int}$ enteroids (Figure 4.4A). Since apical iron import must be matched with basolateral iron efflux through ferroportin (FPN), otherwise iron would accumulate intracellularly, and Fpn is a direct transcriptional target of HIF-2α (Taylor et al., 2011a), we speculated whether Fpn levels would be similarly restored with overexpression of Hif-2α. Indeed, overexpression of Hif-2α in Bpnt1$^{-/fl}$ enteroids normalized Fpn expression (Figure 4.4A). Likewise, we observe restored levels of

Cybrd1 in Bpnt1$^{-/int}$ enteroids complemented with Hif-2α, although Cybrd1 appears to be dispensable for iron absorption (Gunshin et al., 2005b). While iron homeostatic genes were normalized with overexpression of Hif-2α, we did not see appreciable restoration of nucleolar condensation/enlargement, as assessed by immunohistochemical analysis of nucleolar-resident protein fibrillarin and electron microscopy (Figure 4.5A-B). Collectively, our data present an intriguing genetic approach to attenuate the iron homeostatic consequences of metabolic toxicity caused by loss of BPNT1 in mice.

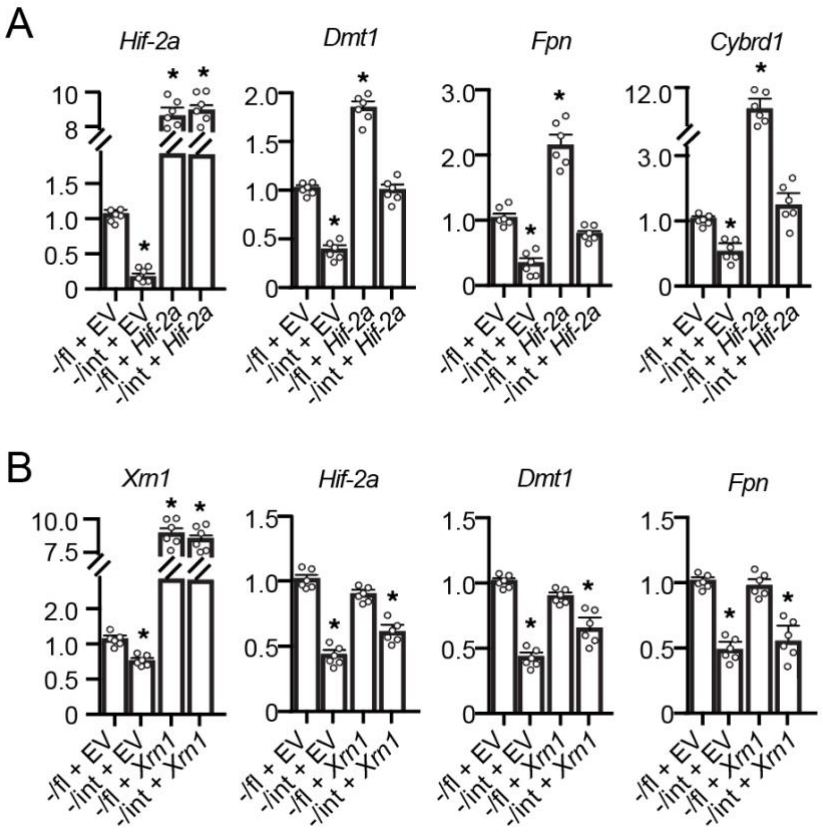

Figure 4.4. Restoration of Hif-2α, but not Xrn1, normalizes iron-regulatory gene expression perturbations in Bpnt1$^{-/int}$ enteroids. qRT-PCR of Hif-2α, Dmt1, Fpn, and Cybrd1 from enteroids isolated from Bpnt1$^{-/fl}$ (-/fl) or Bpnt1$^{-/int}$ (-/int) mice and infected with empty vector (EV) control or a lentivirus expressing mouse Hif-2α (A) or mouse Xrn1 (B). *Represents $p < 0.05$ by two-way ANOVA with Tukey's post-hoc test. Data are represented as mean ± SEM.

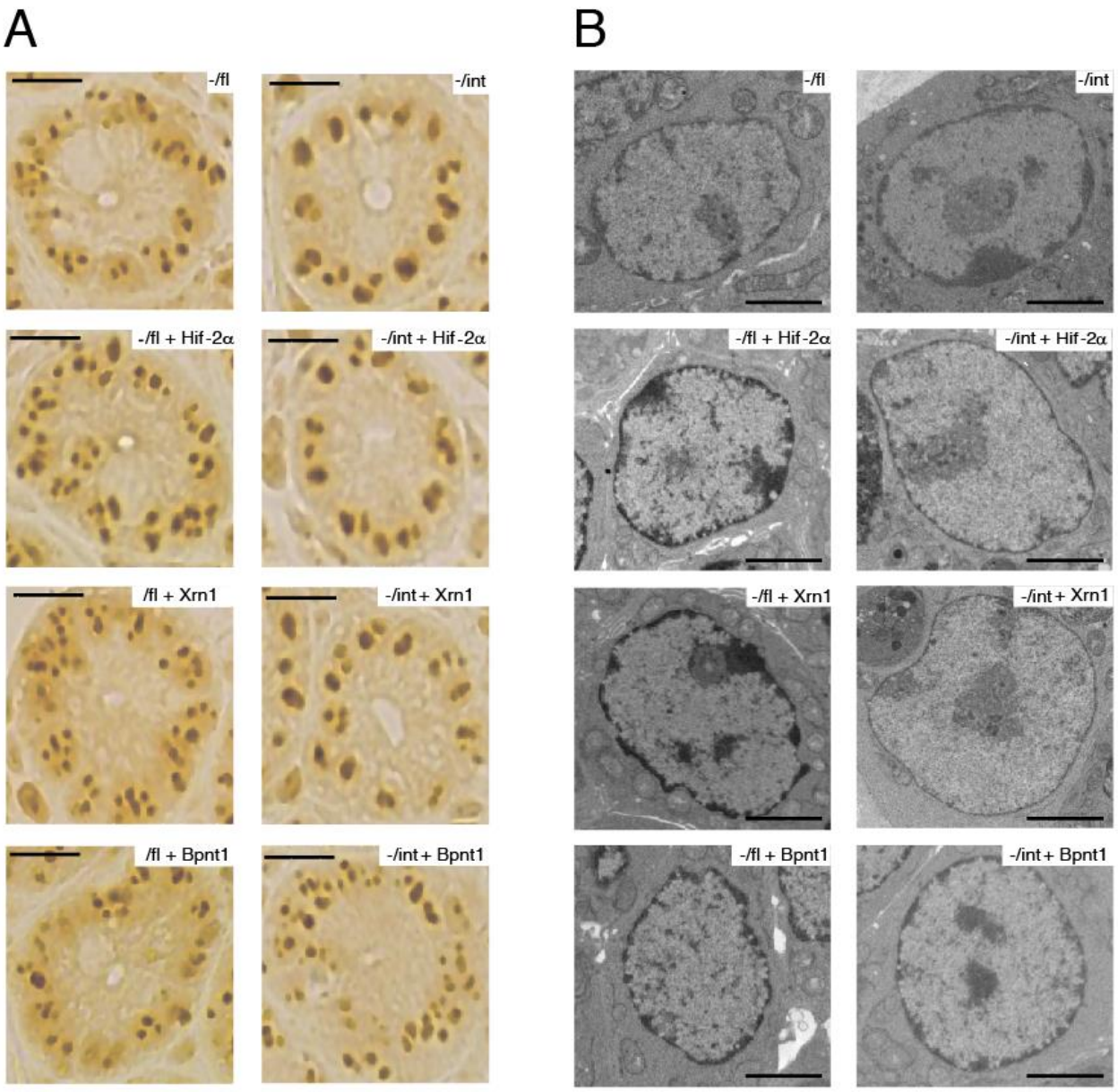

Figure 4.5. Restoration of Hif-2α or Xrn1 does not ameliorate nucleolar condensation or chromatin defects in Bpnt1$^{-/int}$ enteroids. (A) Representative images of fibrillarin-stained enteroids as described in (A-B). Scale bar represents 10 μm. (B) Representative transmission electron microscopy images of -/fl and -/int enteroids complemented with Hif-2α Xrn1 or Bpnt1 taken at 4,400x magnification. Scale bar represents 2 μm. All experiments were performed in triplicate.

Of interest, prior studies in budding yeast identified 5'-3' exoribonuclease 1 (Xrn1), an inhibitor of ribosomal RNA (rRNA) processing, as a mediator of PAP toxicity due to loss of *met22*, the yeast orthologue of Bpnt1 (Dichtl et al., 1997a). Indeed, BPNT1 deficient hepatocytes display elevation of unprocessed rRNA (5.8S "long") consistent with inhibition of XRN1 activity (Hudson et al., 2013). Thus, we postulated that overexpression of Xrn1 in Bpnt1$^{-/int}$ enteroids may modulate effects of PAP toxicity and restore iron homeostatic gene expression. We therefore virally overexpressed Xrn1 in Bpnt1$^{-/int}$ and Bpnt1$^{-/fl}$ control enteroids. We observed a partial restoration of Dmt1, Hif-2α, and Fpn expression in Bpnt1$^{-/int}$ enteroids complemented with Xrn1 (Figure 4.4B). However, nucleolar condensation/enlargement was not appreciably reversed by over-expression of Xrn1 in enteroids from Bpnt1$^{-/int}$ animals (Figure 4.5A-B). Together, our overexpression studies are consistent with both Hif-2α-dependent and -independent mechanisms that lead to iron-regulatory gene expression changes in Bpnt1$^{-/int}$ enteroids.

4.3.4 Hif-2α is epistatic to Bpnt1 in the intestinal epithelium

Since Bpnt1$^{-/int}$ and Hif-2α$^{-/int}$ mice both develop IDA and overexpression of Hif-2α in Bpnt1$^{-/int}$ enteroids restored iron homeostatic gene expression (Figure 4.4A), we aimed to interrogate the genetic interaction between Bpnt1 and Hif-2α *in vivo*. We hypothesized that if Bpnt1 and Hif-2α led to anemia via a shared pathway, then mice lacking both Hif-2α and Bpnt1 would display a similar degree of anemia compared to loss of either gene alone. Conversely, if Bpnt1$^{-/int}$ mice develop IDA independent of Hif-2α deletion of both Bpnt1 and Hif-2α would be expected to exacerbate IDA compared to deletion of either gene alone. Therefore, we generated intestine-specific Bpnt1-Hif-2α double knockout animals (Bpnt1-Hif-2α$^{-/int}$). Indeed, Bpnt1-Hif-

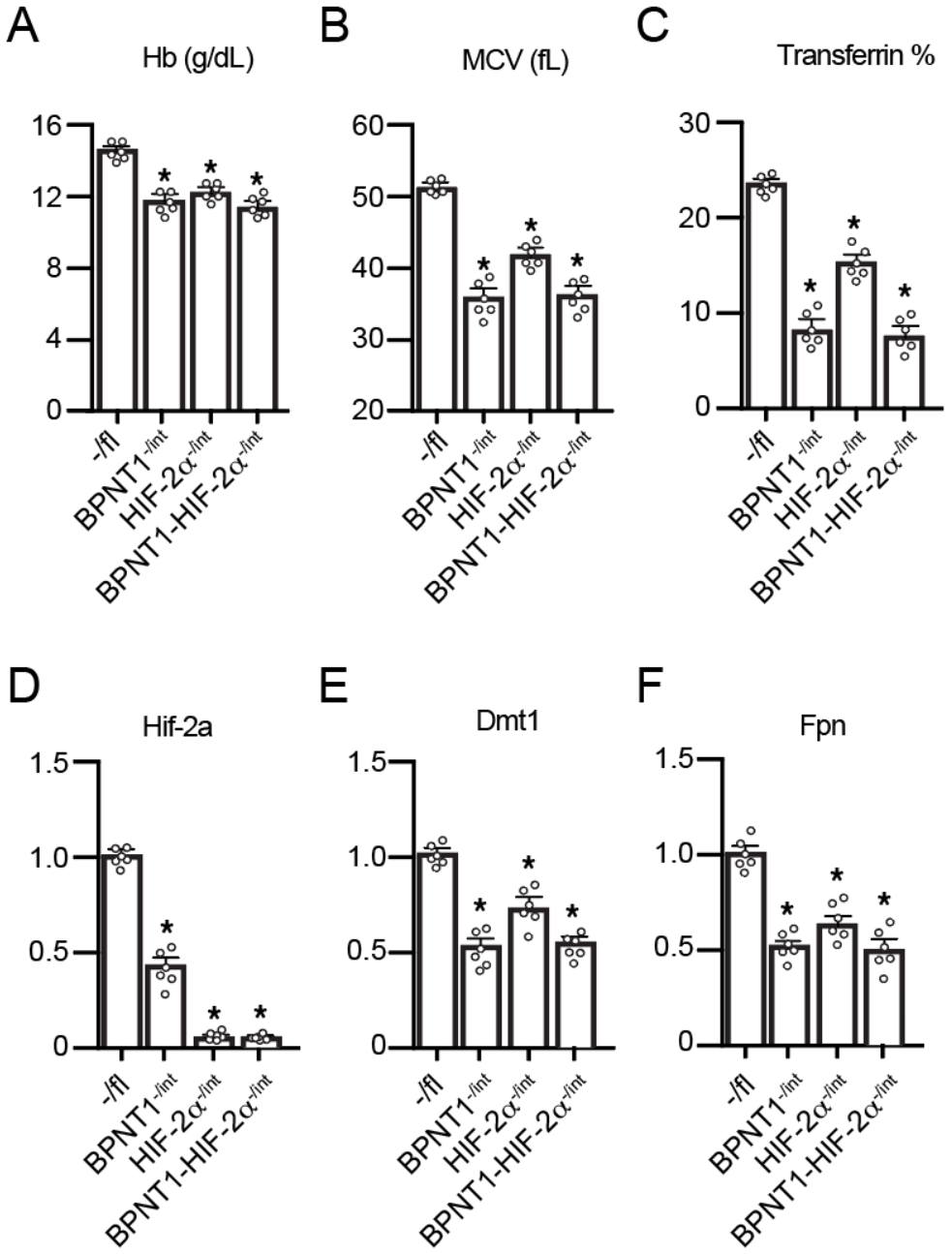

Figure 4.6. Bpnt1 is epistatic to Hif-2α in the intestine. We generated Bpnt1 floxed control mice (-/fl), intestine-specific Bpnt1 knockout mice (Bpnt1$_{-/int}$), intestine-specific HIF-2α knockout mice (HIF-2α$_{-/int}$), and mice lacking both intestine-specific Bpnt1 and HIF-2α (Bpnt1-HIF-2α$_{-/int}$) and measured hemoglobin (Hb, g/dL) (A), mean corpuscular volume (MCV, fL) (B), and transferrin saturation (transferrin %) (C) in 12-16 week mice (n=6 mice per group). qRT-PCR of *Hif-2α* (D), *Dmt1* (E), and *Fpn* (F) in enterocytes (n=6) isolated from mice as described above. *Represents $p < 0.05$ by two-way ANOVA with Tukey's post-hoc test. Data are represented as mean ± SEM.

2α$^{-/int}$ mice display nearly identical hematological parameters (hemoglobin, mean corpuscular volume, and transferrin saturation) compared to Bpnt1$^{-/int}$ mice (Figure 4.6A-C). In addition, transcriptional targets of Hif-2α, Dmt1 and Fpn, were equally repressed in enterocytes isolated from Bpnt1$^{-/int}$ and Bpnt1-Hif-2α$^{-/int}$ mice (Figure 4.6D-F). However, it should be noted that the degree of anemia in Bpnt1$^{-/int}$ mice was more severe than in Hif-2α$^{-/int}$ mice (Figure 4.6A-C). These data suggest that Hif-2α is epistatic to Bpnt1 in the intestine; however, these data also support the conclusion that Hif-2α-independent mechanisms also contribute to IDA in Bpnt1$^{-/int}$ mice.

4.3.5 Intestinal-epithelium specific loss of Bpnt1 attenuates hepatic iron-overload in Hfe^{C282Y} mice

The current treatment for hemochromatosis is phlebotomy, which is effective in many cases, but a targeted pharmacological approach to treat hemochromatosis would reduce morbidity and improve quality of life (Powell et al., 2016). Intriguingly, pharmacological inhibition of HIF-2α has been shown to abrogate exogenous iron-overload in mice (Schwartz et al., 2019). Furthermore, DMT1 function mitigates iron-overload in mice with homozygous C282Y mutations in homeostatic iron regulator (Hfe^{C282Y}) (Levy et al., 2000), the most common genetic cause of hemochromatosis in humans.

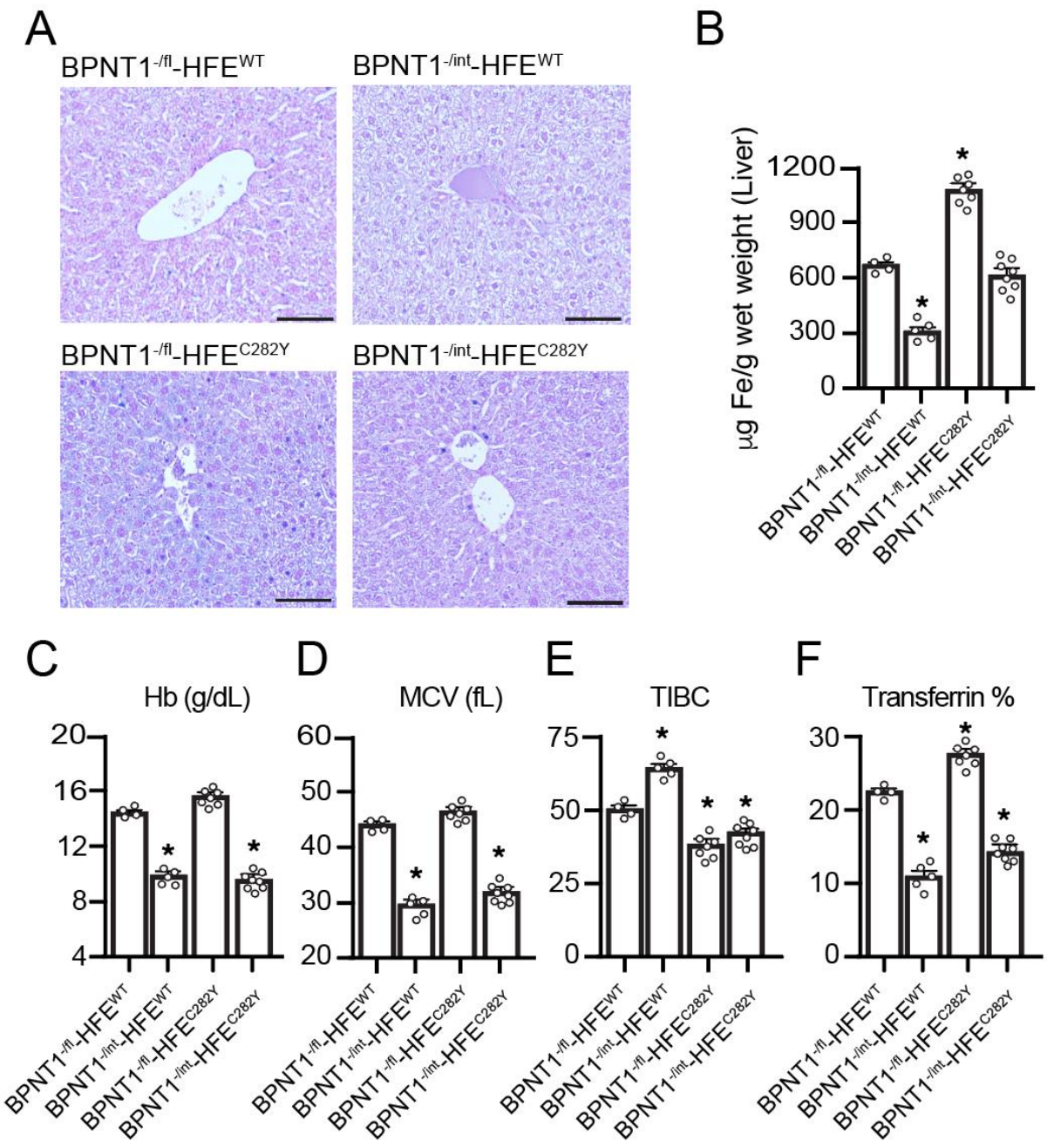

Figure 4.7. Intestinal-specific deletion of Bpnt1 attenuates hepatic iron-overload in Hfe^{C282Y} homozygous mice. (A) Representative Prussian-blue staining from livers isolated from Bpnt1$^{-/fl}$, Bpnt1$^{-/int}$, Hfe^{C282Y}, and Hfe^{C282Y}- Bpnt1$^{-/int}$ mice. (B) Hepatic iron quantification from mice fed normal-chow diet as described in (A). (C) Hemoglobin (Hb, g/dL), (D) mean corpuscular volume (MCV, fL), (E) Total iron binding capacity (TIBC), and (F) percentage transferrin saturation (n=4-8 animals per group). *Represents $p < 0.05$ by two-way ANOVA with Tukey's post-hoc test. Data are represented as mean ± SEM.

Since Bpnt1$^{-/int}$ mice display impaired Dmt1 and Hif-2α expression, we hypothesized that loss of Bpnt1 may be protective against iron-overload. Thus, we crossed intestinal-epithelium specific, Bpnt1 floxed (Bpnt1$^{-/fl}$) mice with global Hfe^{C282Y} mice to obtain Bpnt1$^{-/int}$-Hfe^{C282Y} experimental animals. Analysis of hepatic iron levels revealed a ~50% reduction in hepatic iron stores in Bpnt1$^{-/int}$ mice, whereas Hfe^{C282Y} mice displayed ~2-fold elevation in hepatic iron (Figure 4.7A-B). Remarkably, Bpnt1$^{-/int}$-Hfe^{C282Y} mice displayed normalized hepatic-iron content, but display decreased hemoglobin, mean corpuscular volume, total iron binding capacity, and transferrin saturation compared to control animals (Figure 4.7A-F). Overall, these data suggest that inhibition of intestinal Bpnt1 may be an attractive strategy to treat hemochromatosis.

4.4 Discussion

Our results suggest two orthogonal approaches to overcome metabolic toxicity caused by loss of Bpnt1 and identifies BPNT1 as a potential target for the treatment of hemochromatosis. We demonstrate that a diet containing a minimal amount of methionine can reduce metabolic toxicity and reverse IDA in Bpnt1$^{-/int}$ mice. In addition, we delineate a genetic strategy via overexpression of Hif-2α to overcome metabolic toxicity through restoration of iron homeostatic gene expression in Bpnt1$^{-/int}$ mouse enteroids. Mechanistically, we demonstrate that BPNT1 catalytic activity is required for iron homeostatic gene expression in Bpnt1$^{-/int}$ mouse enteroids. Finally, we demonstrate that loss of intestinal Bpnt1 can suppress hepatic iron overload caused by Hfe^{C282Y}, the most common mutation associated with hemochromatosis in humans. Our study outlines strategies to overcome intestinal metabolic toxicity and identifies an unexpected genetic mechanism to block iron accumulation due to Hfe^{C282Y}.

Although the yeast orthologue of Bpnt1 (*met22/hal2*) was first identified through a screen of methionine auxotrophy (Masselot and De Robichon-Szulmajster, 1975a), the role of Bpnt1 in response to augmentation of dietary methionine in metazoans has not been described. The predominant source of inorganic sulfate in mammals is the breakdown and turnover of sulfur-containing amino acid methionine. Diets containing excess methionine have been shown to cause atherosclerosis in genetically-predisposed mice secondary to hyperproduction of homocysteine (Troen et al., 2003); whereas mice fed a minimal methionine diet are protected from obesity/insulin-resistance but display decreased bone density (Ables et al., 2012). Here, we show that methionine restriction attenuates PAP metabolic toxicity and reverses anemia due to loss of Bpnt1 analogous to introduction of a hypomorphic mutation in Papss2 (Hudson et al., 2013; Hudson et al., 2018). These data illuminate a dietary strategy to overcome pathophysiology caused by loss of Bpnt1 and a mechanism to treat heretofore unidentified patients carrying loss of function mutations in Bpnt1.

Given that ~25% of the transcriptome was differentially-expressed greater than three-fold in Bpnt1$^{-/int}$ enterocytes (Hudson et al., 2018) and Bpnt1$^{-/int}$ display decreased heterochromatin, it is clear that PAP accumulation regulates transcription and chromatin organization. There are several mechanisms by which PAP accumulation may regulate these processes: 1) alteration of nucleosome positioning, 2) impaired interactions between histones and DNA, 3) disruption of nucleosome assembly/disassembly, or 4) block histone deacetylase or acetylase interactions with the histone core, among many other potential mechanisms. Since PAP accumulates to near-equivalent levels of ADP in Bpnt1 null tissue (Hudson et al., 2013), PAP metabolic toxicity may impair multiple processes required for normal cellular function. Since different tissues utilize sulfur assimilation to varying degrees and PAP is elevated (but to a variable degree) only in select

tissues, despite loss of Bpnt1 protein (Hudson and York, 2012, 2014), there are likely tissue-specific molecular consequences of PAP accumulation. Consistent with these data, Bpnt1 null hepatocytes display defects in ribosome biogenesis and develop anasarca due to impaired albumin protein production (Hudson et al., 2013), whereas Bpnt1$^{-/int}$ do not display features associated with gross alterations in protein production (i.e. intestinal barrier breakdown, diarrhea, weight loss, etc.). Given that PAP accumulates ~200-fold in liver vs. ~40-fold in the intestinal-epithelium, these data suggest that PAP may regulate a diverse set of biological targets dependent on tissue type and degree of metabolic toxicity.

PAP accumulation causes abnormal condensation of the nucleolus, the site of rRNA synthesis (Hudson et al., 2013; Hudson et al., 2018; Hudson and York, 2014). Prior analysis of Bpnt1-deficient liver tissue revealed a selective accumulation of unprocessed rRNA species 5.8S "long" and defects in ribosome biogenesis (Hudson et al., 2013). However, restoration of Xrn1 in Bpnt1$^{-/int}$ enteroids did not alter iron-regulatory gene expression changes or reverse nucleolar architecture. These data disfavor, but do not rule out, XRN1-mediated mechanisms contributing to iron homeostatic gene expression or nucleolar condensation in Bpnt1$^{-/int}$ mice. While restoration of Hif-2α normalized Dmt1 and Fpn expression, these effects were independent of nucleolar condensation, as nucleolar-resident fibrillarin staining of Bpnt1$^{-/int}$ enteroids complemented with Hif-2α were indistinguishable from Bpnt1$^{-/int}$ enteroids complemented with empty-vector control. Thus, functional restoration of iron transporter genes would appear to restore iron homeostasis independent of persistent nucleolar condensation.

Interestingly, enterocytes isolated from Bpnt1$^{-/int}$ mice displayed blunted production of Dmt1 and Fpn expression (Hudson et al., 2018), similar to HIF-2α deficient mice (Mastrogiannaki et al., 2009; Shah et al., 2009). Thus, we hypothesized that gain of HIF-2α function could

overcome Dmt1 and Fpn repression, since HIF-2α is a direct transcriptional regulator of both genes (Taylor et al., 2011a). However, if Dmt1 and Fpn repression in Bpnt1$^{-/int}$ was independent of HIF-2α, at least in part, then HIF-2α gain of function would not alter Dmt1 or Fpn levels. Indeed, we find that restoration of HIF-2α normalizes Dmt1 and Fpn expression compared to enteroids isolated from Bpnt1$^{-/fl}$ mice. However, alterations in Hif-2α function in Bpnt1$^{-/int}$ mice may occur pre- or post- transcription or translation (or both) via a direct or indirect mechanism.

Targeting Bpnt1 for the treatment of hemochromatosis may have several advantages over pharmacological inhibition of DMT1 or HIF-2α. Blocking apical iron import through DMT1 may reduce iron absorption, but also inhibit uptake of other divalent metals (Picard et al., 2000). While loss of Bpnt1 impairs DMT1 expression and response to iron deficiency (Hudson et al., 2018), Bpnt1 mutant mice do not display any signs of divalent metal deficiency (seizures, muscle spasms, pernicious anemia etc.) at any age. Furthermore, while nearly ~90% of mice harboring loss of function mutations in Dmt1 die before weaning (Russell et al., 1970), Bpnt1$^{-/int}$ mice display normal lifespan and age-appropriate weight gain (Hudson et al., 2018). Furthermore, while HIF-2α inhibitors have been developed, they present many challenges due to HIF-2α's complex post-translational regulatory mechanisms, interaction with transcriptional coactivators, and nuclear localization (Wigerup et al., 2016). Conversely, loss of BPNT1 impairs Hif-2α mRNA and protein levels (Fig. 2A and (Hudson et al., 2018)), achieving the functional benefits of direct pharmacological inhibition. Our data suggests that inhibition of BPNT1 catalytic activity, leading to select PAP metabolic accumulation in the intestine, may be beneficial for the treatment of hemochromatosis.

Our study reveals an unexpected genetic mechanism, via loss of Bpnt1 in the intestinal-epithelium, to attenuate hepatic iron accumulation in mice harboring biallelic Hfe^{C282Y} mutations, the most common genetic cause of hemochromatosis in humans. These data suggest that inhibition of intestinal Bpnt1 may represent a pharmacologic approach to treat hemochromatosis and other disorders of iron overload. Furthermore, based on the unique phenotype of Bpnt1 deficient mice (severe IDA, anasarca, and liver failure), targeted sequencing of Bpnt1 may be warranted in patients with unknown causes of this unique combination of phenotypes. Should patients with homozygous loss of function mutations Bpnt1 be identified, our studies provide a simple dietary modification to reverse metabolic toxicity and reverse disease pathophysiology. In addition, as BPNT1 is inhibited at therapeutic levels of lithium and mediates lithium-induced toxicity in a variety of organisms (Meisel and Kim, 2016; Spiegelberg et al., 2005; Spiegelberg et al., 1999a), these data represent potential strategies to overcome side effects associated with lithium therapy that may be caused by PAP accumulation.

Chapter 5 Identification of targets of PAP metabolic toxicity

5.1 Introduction

Sulfur assimilation is the evolutionary-conserved pathway of incorporating inorganic sulfate into sulfur-containing amino acids and sulfated end-products (Hudson and York, 2012; Kopriva et al., 2015; Takahashi et al., 2011; Taylor et al., 2011a). The first step of sulfur assimilation is incorporation of inorganic sulfate via the bifunctional enzyme 3'-phosphoadenosine 5'-phosphosulfate synthase 2 (Papss2) to produce 3'-phosphoadenosine 5'-phosphosulfate (PAPS), a high-energy sulfate donor. PAPS can serve as a substrate for cytoplasmic-localized sulfotransferases to produce 3'-phosphoadenosine 5'-phosphate (PAP) or be transported to the Golgi-lumen via the PAPS transporter (Kamiyama et al., 2003). In the cytosol, PAP is hydrolyzed to 5'-AMP by bisphosphate 3'-nucleotidase 1 (Bpnt1), whereas Golgi-localized PAP phosphatase (gPAPP) performs the same enzymatic reaction in the Golgi-lumen. Mice lacking Bpnt1 develop iron-deficiency anemia (IDA) (Hudson et al., 2018), anasarca, and liver failure (Hudson et al., 2013). In contrast, loss of gPAPP in mice is perinatal lethal and mutant mice display impaired chondroitin sulfation that underlies defects in long-bone formation (Frederick et al., 2008), which is phenocopied in human patients with chondrodysplasia carrying biallelic loss of function mutations in gPAPP (Vissers et al., 2011). These data highlight cell-compartment specific roles for 3'-nucleotidases in mammalian physiology.

Our laboratory previously reported that mice lacking Bpnt1 in the intestinal-epithelium (Bpnt1$^{-/int}$) develop iron deficiency anemia (IDA), but none of the other phenotypes observed in the global Bpnt1 knockout animal (Hudson et al., 2018). Loss of Bpnt1 causes ~40-fold elevation

of PAP substrate, and loss of Bpnt1 can be overcome with genetic suppression of PAP synthesis through introduction of a hypomorphic mutation in Papss2 (Hudson et al., 2018). Furthermore, consistent with a mechanism by which PAP metabolic toxicity underlies loss of Bpnt1, we demonstrated that catalytic activity of Bpnt1 is required for iron homeostatic gene expression (Chapter 4). These results strongly suggest that accumulation of PAP, rather than defects in sulfation, cause the phenotypes observed in the Bpnt1 mutant mouse. While PAP has been shown to modulate and/or interact with a diverse set of targets including those regulating nucleoside metabolism (Schneider et al., 1998), rRNA processing (Dichtl et al., 1997a), and sulfation (Lee et al., 2003), among others, it is unclear whether or these factors (or others) are directly mediating the phenotypic consequences of PAP toxicity. Here we use biochemical and molecular approaches to identify targets of PAP metabolic toxicity in enterocytes.

5.2 Methods

5.2.1 PAP agarose affinity chromatography

We used affinity-chromatography (i.e. PAP directly conjugated to agarose beads (Spiegelberg et al., 1999a)) to identify PAP-binding proteins in enterocytes isolated from Bpnt1$^{-/fl}$ and Bpnt1$^{-/int}$ mice. Generation of these mice was described previously (Hudson et al., 2018). Briefly, PAP conjugated to agarose beads (PAP-agarose, Sigma-Aldrich A3640) was swelled in buffer containing 50 mM HEPES (pH= 7.5), 10 mM $CaCl_2$, and 50 mM KCl (PAP-agarose buffer). Enterocytes were isolated as previously described (Hudson et al., 2018) and lysed in PAP-agarose buffer containing 2 mM PMSF by brief sonication. The supernatant was then applied to PAP-agarose, gently resuspended, and rotated at 4°C for 1 hour. Purified Bpnt1 was used as a positive

control. The PAP agarose column was then thoroughly washed in PAP-agarose buffer containing 500 mM NaCl. PAP-binding proteins were then competitively-eluted with 500 μM PAP (Sigma Aldrich A5763). Eluents were then analyzed by SDS page (followed by silver staining or Coomassie blue) or shotgun mass-spectrometry to identify putative PAP-binding proteins.

5.2.2 Histone isolation & post-translational modification analysis

Histone isolation was performed using a commercially available kit (Abcam, ab113476). Eighteen histone H3 post-translational modifications (PTMs) were determined using an ELISA-based kit (Abcam, ab185910). Histone H3 PTM levels were normalized to total H3 protein.

5.3 Results

5.3.1 PAP affinity chromatography identifies PAP binding proteins

Deletion of Bpnt1 in mice causes ~40-200 fold elevation of PAP in select tissues, and PAP metabolic toxicity and disease phenotypes caused by loss of Bpnt1 can be overcome with concomitant downregulation of PAP synthesis through introduction of a hypomorphic mutation in Papss2 (Hudson et al., 2013; Hudson et al., 2018). These data strongly suggest that accumulation of PAP, rather than defects in sulfation, cause the phenotypes observed in Bpnt1 deficient mice. However, the mechanism(s) by which PAP metabolic toxicity impairs cellular function remain largely unknown. PAP has been shown to modulate activity of sulfotransferases (Klaassen and Boles, 1997), nucleoside diphosphate kinase (NDK) (Schneider et al., 1998), 5’-3’ exoribonuclease 1 (Xrn1) (Dichtl et al., 1997a), and poly (ADP-ribose) polymerase 1 (PARP1)

(Toledano et al., 2012), among others. However, it remains unclear if PAP-mediated inhibition of these targets (or others) is responsible for the disease phenotypes and metabolic toxicity observed in Bpnt1 deficient mice.

To identify potential targets of PAP in Bpnt1$^{-/int}$ enterocytes, we adapted an affinity chromatography approach using PAP conjugated to agarose beads (PAP-agarose) as previously described (Spiegelberg et al., 1999a). Briefly, duodenal enterocyte lysates from Bpnt1$^{-/fl}$ or Bpnt1$^{-/int}$ mice were applied to PAP-agarose, washed, competitively eluted with PAP. Purified Bpnt1 was used as a positive control. Eluents were analyzed by SDS page and silver-staining (Figure 5.1A).

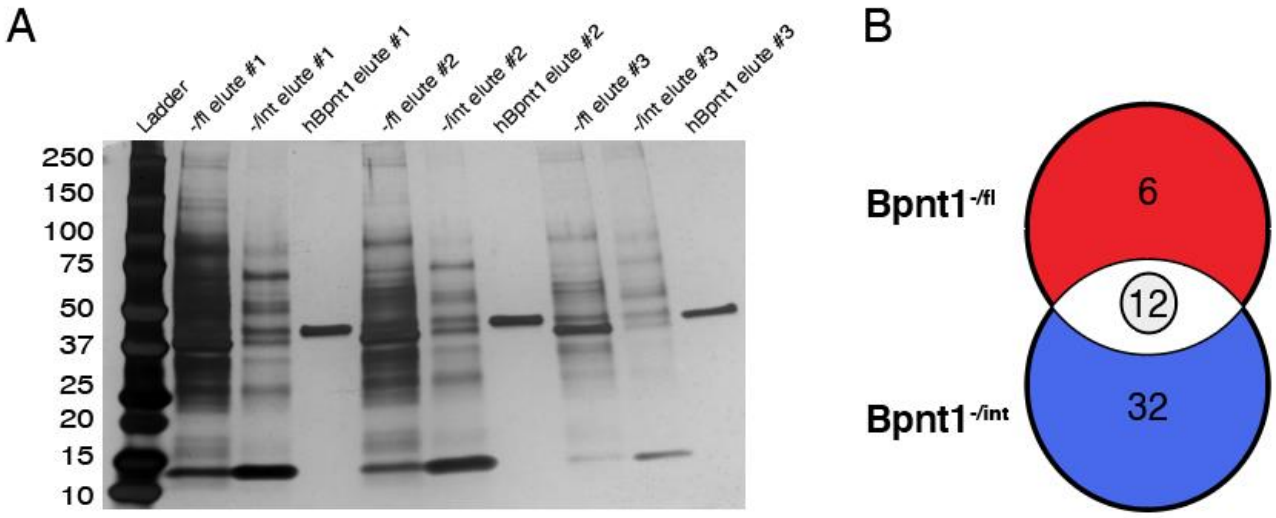

Figure 5.1. Identification of PAP-binding proteins by affinity chromatography in Bpnt1$^{-/fl}$ and Bpnt1$^{-/int}$ enterocyte lysates. (A) 20 μg of enterocyte lysates from Bpnt1$^{-/fl}$ and Bpnt1$^{-/int}$ as well as purified human Bpnt1 (hBpnt1) were applied to a column with PAP-conjugated to agarose beads, washed, and competitively-eluted with PAP in sequential fashion. Proteins in each successive eluent were separated by on a 4-20% SDS-page gel and visualized using silver-stain. (B) Venn-diagram of individual peptides identified by mass spectrometry from Bpnt1$^{-/fl}$ and Bpnt1$^{-/int}$ lysates after eluted from PAP agarose.

We then used shotgun mass-spectrometry to determine protein identity from eluents isolated from Bpnt1$^{-/fl}$ or Bpnt1$^{-/int}$ lysates (Table 1). As a positive control, we identify Bpnt1 in Bpnt1$^{-/fl}$ enterocytes and identify known PAP-binding protein NDK in Bpnt1$^{-/int}$, but not Bpnt1$^{-/fl}$, enterocytes (Table 1). We observed 32 unique peptides in Bpnt1$^{-/int}$ eluents, 12 peptides in both Bpnt1$^{-/int}$ and Bpnt1$^{-/fl}$ eluents, and 6 peptides exclusively in Bpnt1$^{-/fl}$ eluents (Fig. 1B and Table 1). Intriguingly, we identify number of histone species (H1.0, H1.2, H1.5, H2A, H3, and H4) binding to PAP-agarose in Bpnt1$^{-/int}$ lysates.

Protein	Molecular weight (kDa)	Bpnt1-fl eluent	Bpnt1-tint eluent
Actin cytoplasmic 1	42	+	+
Adenosylhomocysteinase	48	-	+
ADP ribosylation factor 3	21	-	+
ADP/ATP translocase	33	-	+
Alkaline phosphatase	60	+	+
Alpha globin 1	15	-	+
Annexin A2	39	-	+
ATP synthase subunit beta, mitochondrial	56	-	+
Attractin like protein 1	152	+	-
Beta globin	16	+	+
Bpnt1	33	+	+
Calmodulin	17	+	-
Carbamoyl phosphate synthase	165	-	+
Catalase	60	+	+
Creatine kinase U-type, mitochondrial	47	-	+
Elongation factor 2	95	-	+
Endoplasmin	92	-	+
Enoyl CoA hydratase	31	+	-
Epithelial cell adhesion molecule	35	-	+
Fructose bisphosphate aldolase	40	+	+
Galectin 4	36	-	+
Glucose regulated protein	72	-	+
Glyceraldehyde 3-phosphate dehydrogenase	36	-	+
Heat shock protein 90 beta	83	+	-
Heat shock protien, mitochrondrial	61	-	+
Histone 1.0	21	-	+
Histone H1.2	21	-	+
Histone H1.5	23	-	+
Histone H2A type I	14	+	+
Histone H3.3C	15	-	+
Histone H4	11	+	+
Junction plakoglobin	82	-	+
Microsomal triglyceride transfer protein large subunit	99	-	+
Myosin 11	227	-	+
Myosin 9	226	-	+
Nucleoside disphosphate kinase	17	-	+
Pancreatic alpha amylase	57	-	+
Phosphate carrier protein	40	-	+
Poly(rC)-binding protein	37	+	+
Protein disulfide isomerase	57	+	+
Protein Gm3940	16	+	-
Protein Krt78	112	+	-
Pyruvate kinase isozymes M1/M2	31	+	+
Serine threonine protein kinase ATR	300	-	+
Sodium/potassium ATPase subunit alpha 1	113	-	+
Transferrin	77	-	+
Tubulin alpha-1C	50	-	+
Tubulin beta-5 chain	50	-	+
UDP glucose 6 dehydrogenase	55	-	+
Voltage dependent anion selective channel protein 2	31	-	+
Zymogen granule membrane protein	18	+	+

Table 5.1. Protein species identified in eluent from Bpnt1$^{-/fl}$ and Bpnt1$^{-/int}$ enterocytes after competitive elution with PAP from PAP-agarose binding experiments. Proteins identified in Bpnt1$^{-/fl}$ or Bpnt1$^{-/int}$ are indicted as (+).

To gain insights into pathways augmented by PAP accumulation, we performed gene set enrichment analysis (GSEA) of proteins eluted from PAP-agarose in Bpnt1$^{-/int}$ lysates. The most significant pathways by GSEA were involved in nucleosome/chromatin regulation, response to hypoxia, and genes upregulated during protein unfolding in Bpnt1$^{-/int}$ lysates, among others (Table 2). These data suggest that PAP may interact with number of targets/pathways that play diverse roles in the cell.

Gene set description	**P value**	**False discovery rate**
Genes involved in nucleosome and chromatin regulation	1.05×10^{-5}	5.14×10^{-4}
Genes upregulated in response to hypoxia	1.18×10^{-5}	5.91×10^{-4}
Genes upregulated during the protein unfolding response	7.08×10^{-5}	1.77×10^{-3}
Genes upregulated through activation of mTORC1 complex	3.81×10^{-4}	4.76×10^{-3}
Genes involved in oxidative phosphorylation	5.82×10^{-3}	4.92×10^{-2}
Genes mediating apoptosis	8.85×10^{-3}	4.93×10^{-2}
Genes encoding components of the apical junction complex	8.87×10^{-3}	4.95×10^{-2}
Genes involved in metabolizing xenobiotics	9.02×10^{-3}	4.99×10^{-2}

Table 5.2. Hallmark pathways identified by Gene Set Enrichment Analysis (false discovery rate $q<0.05$) using proteins identified in Bpnt1$^{-/int}$ enterocytes eluted from PAP-agarose.

5.3.2 Histones isolated from Bpnt1$^{-/int}$ enterocytes interact with PAP agarose

Next, since we observed histones and nucleoside diphosphate kinase (NDK) (very similar molecular weights) interacting with PAP-agarose from Bpnt1$^{-/int}$, but not Bpnt1$^{-/fl}$ control enterocytes, we aimed to isolate histones and attempt to identify the predominant protein species observed in between 10-20 kDa ladder (where both histones and NDK are observed) in the Bpnt1$^{-/int}$ lysate fraction. Thus, we used a commercially-available histone extraction kit to isolate acid-soluble proteins from Bpnt1$^{-/fl}$ control and Bpnt1$^{-/int}$ enterocytes and applied these isolates to PAP-agarose as described above. The input fraction (i.e. contents loaded onto PAP agarose) isolated from Bpnt1$^{-/fl}$ and Bpnt1$^{-/int}$ were largely similar except for the presence of band below H1 in the Bpnt1$^{-/int}$ fraction and a very large band (~200 kDa) in the Bpnt1$^{-/fl}$ fraction (Figure 5.2). Very little protein was observed in the Bpnt1$^{-/fl}$ flow-through suggesting that the majority of protein stably interacts with PAP agarose. Conversely, ~50% of input protein in Bpnt1$^{-/int}$ histone lysate and 50:50 ratio of Bpnt1$^{-/fl}$:Bpnt1$^{-/int}$ protein does not interact with PAP agarose and is observed in the flow-through (Figure 5.2). Intriguingly, only histones isolated from Bpnt1$^{-/int}$ enterocytes are observed in the PAP elution fraction. However, both Bpnt1$^{-/fl}$ and 50:50 ratio of Bpnt1$^{-/fl}$:Bpnt1$^{-/int}$ histones on the boiled beads are observed (Figure 5.2). These data suggest that perhaps there is an acid soluble protein present in Bpnt1$^{-/fl}$ (or conversely loss of Bpnt1$^{-/int}$ histone preparations) that alters the ability of histones to interact with PAP agarose. However, at the time of preparing this dissertation, the commercial production of PAP agarose has been discontinued. Thus, future studies should be aimed at recapitulating these results using a manually-prepared PAP agarose resin.

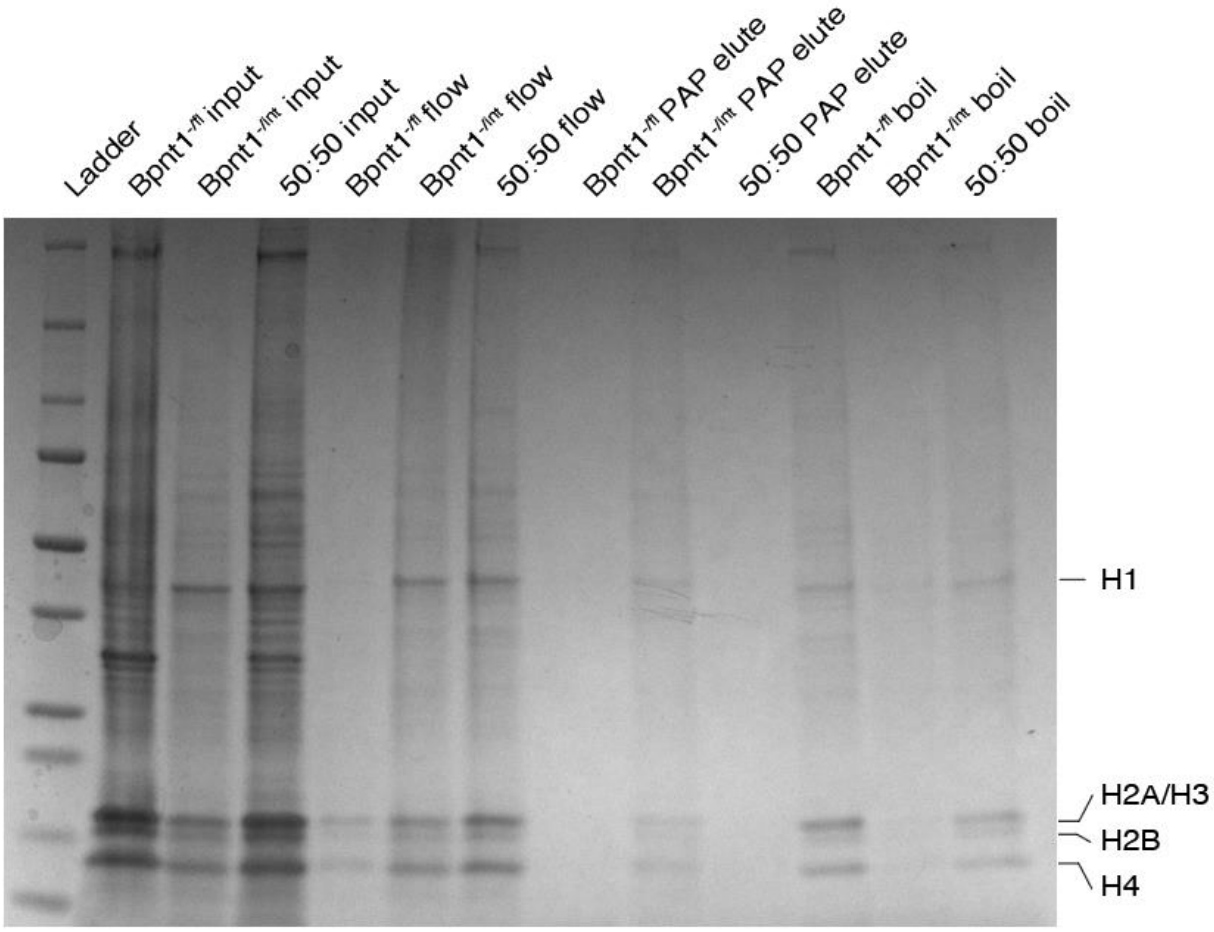

Figure 5.2. Histones isolated from Bpnt1$^{-/fl}$, Bpnt1$^{-/int}$, and a 50:50 ratio of Bpnt1$^{-/fl}$:Bpnt1$^{-/int}$ protein was applied to PAP agarose as described above. Equal volumes (30 μl) were used for flow-through, PAP elution, and boiled fractions to quantify relative amount of protein in each fraction. Flow through represents the quantity and identity of proteins not bound to PAP agarose. Elution was performed using 500 μM PAP. The boiled fraction was PAP agarose buffer mixed with SDS sample buffer applied to PAP agarose beads after PAP elution and boiling for five minutes.

5.3.3 Bpnt1$^{-/int}$ enterocytes display histone post-translational modifications consistent with increased chromosomal accessibility

Since we observed histones interacting with PAP agarose in Bpnt1$^{-/int}$ enterocytes, Bpnt1$^{-/int}$ display broad changes in transcription (Hudson et al., 2018), and GSEA revealed an enrichment

of proteins involved in chromatin/nucleosome regulation, we postulated that PAP toxicity may alter histones. First, to confirm histone binding to PAP-agarose, we purified histones from Bpnt1$^{-/fl}$ and Bpnt1$^{-/int}$ enterocytes and applied them to PAP-agarose (Figure 5.2). Input control revealed no obvious differences in individual histone levels between Bpnt1$^{-/fl}$ and Bpnt1$^{-/int}$ enterocytes (Figure 5.2). Next, we surmised that Bpnt1$^{-/int}$ enterocytes may display alterations in histone post-translational modifications (PTMs) consistent with decreased heterochromatin. To test this hypothesis, we used an enzyme-linked immunosorbent essay (ELISA) based approach to identify relative levels histone H3 PTMs between Bpnt1$^{-/fl}$ and Bpnt1$^{-/int}$ enterocytes. We observed a marked enrichment in H3 PTMs associated with "open" chromatin and a corresponding decrease in heterochromatin-associated H3 PTMs (Figure 5.3). These data identify alterations in histone PTMs consistent with increased chromosome accessibility in Bpnt1$^{-/int}$ enterocytes.

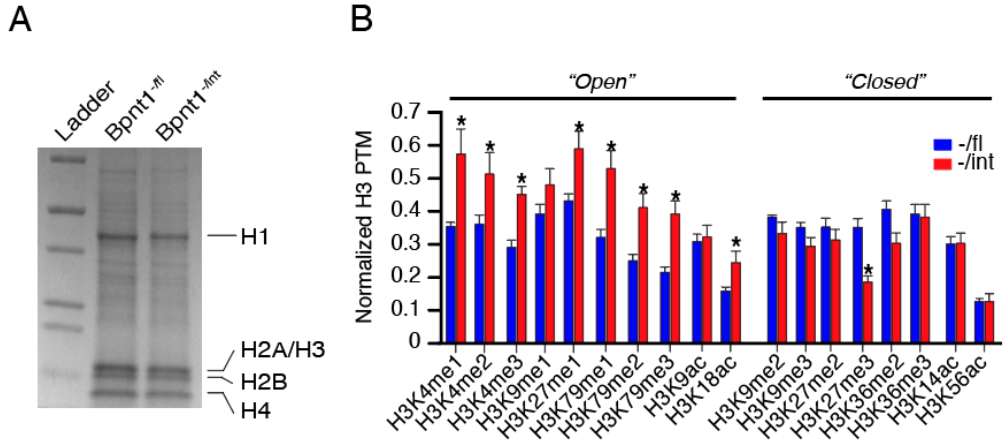

Figure 5.3. Bpnt1$^{-/int}$ enterocytes display enrichment of histone post-translational modifications consistent with increased chromosome accessibility (A) Input control (10 μg) of purified histones from Bpnt1$^{-/fl}$ (lane 2) and Bpnt1$^{-/int}$ (lane 3) enterocytes. Molecular weight ladder is in lane 1. (B) Bpnt1$^{-/int}$ enterocytes display alterations in histone H3 post-translational modifications associated with increased "open" chromatin. Data are normalized to total H3 protein and represented as mean ± standard deviation.

5.4 Discussion

Our study provides insights into potential targets of PAP toxicity in enterocytes isolated from Bpnt1$^{-/int}$ mice. Using an affinity-chromatography approach, we identify known PAP-binding protein nucleoside diphosphate kinase (NDK) (Schneider et al., 1998), but not poly(ADP-ribose) polymerase (PARP1), interacting with PAP-agarose in Bpnt1$^{-/int}$, but not Bpnt1$^{-/fl}$, enterocytes. Interestingly, we also observed PAP broadly interacting with a number of histone proteins (H1.0, H1.2, H1.5, H2A, H3, and H4) and an enrichment of histone PTMs associated with increased euchromatin (i.e. markers of increased chromosome accessibility and thus transcription). These data are consistent with prior studies demonstrating that ~25% of the transcriptome is differentially expressed greater than three-fold in Bpnt1$^{-/int}$ enterocytes. Importantly, there is a ~4:1 ratio of genes upregulated vs. downregulated (Hudson et al., 2018). Despite the disproportionate increase in gene transcription consistent with global enrichment of H3 PTMs, iron homeostatic gene expression is nearly universally repressed. However, the mechanism by which PAP mediates alterations in transcription remains unknown. Overall, our study provides insights into potential targets of PAP metabolic toxicity.

We identified known PAP-interacting protein NDK in enterocytes isolated from Bpnt1$^{-/int}$ mice. While an NDK-mediated mechanism perturbing iron metabolism is disfavored, it cannot be definitively ruled out. Since PAP has a phosphate at the 3' ring position, NDK is not predicted to accommodate PAP as a substrate (Schneider et al., 1998). Although PAP could allosterically regulate NDK, inhibition of NDK would be expected to decrease the ATP:ADP ratio, which is not readily apparent in Bpnt1 null tissue by HPLC analysis (Hudson et al., 2013). However, there is evidence to suggest that loss of NDK in mice leads to severe defects in erythropoiesis (Postel et al., 2009), although this type of anemia is distinct from the iron deficiency anemia observed in

Bpnt1 null mice. Furthermore, NDK null mice do not display any other phenotypes observed in the conventional Bpnt1 knockout mouse.

In addition, Bpnt1 deficient tissue features a modest (~five-fold) accumulation of PAPS (Hudson et al., 2013), and although PAP is the preferred substrate ($k_{cat}/K_m = 4.4x10^7$), Bpnt1 can utilize PAPS as a substrate albeit with indeterminate efficiency (Spiegelberg et al., 1999a). However, PAPS accumulation as a mechanism to impair NDK is also disfavored because PAP has a ~7-fold higher K_d for NDK compared to PAPS (Schneider et al., 1998). While our data does not definitively rule out inhibition of NDK and/or PAPS accumulation as mechanisms contributing to IDA, these mechanisms would appear to be less likely.

We also identified transferrin (non-heme iron carrying protein) and intestinal barrier proteins Myosin 9 (Myo9) and epithelial cell adhesion molecule (EPCAM) from Bpnt1$^{-/int}$ enterocytes interacting with PAP agarose. However, alteration of these targets is disfavored because expression of transferrin in the intestine is negligible compared to hepatic production (Idzerda et al., 1986) and Bpnt1$^{-/int}$ mice do not display any phenotypes associated with loss of Myo9 or EPCAM (Guerra et al., 2012; Zhang et al., 2012a). Interestingly, while Bpnt1 null hepatocytes display defects in ribosome biogenesis and protein production (Hudson et al., 2013), Bpnt1$^{-/int}$ do not display an overt phenotypes associated with global defects in protein production (i.e. intestinal barrier breakdown, diarrhea, weight loss, etc.). Furthermore, since different tissues utilize sulfur assimilation to varying degrees and PAP is elevated to variable degrees in select tissues, despite uniform loss of Bpnt1 protein (Hudson and York, 2012, 2014), both shared and tissue-specific molecular mechanisms of PAP accumulation seem plausible.

There is a growing body of literature linking metabolic toxicity with epigenetic changes in disease (Kaelin and McKnight, 2013). We observed PAP binding to nearly all histone species in

Bpnt1$^{-/int}$, but not Bpnt1$^{-/fl}$ enterocytes, providing some support for PAP directly interacting with the histone/nucleosome machinery. Corollary to these observations, we observed an enrichment of histone H3 PTMs associated with "open" chromatin. Given that ~25% of the transcriptome in Bpnt1$^{-/int}$ enterocytes was differentially-expressed greater than three-fold (Hudson et al., 2018) and Bpnt1 null hepatocytes display decreased heterochromatin by electron microscopy analysis (Hudson and York, 2014), these data are consistent with a role for PAP toxicity and modulation of chromatin. Furthermore, Bpnt1 null enterocytes display a ~4:1 ratio of genes upregulated vs. downregulated greater than three-fold, despite global repression of iron homeostatic genes. However, whether or not direct binding of histones causes the observed changes in transcription remains unclear. Collectively these data suggest that histones may be a target of PAP metabolic toxicity, but the precise mechanism by which this occurs remains unknown. There are many mechanisms by which PAP accumulation may influence chromatin: 1) alter nucleosome positioning, 2) disrupt nucleosome assembly/disassembly, 3) impair interactions between histones and DNA, 4) block histone deacetylase or acetylase interactions with the histone core, or 5) augment recognition or function of chromatin modifying enzymes, among others. Nonetheless, we provide data to suggest that PAP toxicity may act, at least in part, through interaction with histone proteins. However, the mechanism by which PAP accumulation augments transcription and chromosome accessibility remains unknown.

A cellular feature of PAP accumulation is the presence of a single, large nucleolus (the site of rRNA production) identified by electron microscopy and staining for nucleolar-resident proteins fibrillarin and nucleoplasmin/B23 (Hudson et al., 2013; Hudson et al., 2018; Hudson and York, 2014). In addition to alterations in nucleolar structure, we observe a marked accumulation of fibrillarin protein in Bpnt1 null tissue (Hudson et al., 2013). In addition to its role as a marker of

the nucleolus, fibrillarin is a methyltransferase that can modify rRNA and proteins (including histone H2A) (Shubina et al., 2016; Tiku and Antebi, 2018) to regulate gene expression as well as directly regulate translation (Elliott et al., 2019). Thus, it is possible that the nucleolar condensation observed is merely the accumulation of fibrillarin protein that may exert its effects via its methyltransferase activity rather than through modulation of nucleolar function (i.e. rRNA production).

Furthermore, Bpnt1 null hepatocytes display selective elevation of unprocessed rRNA species consistent with inhibition of ribosomal RNA processing enzyme Xrn1 (Hudson et al., 2013), a PAP-sensitive enzyme (Dichtl et al., 1997a). Intriguingly, Xrn1 and the fibrillarin orthologue Nop1 have been shown to genetically and physically interact in budding yeast (Krogan et al., 2004; Wilmes et al., 2008), suggesting a convergent mechanism linked through PAP accumulation. In addition, deletion of the fibrillarin homolog *ncl-1* in *C. Elegans* phenocopies the nucleolar condensation observed in Bpnt1 null tissue (Tiku et al., 2017), suggesting that homeostatic fibrillarin expression is an important regulator of nucleolar architecture. However, the mechanism by which PAP accumulation causes increased fibrillarin expression in the liver, despite global regression of protein synthesis and defects in ribosome biogenesis, is not known. Future studies should be aimed at elucidating this apparent paradox and also a potential role for fibrillarin methyltransferase activity on both rRNA processing and chromosome regulation via glutamine methylation of histone H2A.

In addition, lithium-induced accumulation of PAP has been shown to inhibit poly (ADP-ribose) polymerase 1 (PARP-1) activity on histone modification (Toledano et al., 2012), PARP-1 directly interacts with nucleoplasmin (Meder et al., 2005), and histone H2A variants modulate PARP-1 association with chromatin (Kotova et al., 2011). Finally, loss of PARP-1 function impairs

nucleolar structure and disrupts rRNA processing and ribosome biogenesis (Boamah et al., 2012). Thus, PAP accumulation augments many key steps involved in chromatin regulation, rRNA processing, and nucleolar function, that likely in concert, lead to phenotypes associated with loss of Bpnt1.

Our data outline potential targets of PAP metabolic toxicity in the intestinal epithelium identified by PAP affinity chromatography. While many PAP-dependent mechanisms are likely contributing to IDA in Bpnt1$^{-/int}$ mice, these data provide a link between sulfur assimilation metabolic toxicity and alterations in chromatin. Given that Bpnt1 is potently inhibited by lithium (Spiegelberg et al., 2005; Spiegelberg et al., 1999a), it is possible that elevation of PAP may be mediating the therapeutic and/or toxic effects of lithium pharmacotherapy. Since histones may be a target of PAP metabolic toxicity, these data are particularly very intriguing given the high rate of lithium "non-responders" among patients with bipolar disorder. These data are directly relevant for understanding molecular mechanisms underlying PAP metabolic toxicity and loss of Bpnt1.

Chapter 6 Summary and Future Directions

6.1 Summary

Our work outlined in this dissertation uncovers an unanticipated link between nucleotide hydrolysis in the sulfur assimilation pathway and regulation of iron homeostasis. These data point to a mechanism by which inactivation of the 3'-nucleotidase Bpnt1 in the intestinal-epithelium leads to a massive accumulation PAP substrate. Elevation of PAP prevents the physiological response to low iron levels in mice leading to IDA. Remarkably, by reducing PAP synthesis in the context of nucleotidase deficiency, we are able to completely rescue the pathophysiology of IDA. However, the precise mechanism by which PAP accumulation alters the function of the intestinal-epithelium remains unclear. Our studies suggest that PAP accumulation causes dramatic changes in transcription consistent with broad changes in chromosome accessibility, repression of iron homeostatic gene expression, and condensation of the nucleolar architecture. In addition, our data suggest that iron deficiency anemia caused by loss of Bpnt1 is mediated, at least in part, by inhibition of HIF-2α signaling. We describe both genetic and dietary approaches to overcome PAP metabolic toxicity that act through distinct mechanisms. In addition, we identify modulation of Bpnt1 as a potential target for ameliorating iron overload caused by biallelic C282Y mutations in Hfe, the most common cause of hemochromatosis in humans. Finally, we provide insights into histones as potential molecular targets of PAP metabolic toxicity, leading to broad changes in transcription.

The data outlined in this dissertation support the following conclusions: 1) definition of a new genetic complementation group for IDA through loss of Bpnt1, 2) identification of a genetic approach to overcome IDA caused by loss of Bpnt1 through reduction of PAP synthesis and/or restoration of HIF-2α expression, 3) description of a dietary mechanism to suppress PAP toxicity

and restore iron homeostasis, and 4) identification of a genetic mechanism to suppress iron overload in mice harboring homozygous Hfe^{C282Y} mutations. Additional studies suggest that PAP accumulation may interact with a broad number of targets (outlined in Chapter 5), although many mechanisms may be contributing to iron deficiency anemia due to loss of Bpnt1. In this Chapter, an outline and critical appraisal of potential PAP-mediated mechanisms are highlighted based on our current understanding of PAP metabolic toxicity. This summary provides an outline for future studies aimed at elucidating a mechanistic basis for PAP accumulation.

Regulation of iron metabolism is essential for normal cellular homeostasis and is perturbed in a number of disease states. Thus, identification of mechanisms that modulate iron homeostasis have broad implications for understanding the pathophysiological basis and potential treatment of numerous disorders. Given that PAP has been shown to directly bind upstream sulfotransferases (Rens-Domiano and Roth, 1987) and inhibit RNA processing (Dichtl et al., 1997b), it is conceivable that PAP acts as a broad and potent inhibitor of other proteins involved in varied biological processes that may influence iron metabolism. It is also likely that PAP-mediated mechanisms may differ between cell types, largely dependent on degree of PAP toxicity. Our studies already suggest that PAP elevation may work through differing mechanisms in the liver versus the intestinal epithelium, and this could be due to the varying degree to which tissue types utilize sulfur assimilation metabolism. Our studies summarized in Chapters 3, 4, & 5 demonstrated that PAP accumulation causes ~25% of genes to be differentially expressed, consistent with decreased heterochromatin observed by electron microscopy and an enrichment of histone H3 post-translational modifications associated with increased euchromatin. Despite a 4:1 ratio of genes up-regulated greater than three-fold compared to genes down-regulated, we observe a marked repression of nearly all iron homeostatic genes. In addition, the iron deficiency anemia

phenotype and transcriptional signature are phenocopied in mice lacking intestinal-epithelial expression of Hif-2α. One group has suggested thatthe transcriptional response to iron starvation is, in large part, mediated by HIF-2α (Taylor et al., 2011b). Our data demonstrates that HIF-2α and its downstream targets are decreased at the transcriptional level due to accumulation of PAP. Thus, we surmise that PAP may impair Hif-2α expression, however there are many potential mechanisms by which this could occur.

Our studies also imply that manipulation of sulfur assimilation metabolism may represent a new avenue for therapeutic development. Given that Bpnt1 is potently inhibited by lithium (Spiegelberg et al., 2005; Spiegelberg et al., 1999a), it is possible that lithium may be mediating its toxic effects through accumulation of PAP. Bpnt1 deficient animals display alterations in diverse cellular functions (i.e. ribosome biogenesis, chromosome accessibility, etc.) that could be playing a role in the mechanism of action of lithium, this is certainly a possibility. Furthermore, development of small-molecule inhibitors of Papps2, leading to amelioration of PAP synthesis, may represent a unique approach to treating iron deficiency anemia due to loss of Bpnt1. Similarly, development of Bpnt1 catalytic inhibitors and subsequent accumulation of PAP may represent a strategy to overcome disorders of iron overload.

In summary, we define a new genetic basis for IDA, uncovering an unanticipated link between intestinal-epithelium specific nucleotide hydrolysis in the sulfur assimilation pathway and regulation of iron homeostasis. Our data point to a mechanism by which loss of Bpnt1 leads to massive elevation of PAP which prevents the physiological response to low iron levels by perturbing transcriptional upregulation of iron homeostasis factors, possibly through modulation of HIF-2α activity. Our work identifies a new complementation group for iron deficiency anemia and provides insights into strategies to overcome disease pathophysiology through concomitant

down regulation of PAP synthesis via reduction of PAPSS2 activity. Preliminary biochemical data suggests that histones may be a target of PAP metabolic toxicity, however a precise mechanistic basis for these observations has not been elucidated. The remainder of this chapter will focus on summarizing potential areas of investigation for delineating mechanisms of PAP metabolic toxicity.

6.2 Future Directions

6.2.1 PAP accumulation and histones as targets of metabolic toxicity

Throughout this dissertation and through prior studies from our group, we have demonstrated that PAP accumulation alters transcription and chromosome accessibility using a variety of approaches. However, the mechanism by which PAP toxicity alters transcription remains an important unanswered question. However, it was with great enthusiasm that we identified various histone species isolated from Bpnt1$^{-/int}$ enterocyte lysates binding to PAP-agarose, outlined in Chapter 5. Subsequent studies isolating acid soluble proteins (of which histones are a major component) from Bpnt1$^{-/int}$ and control enterocytes recapitulated histones isolated from Bpnt1$^{-/int}$, but not control, enterocytes interacting with PAP agarose. Only histones isolated from Bpnt1$^{-/int}$, but not control, enterocytes were observed in the competitive elution (500 μM PAP) fraction after wash with buffer containing 500 mM NaCl. However, mixing a 50:50 ratio of Bpnt1$^{-/fl}$:Bpnt1$^{-/int}$ histone isolates to determine if there is an inhibitor of PAP-agarose binding in the Bpnt1$^{-/int}$ histone preparation yielded mixed findings. While isolated histones were observed in the flow-through of the 50:50 sample mix consistent with the Bpnt1$^{-/int}$ sample, competitive PAP elution did not elute histones from the 50:50 sample. Furthermore, histones from Bpnt1$^{-/fl}$ or 50:50

sample ratio were only disrupted after boiling, whereas histones isolated from Bpnt1$^{-/int}$ enterocytes were observed after PAP elution or in the flow-through. These data suggest that perhaps histones in Bpnt1$^{-/int}$ enterocytes are modified in such a way that enable interaction with PAP agarose. Further biochemical characterization of these results are warranted in order to identify a potential mechanistic basis for regulation of sulfur assimilation metabolism and nucleotide hydrolysis augmenting transcription.

PAP accumulation may alter the biochemical properties of histones and modulate transcription in a number of ways: 1) alter nucleosome positioning, 2) disrupt nucleosome assembly/disassembly, 3) impair interactions between histones and DNA, 4) block histone deacetylase or acetylase interactions with the histone core, 5) augment recognition or function of chromatin modifying enzymes, or 6) promote alterations in post-translational modifications, among others. We demonstrated that histones isolated from Bpnt1$^{-/int}$ enterocytes display alterations in histone H3 PTMs, however a global analysis of all histone PTMS may be warranted as understanding the entirety of the histone code may provide insights into how PAP influences histone PTMs. Mass spectrometry based approaches have been used to analyze the range of potential histone PTMs across histone species (Zhao and Garcia, 2015), and may be useful to quantify global changes in histone PTMs.

It appears that the individual components of the histone octamer from Bpnt1$^{-/int}$ enterocytes bind to PAP agarose to a similar degree. Thus, it would be intriguing to delineate if PAP binds specifically to any individual histone protein or rather coordinates the assembly/disassembly of the histone octamer. Furthermore, PAP may alter how the components of the nucleosome assemble on DNA. Since PAP is negatively-charged, PAP-bound histones may electrostatically repel their

interaction with DNA. Delineating the molecular interaction of PAP with histones may provide unique insights into mechanisms underlying PAP metabolic toxicity.

6.2.2 Additional targets of PAP toxicity

Here we applied an affinity-chromatography based approach to identify putative targets of PAP metabolic toxicity. However, PAP can be conjugated to agarose through a number of linkers and at different ring positions. Thus, expanding the biochemical approach to test different affinity chromatography approaches are warranted. Similarly, these approaches only identify proteins that exchange PAP and may thus be assumed to be interacting with PAP through surface residues (i.e. easily accessible to exchange with PAP agarose). Interrogation of proteins that may bind PAP through non-surface exposed motifs is certainly possible, and additional biochemical approaches are needed to answer these questions.

One group identified poly(ADP-ribose) polymerase (PARP-1) isolated from nuclear extracts of HeLa cells binding to PAP agarose (Toledano et al., 2012). However, this group's approach differed substantially from the approach taken herein. First, they used nuclear extracts instead of whole-cell lysates, which inevitably disregard cytoplasmic and other organelle-bound proteins. Second, these authors only used heat (65 °C for 15 minutes) to elute putative PAP-binding proteins from the agarose beads. In addition, these authors observed excess PAP (3 mM) blocking PARP-1 interaction with PAP-agarose beads. However, this concentration of PAP far exceeds the physiological levels of PAP that our group observes even in the Bpnt1 knockout animal (~80 nmol/g tissue). Perhaps most relevant to the studies outlined in this dissertation, these authors did not isolate cells from Bpnt1 null mice displaying PAP metabolic toxicity and compare

characteristics of PAP-agarose. Interestingly, these authors provide data to suggest that PAP-mediated inhibition of PARP-1 poly(ADP-ribosyl)ation activity can inhibit histone H1 poly(ADP-ribosyl)ation, but only at ~0.1-1.0 μM PAP (Toledano et al., 2012). These data were also recapitulated in HeLa cells treated with lithium. Thus, there is some evidence to suggest that inhibition of PARP-1 may be a relevant target of PAP metabolic toxicity.

Although not identified through the PAP affinity chromatography approach described here, PARP-1 has been shown to interact with PAP agarose. In addition, PARP-1 ADP-ribosylation activity is inhibited by PAP *in vitro* (Toledano et al., 2012). PARP-1 has also been shown to associate with chromatin and regulate nucleosome remodeling (Althaus et al., 1994; Martinez-Zamudio and Ha, 2012; Realini and Althaus, 1992). Some have suggested that PARP-1 can directly regulate mRNA processing through inhibition of mRNA binding proteins (Ryu et al., 2015). However, PARP-1 has also been shown to mediate the response to hypoxia via Hif-2α at the transcriptional and translational levels (Gonzalez-Flores et al., 2014). These authors also demonstrate that PARP-1 forms a complex with HIF-2α and that HIF-2α-dependent transcriptional programs require PARP-1 activity (Gonzalez-Flores et al., 2014). Finally, deletion of PARP-1 in mice results in decreased erythropoietin production, blunted red blood cell production in response to hypoxia, and increased genome instability due to loss of PARP-1 DNA repair activity (de Murcia et al., 1997; Gonzalez-Flores et al., 2014). However, these phenotypes associated with impaired PARP-1, while peripherally related to anemia, are not consistent with impaired iron absorption, but rather due to primary defects in hematopoiesis. Nonetheless, it seems feasible that PARP-1 may be a target of PAP metabolic toxicity, and investigation of a PARP-1 dependent mechanism is warranted.

PAP has been shown to bind and inhibit nucleoside diphosphase kinase (NDK), although PAP has a ~7-fold higher K_d for NDK compared to PAPS (Schneider et al., 1998). While Bpnt1 can utilize PAPS as a substrate (Spiegelberg et al., 1999a), the accumulation of PAPS is modest (~5 fold) compared to ~40 fold increase in PAP levels in Bpnt1 null tissue. Perhaps contrary to the biochemical rationale presented above, deletion of both isoforms of NDK in mice leads to severe anemia (Postel et al., 2009). While Bpnt1 null mice develop anemia due to impaired intestinal iron absorption (Hudson et al., 2018), NDK null mice display defects in erythroblast development (i.e. nucleated red blood cells) and perinatal death (Postel et al., 2009). The NDK double heterozygous mice, however, display mild iron deficiency anemia at embryonic day 18.5. Thus, it is possible that inhibition of NDK contributes, at least in part, to the anemia phenotype observed in Bpnt1 null mice. However, the type of anemia observed in the NDK mutant animal (i.e. defective erythropoiesis) is substantially different than the anemia observed in the Bpnt1$^{-/int}$ animal due to defects in intestinal iron absorption.

6.2.3 Phase separation as a potential mechanistic consequence of PAP toxicity

Studies detailed in this dissertation revealed a role for PAP accumulation in Bpnt1 null tissue mediating broad changes in transcription and chromatin structure based on the observation that ~25% of the transcriptome is differentially expressed greater than three-fold and Bpnt1 null enterocytes display decreased heterochromatin by electron microscopy. In addition, preliminary biochemical approaches suggest that histones may be a target of PAP metabolic toxicity and histones isolated from Bpnt1$^{-/int}$ enterocytes display an enrichment of post-translational modifications consistent with increased chromosomal accessibility. One potential mechanism by which chromatin is organized is dependent on phase separation, the process by which two mutually

soluble components come apart into distinct compartments (Yoo et al., 2019). Phase separation and control of gene expression is a topic of recent interest in the scientific literature (Hnisz et al., 2017), and the mechanistic basis of these processes is currently under active investigation. Relevant to the studies presented in this dissertation, many groups have implicated histone modifications as playing a major role in regulating euchromatin vs. heterochromatin via a phase separation mechanism (Gibson et al., 2019; Larson and Narlikar, 2018; Strom et al., 2017; Wang et al., 2019). Furthermore, given the abnormal condensation (and potentially separation) of the nucleolus in Bpnt1 null cells, it is possible that PAP accumulation broadly regulates subcellular phase separation. It is possible that PAP accumulation therefore may regulate a phase separation mechanism via alteration of histone modifications and/or modulation of nucleolar architecture. Thus, biophysical approaches may be useful in determining the molecular mechanisms of PAP metabolic toxicity.

6.2.4 rRNA processing and modifications

In addition to alterations in chromatin organization, loss of Bpnt1 and PAP accumulation causes condensation of the nucleolus, determined by immunohistochemical analysis of nucleolar-resident proteins fibrillarin/nucleoplasmin and by electron microscopy (Hudson et al., 2013; Hudson et al., 2018). Thus, a phase separation mechanism perturbing nucleolar structure and organization may also underly PAP metabolic toxicity. Fibrillarin is a component of ribonucleoproteins and has known roles in rRNA processing and ribosome biogenesis (Amin et al., 2007). Furthermore, recent evidence suggests that fibrillarin can methylate a glutamine residue on H2A in the nucleolus to regulate transcription through binding of the facilitator of chromatin transcription (FACT) complex (Elliott et al., 2019; Tessarz et al., 2014). Furthermore, fibrillarin

has rRNA 2'-O-methylation activity that when lost, results in attenuated ribosome biogenesis (Erales et al., 2017). Since Bpnt1 null tissue displays increased expression of fibrillarin, increased methyltransferase and/or rRNA 2'-O-methylation activity may be a consequence of PAP metabolic toxicity.

Lastly, prior studies from our group and others demonstrated that PAP accumulation inhibits rRNA processing through inhibition of XRN (Dichtl et al., 1997a; Hudson et al., 2013). While restoration of Xrn1 expression in Bpnt1$^{-/int}$ enteroids partially suppressed iron homeostatic gene expression (see Chapter 4), it is possible that expression levels were not high enough to stoichiometrically match the levels of PAP in the cell. Furthermore, it may be useful to perform Xrn1-Bpnt1 epistasis experiments to see if deletion of Xrn1 mirrors defects in iron homeostatic gene expression in enteroids. While modest elevation of the "long" form of 5.8S rRNA were observed in Bpnt1 hepatocytes, there were no gross changes in individual rRNA species levels despite marked defects in ribosome biogenesis (Hudson et al., 2013). Whether or not the rRNA species in Bpnt1 null tissue were functional and appropriately post-transcriptionally modified remains unknown. One potential approach to understanding the genetic relationship between Bpnt1 and Xrn1 is to knockdown Xrn1 expression in Bpnt1 enteroids. However, gene deletion via siRNA or shRNA may be difficult in primary mouse enteroids.

Overall, the studies outlined in this dissertation provide insights into the role of sulfur assimilation metabolism and nucleotide hydrolysis in regulating iron metabolism. We define a mechanism by which iron deficiency anemia caused loss of Bpnt1 can be overcome with forward genetic disruption of PAP substrate synthesis. In addition, PAP metabolic toxicity can be overcome with dietary restriction of methionine leading to iron homeostasis and decreased PAP accumulation *in vivo*. We also identify a genetic approach to restore iron homeostatic gene

expression in Bpnt1$^{-/int}$ enteroids through overexpression of key iron-regulatory transcriptional regulator Hif-2α. We then identify Bpnt1 as a genetic modifier of iron overload caused by hereditary hemochromatosis, suggesting that modulation of sulfur assimilation metabolism may be an attractive strategy to treat iron overload. Finally, we provide preliminary evidence that histones may be a target of PAP metabolic toxicity. Future studies should be aimed at identifying the molecular basis of PAP accumulation and further identifying cellular consequences of PAP metabolic toxicity.

Bibliography

Abboud, S., and Haile, D.J. (2000). A novel mammalian iron-regulated protein involved in intracellular iron metabolism. The Journal of biological chemistry *275*, 19906-19912.

Ables, G.P., Perrone, C.E., Orentreich, D., and Orentreich, N. (2012). Methionine-restricted C57BL/6J mice are resistant to diet-induced obesity and insulin resistance but have low bone density. PloS one *7*, e51357.

Adams, M.D., Soares, M.B., Kerlavage, A.R., Fields, C., and Venter, J.C. (1993). Rapid cDNA sequencing (expressed sequence tags) from a directionally cloned human infant brain cDNA library. Nat Genet *4*, 373-380.

Alonge, K.M., Logsdon, A.F., Murphree, T.A., Banks, W.A., Keene, C.D., Edgar, J.S., Whittington, D., Schwartz, M.W., and Guttman, M. (2019). Quantitative analysis of chondroitin sulfate disaccharides from human and rodent fixed brain tissue by electrospray ionization-tandem mass spectrometry. Glycobiology *29*, 847-860.

Althaus, F.R., Hofferer, L., Kleczkowska, H.E., Malanga, M., Naegeli, H., Panzeter, P.L., and Realini, C.A. (1994). Histone shuttling by poly ADP-ribosylation. Mol Cell Biochem *138*, 53-59.

Amin, M.A., Matsunaga, S., Ma, N., Takata, H., Yokoyama, M., Uchiyama, S., and Fukui, K. (2007). Fibrillarin, a nucleolar protein, is required for normal nuclear morphology and cellular growth in HeLa cells. Biochem Biophys Res Commun *360*, 320-326.

Anders, S., and Huber, W. (2010). Differential expression analysis for sequence count data. Genome Biol *11*, R106.

Anders, S., Pyl, P.T., and Huber, W. (2015). HTSeq--a Python framework to work with high-throughput sequencing data. Bioinformatics *31*, 166-169.

Anderson, E.R., Taylor, M., Xue, X., Ramakrishnan, S.K., Martin, A., Xie, L., Bredell, B.X., Gardenghi, S., Rivella, S., and Shah, Y.M. (2013a). Intestinal HIF2alpha promotes tissue-iron accumulation in disorders of iron overload with anemia. Proc Natl Acad Sci U S A *110*, E4922-4930.

Anderson, S.A., Nizzi, C.P., Chang, Y.I., Deck, K.M., Schmidt, P.J., Galy, B., Damnernsawad, A., Broman, A.T., Kendziorski, C., Hentze, M.W., *et al.* (2013b). The IRP1-HIF-2alpha axis coordinates iron and oxygen sensing with erythropoiesis and iron absorption. Cell Metab *17*, 282-290.

Andrews, N.C. (2008). Forging a field: the golden age of iron biology. Blood *112*, 219-230.

Andrews, N.C. (2010). Ferrit(in)ing out new mechanisms in iron homeostasis. Cell Metab *12*, 203-204.

Arredondo, M., Mendiburo, M.J., Flores, S., Singleton, S.T., and Garrick, M.D. (2014). Mouse divalent metal transporter 1 is a copper transporter in HEK293 cells. Biometals *27*, 115-123.

Asano, T., Komatsu, M., Yamaguchi-Iwai, Y., Ishikawa, F., Mizushima, N., and Iwai, K. (2011). Distinct mechanisms of ferritin delivery to lysosomes in iron-depleted and iron-replete cells. Mol Cell Biol *31*, 2040-2052.

Bersten, D.C., Sullivan, A.E., Peet, D.J., and Whitelaw, M.L. (2013). bHLH-PAS proteins in cancer. Nat Rev Cancer *13*, 827-841.

Besset, S., Vincourt, J.B., Amalric, F., and Girard, J.P. (2000). Nuclear localization of PAPS synthetase 1: a sulfate activation pathway in the nucleus of eukaryotic cells. Faseb j *14*, 345-354.

Blanchard, R.L., Freimuth, R.R., Buck, J., Weinshilboum, R.M., and Coughtrie, M.W. (2004). A proposed nomenclature system for the cytosolic sulfotransferase (SULT) superfamily. Pharmacogenetics *14*, 199-211.

Blanco, E., Kannengiesser, C., Grandchamp, B., Tasso, M., and Beaumont, C. (2009). Not all DMT1 mutations lead to iron overload. Blood Cells Mol Dis *43*, 199-201.

Boamah, E.K., Kotova, E., Garabedian, M., Jarnik, M., and Tulin, A.V. (2012). Poly(ADP-Ribose) polymerase 1 (PARP-1) regulates ribosomal biogenesis in Drosophila nucleoli. PLoS Genet *8*, e1002442.

Bowes, O., Baxter, K., Elsey, T., Snead, M., and Cox, T. (2014). Hereditary hyperferritinaemia cataract syndrome. Lancet *383*, 1520.

Boyd, D., Jain, S.K., Crampton, J., Barrett, K.J., and Drysdale, J. (1984). Isolation and characterization of a cDNA clone for human ferritin heavy chain. Proc Natl Acad Sci U S A *81*, 4751-4755.

Brissot, P., Pietrangelo, A., Adams, P.C., de Graaff, B., McLaren, C.E., and Loreal, O. (2018). Haemochromatosis. Nature reviews Disease primers *4*, 18016.

Brittenham, G.M. (2011). Iron-chelating therapy for transfusional iron overload. N Engl J Med *364*, 146-156.

Cade, J.F. (1949). Lithium salts in the treatment of psychotic excitement. Med J Aust *2*, 349-352.

Camaschella, C. (2015). Iron-deficiency anemia. N Engl J Med *372*, 1832-1843.

Camaschella, C. (2019). Iron deficiency. Blood *133*, 30-39.

Cameron, B.M., and Neufeld, L.M. (2011). Estimating the prevalence of iron deficiency in the first two years of life: technical and measurement issues. Nutr Rev *69 Suppl 1*, S49-56.

Carlini, E.J., Raftogianis, R.B., Wood, T.C., Jin, F., Zheng, W., Rebbeck, T.R., and Weinshilboum, R.M. (2001). Sulfation pharmacogenetics: SULT1A1 and SULT1A2 allele frequencies in Caucasian, Chinese and African-American subjects. Pharmacogenetics *11*, 57-68.

Chen, A.C., Donovan, A., Ned-Sykes, R., and Andrews, N.C. (2015a). Noncanonical role of transferrin receptor 1 is essential for intestinal homeostasis. Proc Natl Acad Sci U S A *112*, 11714-11719.

Chen, B.H., Wang, C.C., Hou, Y.H., Mao, Y.C., and Yang, Y.S. (2015b). Mechanism of sulfotransferase pharmacogenetics in altered xenobiotic metabolism. Expert Opin Drug Metab Toxicol *11*, 1053-1071.

Choudhry, H., and Harris, A.L. (2018). Advances in Hypoxia-Inducible Factor Biology. Cell Metab *27*, 281-298.

Cortes, M., Baria, A.T., and Schwartz, N.B. (2009). Sulfation of chondroitin sulfate proteoglycans is necessary for proper Indian hedgehog signaling in the developing growth plate. Development *136*, 1697-1706.

Darshan, D., Vanoaica, L., Richman, L., Beermann, F., and Kuhn, L.C. (2009). Conditional deletion of ferritin H in mice induces loss of iron storage and liver damage. Hepatology (Baltimore, Md) *50*, 852-860.

De Domenico, I., Vaughn, M.B., Li, L., Bagley, D., Musci, G., Ward, D.M., and Kaplan, J. (2006). Ferroportin-mediated mobilization of ferritin iron precedes ferritin degradation by the proteasome. Embo j *25*, 5396-5404.

De Falco, L., Sanchez, M., Silvestri, L., Kannengiesser, C., Muckenthaler, M.U., Iolascon, A., Gouya, L., Camaschella, C., and Beaumont, C. (2013). Iron refractory iron deficiency anemia. Haematologica *98*, 845-853.

de Murcia, J.M., Niedergang, C., Trucco, C., Ricoul, M., Dutrillaux, B., Mark, M., Oliver, F.J., Masson, M., Dierich, A., LeMeur, M., *et al.* (1997). Requirement of poly(ADP-ribose) polymerase in recovery from DNA damage in mice and in cells. Proc Natl Acad Sci U S A *94*, 7303-7307.

DeLoughery, T.G. (2014). Microcytic anemia. N Engl J Med *371*, 1324-1331.

Dichtl, B., Stevens, A., and Tollervey, D. (1997a). Lithium toxicity in yeast is due to the inhibition of RNA processing enzymes. Embo j *16*, 7184-7195.

Dichtl, B., Stevens, A., and Tollervey, D. (1997b). Lithium toxicity in yeast is due to the inhibition of RNA processing enzymes. In The EMBO journal, pp. 7184-7195.

Dick, G., Akslen-Hoel, L.K., Grondahl, F., Kjos, I., Maccarana, M., and Prydz, K. (2015). PAPST1 regulates sulfation of heparan sulfate proteoglycans in epithelial MDCK II cells. Glycobiology *25*, 30-41.

Donovan, A., Brownlie, A., Zhou, Y., Shepard, J., Pratt, S.J., Moynihan, J., Paw, B.H., Drejer, A., Barut, B., Zapata, A., *et al.* (2000). Positional cloning of zebrafish ferroportin1 identifies a conserved vertebrate iron exporter. Nature *403*, 776-781.

Donovan, A., Lima, C.A., Pinkus, J.L., Pinkus, G.S., Zon, L.I., Robine, S., and Andrews, N.C. (2005). The iron exporter ferroportin/Slc40a1 is essential for iron homeostasis. Cell Metab *1*, 191-200.

Drakesmith, H., Nemeth, E., and Ganz, T. (2015). Ironing out Ferroportin. Cell Metab *22*, 777-787.

Elliott, B.A., Ho, H.T., Ranganathan, S.V., Vangaveti, S., Ilkayeva, O., Abou Assi, H., Choi, A.K., Agris, P.F., and Holley, C.L. (2019). Modification of messenger RNA by 2'-O-methylation regulates gene expression in vivo. Nat Commun *10*, 3401.

Emerit, J., Beaumont, C., and Trivin, F. (2001). Iron metabolism, free radicals, and oxidative injury. Biomed Pharmacother *55*, 333-339.

Erales, J., Marchand, V., Panthu, B., Gillot, S., Belin, S., Ghayad, S.E., Garcia, M., Laforets, F., Marcel, V., Baudin-Baillieu, A., *et al.* (2017). Evidence for rRNA 2'-O-methylation plasticity: Control of intrinsic translational capabilities of human ribosomes. Proc Natl Acad Sci U S A *114*, 12934-12939.

Erbel, P.J., Card, P.B., Karakuzu, O., Bruick, R.K., and Gardner, K.H. (2003). Structural basis for PAS domain heterodimerization in the basic helix--loop--helix-PAS transcription factor hypoxia-inducible factor. Proc Natl Acad Sci U S A *100*, 15504-15509.

Faiyaz ul Haque, M., King, L.M., Krakow, D., Cantor, R.M., Rusiniak, M.E., Swank, R.T., Superti-Furga, A., Haque, S., Abbas, H., Ahmad, W., *et al.* (1998). Mutations in orthologous genes in human spondyloepimetaphyseal dysplasia and the brachymorphic mouse. Nat Genet *20*, 157-162.

Ferreira, C., Santambrogio, P., Martin, M.E., Andrieu, V., Feldmann, G., Henin, D., and Beaumont, C. (2001). H ferritin knockout mice: a model of hyperferritinemia in the absence of iron overload. Blood *98*, 525-532.

Fillebeen, C., Charlebois, E., Wagner, J., Katsarou, A., Mui, J., Vali, H., Garcia-Santos, D., Ponka, P., Presley, J., and Pantopoulos, K. (2019). Transferrin receptor 1 controls systemic iron homeostasis by fine-tuning hepcidin expression to hepatocellular iron load. Blood *133*, 344-355.

Fleming, M.D., Romano, M.A., Su, M.A., Garrick, L.M., Garrick, M.D., and Andrews, N.C. (1998). Nramp2 is mutated in the anemic Belgrade (b) rat: evidence of a role for Nramp2 in endosomal iron transport. Proc Natl Acad Sci U S A *95*, 1148-1153.

Fleming, M.D., Trenor, C.C., 3rd, Su, M.A., Foernzler, D., Beier, D.R., Dietrich, W.F., and Andrews, N.C. (1997). Microcytic anaemia mice have a mutation in Nramp2, a candidate iron transporter gene. Nat Genet *16*, 383-386.

Fleming, R.E., Ahmann, J.R., Migas, M.C., Waheed, A., Koeffler, H.P., Kawabata, H., Britton, R.S., Bacon, B.R., and Sly, W.S. (2002). Targeted mutagenesis of the murine transferrin receptor-2 gene produces hemochromatosis. Proc Natl Acad Sci U S A *99*, 10653-10658.

Foot, N.J., Dalton, H.E., Shearwin-Whyatt, L.M., Dorstyn, L., Tan, S.S., Yang, B., and Kumar, S. (2008). Regulation of the divalent metal ion transporter DMT1 and iron homeostasis by a ubiquitin-dependent mechanism involving Ndfips and WWP2. Blood *112*, 4268-4275.

Forlino, A., Piazza, R., Tiveron, C., Della Torre, S., Tatangelo, L., Bonafe, L., Gualeni, B., Romano, A., Pecora, F., Superti-Furga, A., *et al.* (2005). A diastrophic dysplasia sulfate transporter (SLC26A2) mutant mouse: morphological and biochemical characterization of the resulting chondrodysplasia phenotype. Human molecular genetics *14*, 859-871.

Foster, P.A., and Mueller, J.W. (2018). SULFATION PATHWAYS: Insights into steroid sulfation and desulfation pathways. J Mol Endocrinol *61*, T271-t283.

Frederick, J.P., Tafari, A.T., Wu, S.M., Megosh, L.C., Chiou, S.T., Irving, R.P., and York, J.D. (2008). A role for a lithium-inhibited Golgi nucleotidase in skeletal development and sulfation. Proc Natl Acad Sci U S A *105*, 11605-11612.

Freimuth, R.R., Wiepert, M., Chute, C.G., Wieben, E.D., and Weinshilboum, R.M. (2004). Human cytosolic sulfotransferase database mining: identification of seven novel genes and pseudogenes. Pharmacogenomics J *4*, 54-65.

Freland, L., and Beaulieu, J.M. (2012). Inhibition of GSK3 by lithium, from single molecules to signaling networks. Front Mol Neurosci *5*, 14.

Frise, M.C., Cheng, H.Y., Nickol, A.H., Curtis, M.K., Pollard, K.A., Roberts, D.J., Ratcliffe, P.J., Dorrington, K.L., and Robbins, P.A. (2016). Clinical iron deficiency disturbs normal human responses to hypoxia. J Clin Invest *126*, 2139-2150.

Ganz, T. (2011). Hepcidin and iron regulation, 10 years later. Blood *117*, 4425-4433.

Gao, J., Chen, J., Kramer, M., Tsukamoto, H., Zhang, A.S., and Enns, C.A. (2009). Interaction of the hereditary hemochromatosis protein HFE with transferrin receptor 2 is required for transferrin-induced hepcidin expression. Cell Metab *9*, 217-227.

Ghosh, M.C., Zhang, D.L., Jeong, S.Y., Kovtunovych, G., Ollivierre-Wilson, H., Noguchi, A., Tu, T., Senecal, T., Robinson, G., Crooks, D.R., *et al.* (2013). Deletion of iron regulatory protein 1 causes polycythemia and pulmonary hypertension in mice through translational derepression of HIF2alpha. Cell Metab *17*, 271-281.

Gibson, B.A., Doolittle, L.K., Schneider, M.W.G., Jensen, L.E., Gamarra, N., Henry, L., Gerlich, D.W., Redding, S., and Rosen, M.K. (2019). Organization of Chromatin by Intrinsic and Regulated Phase Separation. Cell *179*, 470-484.e421.

Gigolashvili, T., Geier, M., Ashykhmina, N., Frerigmann, H., Wulfert, S., Krueger, S., Mugford, S.G., Kopriva, S., Haferkamp, I., and Flugge, U.I. (2012). The Arabidopsis thylakoid ADP/ATP

carrier TAAC has an additional role in supplying plastidic phosphoadenosine 5'-phosphosulfate to the cytosol. Plant Cell *24*, 4187-4204.

Girard, J.P., Baekkevold, E.S., and Amalric, F. (1998). Sulfation in high endothelial venules: cloning and expression of the human PAPS synthetase. Faseb j *12*, 603-612.

Gleadle, J.M., and Ratcliffe, P.J. (1998). Hypoxia and the regulation of gene expression. Mol Med Today *4*, 122-129.

Goda, E., Kamiyama, S., Uno, T., Yoshida, H., Ueyama, M., Kinoshita-Toyoda, A., Toyoda, H., Ueda, R., and Nishihara, S. (2006). Identification and characterization of a novel Drosophila 3'-phosphoadenosine 5'-phosphosulfate transporter. The Journal of biological chemistry *281*, 28508-28517.

Gonzalez-Flores, A., Aguilar-Quesada, R., Siles, E., Pozo, S., Rodriguez-Lara, M.I., Lopez-Jimenez, L., Lopez-Rodriguez, M., Peralta-Leal, A., Villar, D., Martin-Oliva, D., *et al.* (2014). Interaction between PARP-1 and HIF-2alpha in the hypoxic response. Oncogene *33*, 891-898.

Gruber, M., Hu, C.J., Johnson, R.S., Brown, E.J., Keith, B., and Simon, M.C. (2007). Acute postnatal ablation of Hif-2alpha results in anemia. Proc Natl Acad Sci U S A *104*, 2301-2306.

Grunfeld, J.P., and Rossier, B.C. (2009). Lithium nephrotoxicity revisited. Nature reviews Nephrology *5*, 270-276.

Guerra, E., Lattanzio, R., La Sorda, R., Dini, F., Tiboni, G.M., Piantelli, M., and Alberti, S. (2012). mTrop1/Epcam knockout mice develop congenital tufting enteropathy through dysregulation of intestinal E-cadherin/beta-catenin. PloS one *7*, e49302.

Gulec, S., Anderson, G.J., and Collins, J.F. (2014). Mechanistic and regulatory aspects of intestinal iron absorption. Am J Physiol Gastrointest Liver Physiol *307*, G397-409.

Gunal, S., Hardman, R., Kopriva, S., and Mueller, J.W. (2019). Sulfation pathways from red to green. The Journal of biological chemistry *294*, 12293-12312.

Gunshin, H., Fujiwara, Y., Custodio, A.O., Direnzo, C., Robine, S., and Andrews, N.C. (2005a). Slc11a2 is required for intestinal iron absorption and erythropoiesis but dispensable in placenta and liver. J Clin Invest *115*, 1258-1266.

Gunshin, H., Mackenzie, B., Berger, U.V., Gunshin, Y., Romero, M.F., Boron, W.F., Nussberger, S., Gollan, J.L., and Hediger, M.A. (1997). Cloning and characterization of a mammalian proton-coupled metal-ion transporter. In Nature, pp. 482-488.

Gunshin, H., Starr, C.N., Direnzo, C., Fleming, M.D., Jin, J., Greer, E.L., Sellers, V.M., Galica, S.M., and Andrews, N.C. (2005b). Cybrd1 (duodenal cytochrome b) is not necessary for dietary iron absorption in mice. Blood *106*, 2879-2883.

Guo, Y., Zhao, S., Sheng, Q., Ye, F., Li, J., Lehmann, B., Pietenpol, J., Samuels, D.C., and Shyr, Y. (2014). Multi-perspective quality control of Illumina exome sequencing data using QC3. Genomics *103*, 323-328.

Gy, I., Gasciolli, V., Lauressergues, D., Morel, J.B., Gombert, J., Proux, F., Proux, C., Vaucheret, H., and Mallory, A.C. (2007). Arabidopsis FIERY1, XRN2, and XRN3 are endogenous RNA silencing suppressors. Plant Cell *19*, 3451-3461.

Haase, V.H. (2010). Hypoxic regulation of erythropoiesis and iron metabolism. Am J Physiol Renal Physiol *299*, F1-13.

Haila, S., Hastbacka, J., Bohling, T., Karjalainen-Lindsberg, M.L., Kere, J., and Saarialho-Kere, U. (2001). SLC26A2 (diastrophic dysplasia sulfate transporter) is expressed in developing and mature cartilage but also in other tissues and cell types. J Histochem Cytochem *49*, 973-982.

Harding, C., Heuser, J., and Stahl, P. (1983). Receptor-mediated endocytosis of transferrin and recycling of the transferrin receptor in rat reticulocytes. J Cell Biol *97*, 329-339.

Harjes, S., Bayer, P., and Scheidig, A.J. (2005). The crystal structure of human PAPS synthetase 1 reveals asymmetry in substrate binding. J Mol Biol *347*, 623-635.

Hastbacka, J., de la Chapelle, A., Mahtani, M.M., Clines, G., Reeve-Daly, M.P., Daly, M., Hamilton, B.A., Kusumi, K., Trivedi, B., Weaver, A., *et al.* (1994). The diastrophic dysplasia gene encodes a novel sulfate transporter: positional cloning by fine-structure linkage disequilibrium mapping. Cell *78*, 1073-1087.

Hastbacka, J., Superti-Furga, A., Wilcox, W.R., Rimoin, D.L., Cohn, D.H., and Lander, E.S. (1996). Atelosteogenesis type II is caused by mutations in the diastrophic dysplasia sulfate-transporter gene (DTDST): evidence for a phenotypic series involving three chondrodysplasias. Am J Hum Genet *58*, 255-262.

Hazelton, G.A., Hjelle, J.J., Dills, R.L., and Klaassen, C.D. (1985). A radiometric method for the measurement of adenosine 3'-phosphate 5'-phosphosulfate in rat and mouse liver. Drug Metab Dispos *13*, 30-34.

He, H., Qiao, Y., Zhang, Z., Wu, Z., Liu, D., Liao, Z., Yin, D., and He, M. (2018). Dual action of vitamin C in iron supplement therapeutics for iron deficiency anemia: prevention of liver damage induced by iron overload. Food Funct *9*, 5390-5401.

Hentze, M.W., Muckenthaler, M.U., Galy, B., and Camaschella, C. (2010). Two to tango: regulation of Mammalian iron metabolism. Cell *142*, 24-38.

Hermanns, P., Unger, S., Rossi, A., Perez-Aytes, A., Cortina, H., Bonafe, L., Boccone, L., Setzu, V., Dutoit, M., Sangiorgi, L., *et al.* (2008). Congenital joint dislocations caused by carbohydrate sulfotransferase 3 deficiency in recessive Larsen syndrome and humero-spinal dysostosis. Am J Hum Genet *82*, 1368-1374.

Hindupur, S.K., Colombi, M., Fuhs, S.R., Matter, M.S., Guri, Y., Adam, K., Cornu, M., Piscuoglio, S., Ng, C.K.Y., Betz, C., *et al.* (2018). The protein histidine phosphatase LHPP is a tumour suppressor. Nature *555*, 678-682.

Hnisz, D., Shrinivas, K., Young, R.A., Chakraborty, A.K., and Sharp, P.A. (2017). A Phase Separation Model for Transcriptional Control. Cell *169*, 13-23.

Huang da, W., Sherman, B.T., and Lempicki, R.A. (2009a). Bioinformatics enrichment tools: paths toward the comprehensive functional analysis of large gene lists. Nucleic Acids Res *37*, 1-13.

Huang da, W., Sherman, B.T., and Lempicki, R.A. (2009b). Systematic and integrative analysis of large gene lists using DAVID bioinformatics resources. Nat Protoc *4*, 44-57.

Hudson, B.H., Frederick, J.P., Drake, L.Y., Megosh, L.C., Irving, R.P., and York, J.D. (2013). Role for cytoplasmic nucleotide hydrolysis in hepatic function and protein synthesis. Proc Natl Acad Sci U S A *110*, 5040-5045.

Hudson, B.H., Hale, A.T., Irving, R.P., Li, S., and York, J.D. (2018). Modulation of intestinal sulfur assimilation metabolism regulates iron homeostasis. Proc Natl Acad Sci U S A *115*, 3000-3005.

Hudson, B.H., and York, J.D. (2012). Roles for nucleotide phosphatases in sulfate assimilation and skeletal disease. Adv Biol Regul *52*, 229-238.

Hudson, B.H., and York, J.D. (2014). Tissue-specific regulation of 3'-nucleotide hydrolysis and nucleolar architecture. Adv Biol Regul *54*, 208-213.

Idzerda, R.L., Huebers, H., Finch, C.A., and McKnight, G.S. (1986). Rat transferrin gene expression: tissue-specific regulation by iron deficiency. Proc Natl Acad Sci U S A *83*, 3723-3727.

Ivan, M., Kondo, K., Yang, H., Kim, W., Valiando, J., Ohh, M., Salic, A., Asara, J.M., Lane, W.S., and Kaelin, W.G., Jr. (2001). HIFalpha targeted for VHL-mediated destruction by proline hydroxylation: implications for O2 sensing. Science (New York, NY) *292*, 464-468.

Jaakkola, P., Mole, D.R., Tian, Y.M., Wilson, M.I., Gielbert, J., Gaskell, S.J., von Kriegsheim, A., Hebestreit, H.F., Mukherji, M., Schofield, C.J., *et al.* (2001). Targeting of HIF-alpha to the von Hippel-Lindau ubiquitylation complex by O2-regulated prolyl hydroxylation. Science (New York, NY) *292*, 468-472.

James, M.O., and Ambadapadi, S. (2013). Interactions of cytosolic sulfotransferases with xenobiotics. Drug metabolism reviews *45*, 401-414.

Kaelin, W.G. (2007). Von Hippel-Lindau disease. Annual review of pathology *2*, 145-173.

Kaelin, W.G., Jr. (2005). The von Hippel-Lindau protein, HIF hydroxylation, and oxygen sensing. Biochem Biophys Res Commun *338*, 627-638.

Kaelin, W.G., Jr. (2008). The von Hippel-Lindau tumour suppressor protein: O2 sensing and cancer. Nat Rev Cancer *8*, 865-873.

Kaelin, W.G., Jr., and McKnight, S.L. (2013). Influence of metabolism on epigenetics and disease. Cell *153*, 56-69.

Kaelin, W.G., Jr., and Ratcliffe, P.J. (2008). Oxygen sensing by metazoans: the central role of the HIF hydroxylase pathway. Molecular cell *30*, 393-402.

Kamiyama, S., Sasaki, N., Goda, E., Ui-Tei, K., Saigo, K., Narimatsu, H., Jigami, Y., Kannagi, R., Irimura, T., and Nishihara, S. (2006). Molecular cloning and characterization of a novel 3'-phosphoadenosine 5'-phosphosulfate transporter, PAPST2. The Journal of biological chemistry *281*, 10945-10953.

Kamiyama, S., Suda, T., Ueda, R., Suzuki, M., Okubo, R., Kikuchi, N., Chiba, Y., Goto, S., Toyoda, H., Saigo, K., *et al.* (2003). Molecular cloning and identification of 3'-phosphoadenosine 5'-phosphosulfate transporter. The Journal of biological chemistry *278*, 25958-25963.

Karniski, L.P. (2001). Mutations in the diastrophic dysplasia sulfate transporter (DTDST) gene: correlation between sulfate transport activity and chondrodysplasia phenotype. Human molecular genetics *10*, 1485-1490.

Karniski, L.P. (2004). Functional expression and cellular distribution of diastrophic dysplasia sulfate transporter (DTDST) gene mutations in HEK cells. Human molecular genetics *13*, 2165-2171.

Kawabata, H., Yang, R., Hirama, T., Vuong, P.T., Kawano, S., Gombart, A.F., and Koeffler, H.P. (1999). Molecular cloning of transferrin receptor 2. A new member of the transferrin receptor-like family. The Journal of biological chemistry *274*, 20826-20832.

Kim, D., Pertea, G., Trapnell, C., Pimentel, H., Kelley, R., and Salzberg, S.L. (2013). TopHat2: accurate alignment of transcriptomes in the presence of insertions, deletions and gene fusions. Genome Biol *14*, R36.

Kim, M.S., Shigenaga, J., Moser, A., Grunfeld, C., and Feingold, K.R. (2004). Suppression of DHEA sulfotransferase (Sult2A1) during the acute-phase response. Am J Physiol Endocrinol Metab *287*, E731-738.

Kinoshita, K., Kikuchi, Y., Sasakura, Y., Suzuki, M., Fujii-Kuriyama, Y., and Sogawa, K. (2004). Altered DNA binding specificity of Arnt by selection of partner bHLH-PAS proteins. Nucleic Acids Res *32*, 3169-3179.

Kirn-Safran, C.B., Gomes, R.R., Brown, A.J., and Carson, D.D. (2004). Heparan sulfate proteoglycans: coordinators of multiple signaling pathways during chondrogenesis. Birth Defects Res C Embryo Today *72*, 69-88.

Klaassen, C.D., and Boles, J.W. (1997). Sulfation and sulfotransferases 5: the importance of 3'-phosphoadenosine 5'-phosphosulfate (PAPS) in the regulation of sulfation. Faseb j *11*, 404-418.

Kluppel, M., Wight, T.N., Chan, C., Hinek, A., and Wrana, J.L. (2005). Maintenance of chondroitin sulfation balance by chondroitin-4-sulfotransferase 1 is required for chondrocyte development and growth factor signaling during cartilage morphogenesis. Development *132*, 3989-4003.

Knutson, M., and Wessling-Resnick, M. (2003). Iron metabolism in the reticuloendothelial system. Crit Rev Biochem Mol Biol *38*, 61-88.

Knutson, M.D. (2010). Iron-sensing proteins that regulate hepcidin and enteric iron absorption. Annu Rev Nutr *30*, 149-171.

Kopriva, S., Talukdar, D., Takahashi, H., Hell, R., Sirko, A., D'Souza, S.F., and Talukdar, T. (2015). Editorial: Frontiers of Sulfur Metabolism in Plant Growth, Development, and Stress Response. Front Plant Sci *6*, 1220.

Kosho, T., Miyake, N., Hatamochi, A., Takahashi, J., Kato, H., Miyahara, T., Igawa, Y., Yasui, H., Ishida, T., Ono, K., *et al.* (2010). A new Ehlers-Danlos syndrome with craniofacial characteristics, multiple congenital contractures, progressive joint and skin laxity, and multisystem fragility-related manifestations. Am J Med Genet A *152a*, 1333-1346.

Kotova, E., Lodhi, N., Jarnik, M., Pinnola, A.D., Ji, Y., and Tulin, A.V. (2011). Drosophila histone H2A variant (H2Av) controls poly(ADP-ribose) polymerase 1 (PARP1) activation in chromatin. Proc Natl Acad Sci U S A *108*, 6205-6210.

Krogan, N.J., Peng, W.T., Cagney, G., Robinson, M.D., Haw, R., Zhong, G., Guo, X., Zhang, X., Canadien, V., Richards, D.P., *et al.* (2004). High-definition macromolecular composition of yeast RNA-processing complexes. Molecular cell *13*, 225-239.

Kuhn, L.C., McClelland, A., and Ruddle, F.H. (1984). Gene transfer, expression, and molecular cloning of the human transferrin receptor gene. Cell *37*, 95-103.

Kurima, K., Warman, M.L., Krishnan, S., Domowicz, M., Krueger, R.C., Jr., Deyrup, A., and Schwartz, N.B. (1998). A member of a family of sulfate-activating enzymes causes murine brachymorphism. Proc Natl Acad Sci U S A *95*, 8681-8685.

Kwak, E.L., Torti, S.V., and Torti, F.M. (1990). Murine ferritin heavy chain: isolation and characterization of a functional gene. Gene *94*, 255-261.

Lane, P.W., and Dickie, M.M. (1968). Three recessive mutations producing disproportionate dwarfing in mice: achondroplasia, brachymorphic, and stubby. The Journal of heredity *59*, 300-308.

Langford, R., Hurrion, E., and Dawson, P.A. (2017). Genetics and pathophysiology of mammalian sulfate biology. J Genet Genomics *44*, 7-20.

Larson, A.G., and Narlikar, G.J. (2018). The Role of Phase Separation in Heterochromatin Formation, Function, and Regulation. Biochemistry *57*, 2540-2548.

Latunde-Dada, G.O., Xiang, L., Simpson, R.J., and McKie, A.T. (2011). Duodenal cytochrome b (Cybrd 1) and HIF-2alpha expression during acute hypoxic exposure in mice. Eur J Nutr *50*, 699-704.

Ledford, H., and Callaway, E. (2019). Biologists who decoded how cells sense oxygen win medicine Nobel. Nature *574*, 161-162.

Lee, K.A., Fuda, H., Lee, Y.C., Negishi, M., Strott, C.A., and Pedersen, L.C. (2003). Crystal structure of human cholesterol sulfotransferase (SULT2B1b) in the presence of pregnenolone and 3'-phosphoadenosine 5'-phosphate. Rationale for specificity differences between prototypical SULT2A1 and the SULT2BG1 isoforms. The Journal of biological chemistry *278*, 44593-44599.

Leidgens, S., Bullough, K.Z., Shi, H., Li, F., Shakoury-Elizeh, M., Yabe, T., Subramanian, P., Hsu, E., Natarajan, N., Nandal, A., *et al.* (2013). Each member of the poly-r(C)-binding protein 1 (PCBP) family exhibits iron chaperone activity toward ferritin. The Journal of biological chemistry *288*, 17791-17802.

Lesbordes-Brion, J.C., Viatte, L., Bennoun, M., Lou, D.Q., Ramey, G., Houbron, C., Hamard, G., Kahn, A., and Vaulont, S. (2006). Targeted disruption of the hepcidin 1 gene results in severe hemochromatosis. Blood *108*, 1402-1405.

Leushacke, M., and Barker, N. (2014). Ex vivo culture of the intestinal epithelium: strategies and applications. Gut *63*, 1345-1354.

Levy, J.E., Montross, L.K., and Andrews, N.C. (2000). Genes that modify the hemochromatosis phenotype in mice. J Clin Invest *105*, 1209-1216.

Lewis, D., Davies, Y., Nieduszynski, I.A., Lawrence, F., Quantock, A.J., Bonshek, R., and Fullwood, N.J. (2000). Ultrastructural localization of sulfated and unsulfated keratan sulfate in normal and macular corneal dystrophy type I. Glycobiology *10*, 305-312.

Leyh, T.S., Cook, I., and Wang, T. (2013). Structure, dynamics and selectivity in the sulfotransferase family. Drug metabolism reviews *45*, 423-430.

Li, H., Deyrup, A., Mensch, J.R., Jr., Domowicz, M., Konstantinidis, A.K., and Schwartz, N.B. (1995). The isolation and characterization of cDNA encoding the mouse bifunctional ATP sulfurylase-adenosine 5'-phosphosulfate kinase. The Journal of biological chemistry *270*, 29453-29459.

Li, W., Jia, H., Li, Q., Cui, J., Li, R., Zou, Z., and Hong, X. (2018). Glycerophosphatidylcholine PC(36:1) absence and 3'-phosphoadenylate (pAp) accumulation are hallmarks of the human glioma metabolome. Scientific reports *8*, 14783.

Lin, E.S., and Yang, Y.S. (1998). Colorimetric determination of the purity of 3'-phospho adenosine 5'-phosphosulfate and natural abundance of 3'-phospho adenosine 5'-phosphate at picomole quantities. Anal Biochem *264*, 111-117.

Linder, M.C. (2013). Mobilization of stored iron in mammals: a review. Nutrients *5*, 4022-4050.

Liu, Q., Davidoff, O., Niss, K., and Haase, V.H. (2012). Hypoxia-inducible factor regulates hepcidin via erythropoietin-induced erythropoiesis. J Clin Invest *122*, 4635-4644.

Lopez-Coronado, J.M., Belles, J.M., Lesage, F., Serrano, R., and Rodriguez, P.L. (1999). A novel mammalian lithium-sensitive enzyme with a dual enzymatic activity, 3'-phosphoadenosine 5'-phosphate phosphatase and inositol-polyphosphate 1-phosphatase. The Journal of biological chemistry *274*, 16034-16039.

Lun, M.P., Monuki, E.S., and Lehtinen, M.K. (2015). Development and functions of the choroid plexus-cerebrospinal fluid system. Nat Rev Neurosci *16*, 445-457.

Mackenzie, B., Takanaga, H., Hubert, N., Rolfs, A., and Hediger, M.A. (2007). Functional properties of multiple isoforms of human divalent metal-ion transporter 1 (DMT1). The Biochemical journal *403*, 59-69.

Madison, B.B., Dunbar, L., Qiao, X.T., Braunstein, K., Braunstein, E., and Gumucio, D.L. (2002). Cis elements of the villin gene control expression in restricted domains of the vertical (crypt) and horizontal (duodenum, cecum) axes of the intestine. The Journal of biological chemistry *277*, 33275-33283.

Malfait, F., Syx, D., Vlummens, P., Symoens, S., Nampoothiri, S., Hermanns-Le, T., Van Laer, L., and De Paepe, A. (2010). Musculocontractural Ehlers-Danlos Syndrome (former EDS type VIB) and adducted thumb clubfoot syndrome (ATCS) represent a single clinical entity caused by mutations in the dermatan-4-sulfotransferase 1 encoding CHST14 gene. Hum Mutat *31*, 1233-1239.

Martinez-Zamudio, R., and Ha, H.C. (2012). Histone ADP-ribosylation facilitates gene transcription by directly remodeling nucleosomes. Mol Cell Biol *32*, 2490-2502.

Marto, N., Morello, J., Monteiro, E.C., and Pereira, S.A. (2017). Implications of sulfotransferase activity in interindividual variability in drug response: clinical perspective on current knowledge. Drug metabolism reviews *49*, 357-371.

Masselot, M., and De Robichon-Szulmajster, H. (1975a). Methionine biosynthesis in Saccharomyces cerevisiae. I. Genetical analysis of auxotrophic mutants. Molecular & general genetics : MGG *139*, 121-132.

Masselot, M., and De Robichon-Szulmajster, H. (1975b). Methionine biosynthesis in Saccharomyces cerevisiae. I. Genetical analysis of auxotrophic mutants. Mol Gen Genet *139*, 121-132.

Mastrogiannaki, M., Matak, P., Keith, B., Simon, M.C., Vaulont, S., and Peyssonnaux, C. (2009). HIF-2alpha, but not HIF-1alpha, promotes iron absorption in mice. J Clin Invest *119*, 1159-1166.

Mastrogiannaki, M., Matak, P., and Peyssonnaux, C. (2013). The gut in iron homeostasis: role of HIF-2 under normal and pathological conditions. Blood *122*, 885-892.

Matak, P., Matak, A., Moustafa, S., Aryal, D.K., Benner, E.J., Wetsel, W., and Andrews, N.C. (2016). Disrupted iron homeostasis causes dopaminergic neurodegeneration in mice. Proc Natl Acad Sci U S A *113*, 3428-3435.

McKie, A.T., Marciani, P., Rolfs, A., Brennan, K., Wehr, K., Barrow, D., Miret, S., Bomford, A., Peters, T.J., Farzaneh, F., *et al.* (2000). A novel duodenal iron-regulated transporter, IREG1, implicated in the basolateral transfer of iron to the circulation. Molecular cell *5*, 299-309.

McKnight, R.F., Adida, M., Budge, K., Stockton, S., Goodwin, G.M., and Geddes, J.R. (2012). Lithium toxicity profile: a systematic review and meta-analysis. Lancet *379*, 721-728.

Meder, V.S., Boeglin, M., de Murcia, G., and Schreiber, V. (2005). PARP-1 and PARP-2 interact with nucleophosmin/B23 and accumulate in transcriptionally active nucleoli. J Cell Sci *118*, 211-222.

Meisel, J.D., and Kim, D.H. (2016). Inhibition of Lithium-Sensitive Phosphatase BPNT-1 Causes Selective Neuronal Dysfunction in C. elegans. Curr Biol *26*, 1922-1928.

Mikami, T., and Kitagawa, H. (2013). Biosynthesis and function of chondroitin sulfate. Biochim Biophys Acta *1830*, 4719-4733.

Miki, T.S., Carl, S.H., Stadler, M.B., and Grosshans, H. (2016). XRN2 Autoregulation and Control of Polycistronic Gene Expresssion in Caenorhabditis elegans. PLoS Genet *12*, e1006313.

Mims, M.P., Guan, Y., Pospisilova, D., Priwitzerova, M., Indrak, K., Ponka, P., Divoky, V., and Prchal, J.T. (2005). Identification of a human mutation of DMT1 in a patient with microcytic anemia and iron overload. Blood *105*, 1337-1342.

Mims, M.P., and Prchal, J.T. (2005). Divalent metal transporter 1. Hematology *10*, 339-345.

Miyake, N., Kosho, T., Mizumoto, S., Furuichi, T., Hatamochi, A., Nagashima, Y., Arai, E., Takahashi, K., Kawamura, R., Wakui, K., *et al.* (2010). Loss-of-function mutations of CHST14 in a new type of Ehlers-Danlos syndrome. Hum Mutat *31*, 966-974.

Miyoshi, H., and Stappenbeck, T.S. (2013). In vitro expansion and genetic modification of gastrointestinal stem cells in spheroid culture. Nature protocols *8*, 2471.

Montemiglio, L.C., Testi, C., Ceci, P., Falvo, E., Pitea, M., Savino, C., Arcovito, A., Peruzzi, G., Baiocco, P., Mancia, F., *et al.* (2019). Cryo-EM structure of the human ferritin-transferrin receptor 1 complex. Nat Commun *10*, 1121.

Mountain, H.A., Bystrom, A.S., Larsen, J.T., and Korch, C. (1991). Four major transcriptional responses in the methionine/threonine biosynthetic pathway of Saccharomyces cerevisiae. Yeast (Chichester, England) *7*, 781-803.

Mueller, J.W., Idkowiak, J., Gesteira, T.F., Vallet, C., Hardman, R., van den Boom, J., Dhir, V., Knauer, S.K., Rosta, E., and Arlt, W. (2018). Human DHEA sulfation requires direct interaction between PAPS synthase 2 and DHEA sulfotransferase SULT2A1. The Journal of biological chemistry *293*, 9724-9735.

Nandal, A., Ruiz, J.C., Subramanian, P., Ghimire-Rijal, S., Sinnamon, R.A., Stemmler, T.L., Bruick, R.K., and Philpott, C.C. (2011). Activation of the HIF prolyl hydroxylase by the iron chaperones PCBP1 and PCBP2. Cell Metab *14*, 647-657.

Nemeth, E., Tuttle, M.S., Powelson, J., Vaughn, M.B., Donovan, A., Ward, D.M., Ganz, T., and Kaplan, J. (2004). Hepcidin regulates cellular iron efflux by binding to ferroportin and inducing its internalization. Science *306*, 2090-2093.

Nicolas, G., Chauvet, C., Viatte, L., Danan, J.L., Bigard, X., Devaux, I., Beaumont, C., Kahn, A., and Vaulont, S. (2002). The gene encoding the iron regulatory peptide hepcidin is regulated by anemia, hypoxia, and inflammation. The Journal of clinical investigation *110*, 1037-1044.

Nizon, M., Alanay, Y., Tuysuz, B., Kiper, P.O., Genevieve, D., Sillence, D., Huber, C., Munnich, A., and Cormier-Daire, V. (2012). IMPAD1 mutations in two Catel-Manzke like patients. Am J Med Genet A *158a*, 2183-2187.

Ogura, M., Endo, R., Ishikawa, H., Takeda, Y., Uchida, T., Iwai, K., Kobayashi, K., and Ishimori, K. (2018). Redox-dependent axial ligand replacement and its functional significance in heme-bound iron regulatory proteins. J Inorg Biochem *182*, 238-248.

Ohana, E., Shcheynikov, N., Park, M., and Muallem, S. (2012). Solute carrier family 26 member a2 (Slc26a2) protein functions as an electroneutral SOFormula/OH-/Cl- exchanger regulated by extracellular Cl. The Journal of biological chemistry *287*, 5122-5132.

Parris, T.Z., Kovacs, A., Hajizadeh, S., Nemes, S., Semaan, M., Levin, M., Karlsson, P., and Helou, K. (2014). Frequent MYC coamplification and DNA hypomethylation of multiple genes on 8q in 8p11-p12-amplified breast carcinomas. Oncogenesis *3*, e95.

Patel, S.A., and Simon, M.C. (2008). Biology of hypoxia-inducible factor-2alpha in development and disease. Cell Death Differ *15*, 628-634.

Patron, N.J., Durnford, D.G., and Kopriva, S. (2008). Sulfate assimilation in eukaryotes: fusions, relocations and lateral transfers. BMC Evol Biol *8*, 39.

Perutz, M.F., Rossmann, M.G., Cullis, A.F., Muirhead, H., Will, G., and North, A.C. (1960). Structure of haemoglobin: a three-dimensional Fourier synthesis at 5.5-A. resolution, obtained by X-ray analysis. Nature *185*, 416-422.

Philpott, C.C., Ryu, M.S., Frey, A., and Patel, S. (2017). Cytosolic iron chaperones: Proteins delivering iron cofactors in the cytosol of mammalian cells. The Journal of biological chemistry *292*, 12764-12771.

Picard, V., Govoni, G., Jabado, N., and Gros, P. (2000). Nramp 2 (DCT1/DMT1) expressed at the plasma membrane transports iron and other divalent cations into a calcein-accessible cytoplasmic pool. The Journal of biological chemistry *275*, 35738-35745.

Pomin, V.H., and Mulloy, B. (2018). Glycosaminoglycans and Proteoglycans. Pharmaceuticals (Basel) *11*.

Postel, E.H., Wohlman, I., Zou, X., Juan, T., Sun, N., D'Agostin, D., Cuellar, M., Choi, T., Notterman, D.A., and La Perle, K.M. (2009). Targeted deletion of Nm23/nucleoside diphosphate kinase A and B reveals their requirement for definitive erythropoiesis in the mouse embryo. Dev Dyn *238*, 775-787.

Powell, L.W., Seckington, R.C., and Deugnier, Y. (2016). Haemochromatosis. Lancet *388*, 706-716.

Realini, C.A., and Althaus, F.R. (1992). Histone shuttling by poly(ADP-ribosylation). The Journal of biological chemistry *267*, 18858-18865.

Reddy, V.K., Short, S.P., Barrett, C.W., Mittal, M.K., Keating, C.E., Thompson, J.J., Harris, E.I., Revetta, F., Bader, D.M., Brand, T., *et al.* (2016). BVES Regulates Intestinal Stem Cell Programs and Intestinal Crypt Viability after Radiation. Stem cells (Dayton, Ohio) *34*, 1626-1636.

Rens-Domiano, S.S., and Roth, J.A. (1987). Inhibition of M and P phenol sulfotransferase by analogues of 3'-phosphoadenosine-5'-phosphosulfate. Journal of neurochemistry *48*, 1411-1415.

Riches, Z., Stanley, E.L., Bloomer, J.C., and Coughtrie, M.W. (2009). Quantitative evaluation of the expression and activity of five major sulfotransferases (SULTs) in human tissues: the SULT "pie". Drug Metab Dispos *37*, 2255-2261.

Russell, E.S., McFarland, E.C., and Kent, E.L. (1970). Low viability, skin lesions, and reduced fertility associated with microcytic anemia in the mouse. Transplantation proceedings *2*, 144-151.

Rybakowski, J.K. (2014). Response to lithium in bipolar disorder: clinical and genetic findings. ACS Chem Neurosci *5*, 413-421.

Ryu, K.W., Kim, D.S., and Kraus, W.L. (2015). New facets in the regulation of gene expression by ADP-ribosylation and poly(ADP-ribose) polymerases. Chem Rev *115*, 2453-2481.

Sasaki, N., Hirano, T., Ichimiya, T., Wakao, M., Hirano, K., Kinoshita-Toyoda, A., Toyoda, H., Suda, Y., and Nishihara, S. (2009). The 3'-phosphoadenosine 5'-phosphosulfate transporters, PAPST1 and 2, contribute to the maintenance and differentiation of mouse embryonic stem cells. PloS one *4*, e8262.

Sato, T., Vries, R.G., Snippert, H.J., van de Wetering, M., Barker, N., Stange, D.E., van Es, J.H., Abo, A., Kujala, P., Peters, P.J., *et al.* (2009). Single Lgr5 stem cells build crypt-villus structures in vitro without a mesenchymal niche. Nature *459*, 262-265.

Schaefer, C.F., Anthony, K., Krupa, S., Buchoff, J., Day, M., Hannay, T., and Buetow, K.H. (2009). PID: the Pathway Interaction Database. Nucleic Acids Res *37*, D674-679.

Schneider, B., Xu, Y.W., Janin, J., Veron, M., and Deville-Bonne, D. (1998). 3'-Phosphorylated nucleotides are tight binding inhibitors of nucleoside diphosphate kinase activity. The Journal of biological chemistry *273*, 28773-28778.

Schroder, E., Gebel, L., Eremeev, A.A., Morgner, J., Grum, D., Knauer, S.K., Bayer, P., and Mueller, J.W. (2012). Human PAPS synthase isoforms are dynamically regulated enzymes with access to nucleus and cytoplasm. PloS one *7*, e29559.

Schwartz, A.J., Das, N.K., Ramakrishnan, S.K., Jain, C., Jurkovic, M.T., Wu, J., Nemeth, E., Lakhal-Littleton, S., Colacino, J.A., and Shah, Y.M. (2019). Hepatic hepcidin/intestinal HIF-2alpha axis maintains iron absorption during iron deficiency and overload. J Clin Invest *129*, 336-348.

Schwartz, N.B., Ostrowski, V., Brown, K.S., and Pratt, R.M. (1978). Defective PAPS-synthesis in epiphyseal cartilage from brachymorphic mice. Biochem Biophys Res Commun *82*, 173-178.

Sengupta, P., and Samuel, A.D. (2009). Caenorhabditis elegans: a model system for systems neuroscience. Current opinion in neurobiology *19*, 637-643.

Shah, Y.M., Matsubara, T., Ito, S., Yim, S.H., and Gonzalez, F.J. (2009). Intestinal hypoxia-inducible transcription factors are essential for iron absorption following iron deficiency. Cell Metab *9*, 152-164.

Sharp, P., and Srai, S.K. (2007). Molecular mechanisms involved in intestinal iron absorption. World J Gastroenterol *13*, 4716-4724.

Shawki, A., Knight, P.B., Maliken, B.D., Niespodzany, E.J., and Mackenzie, B. (2012). H(+)-coupled divalent metal-ion transporter-1: functional properties, physiological roles and therapeutics. Curr Top Membr *70*, 169-214.

Shi, H., Bencze, K.Z., Stemmler, T.L., and Philpott, C.C. (2008). A cytosolic iron chaperone that delivers iron to ferritin. Science (New York, NY) *320*, 1207-1210.

Shimizu, K., Okamoto, N., Miyake, N., Taira, K., Sato, Y., Matsuda, K., Akimaru, N., Ohashi, H., Wakui, K., Fukushima, Y., *et al.* (2011). Delineation of dermatan 4-O-sulfotransferase 1 deficient Ehlers-Danlos syndrome: observation of two additional patients and comprehensive review of 20 reported patients. Am J Med Genet A *155a*, 1949-1958.

Shubina, M.Y., Musinova, Y.R., and Sheval, E.V. (2016). Nucleolar Methyltransferase Fibrillarin: Evolution of Structure and Functions. Biochemistry (Mosc) *81*, 941-950.

Siddique, A., and Kowdley, K.V. (2012). Review article: the iron overload syndromes. Aliment Pharmacol Ther *35*, 876-893.

Silver, D.J., Siebzehnrubl, F.A., Schildts, M.J., Yachnis, A.T., Smith, G.M., Smith, A.A., Scheffler, B., Reynolds, B.A., Silver, J., and Steindler, D.A. (2013). Chondroitin sulfate proteoglycans potently inhibit invasion and serve as a central organizer of the brain tumor microenvironment. J Neurosci *33*, 15603-15617.

Simpson, R.J., and McKie, A.T. (2009). Regulation of intestinal iron absorption: the mucosa takes control? Cell Metab *10*, 84-87.

Singh, N., Haldar, S., Tripathi, A.K., Horback, K., Wong, J., Sharma, D., Beserra, A., Suda, S., Anbalagan, C., Dev, S., *et al.* (2014). Brain iron homeostasis: from molecular mechanisms to clinical significance and therapeutic opportunities. Antioxid Redox Signal *20*, 1324-1363.

Soares da Costa, D., Reis, R.L., and Pashkuleva, I. (2017). Sulfation of Glycosaminoglycans and Its Implications in Human Health and Disorders. Annual review of biomedical engineering *19*, 1-26.

Sohaskey, M.L., Yu, J., Diaz, M.A., Plaas, A.H., and Harland, R.M. (2008). JAWS coordinates chondrogenesis and synovial joint positioning. Development *135*, 2215-2220.

Sonoda, J., Xie, W., Rosenfeld, J.M., Barwick, J.L., Guzelian, P.S., and Evans, R.M. (2002). Regulation of a xenobiotic sulfonation cascade by nuclear pregnane X receptor (PXR). Proc Natl Acad Sci U S A *99*, 13801-13806.

Spiegelberg, B.D., Dela Cruz, J., Law, T.H., and York, J.D. (2005). Alteration of lithium pharmacology through manipulation of phosphoadenosine phosphate metabolism. The Journal of biological chemistry *280*, 5400-5405.

Spiegelberg, B.D., Xiong, J.P., Smith, J.J., Gu, R.F., and York, J.D. (1999a). Cloning and characterization of a mammalian lithium-sensitive bisphosphate 3'-nucleotidase inhibited by inositol 1,4-bisphosphate. The Journal of biological chemistry *274*, 13619-13628.

Spiegelberg, B.D., Xiong, J.P., Smith, J.J., Gu, R.F., and York, J.D. (1999b). Cloning and characterization of a mammalian lithium-sensitive bisphosphate 3'-nucleotidase inhibited by inositol 1,4-bisphosphate. J Biol Chem *274*, 13619-13628.

Strom, A.R., Emelyanov, A.V., Mir, M., Fyodorov, D.V., Darzacq, X., and Karpen, G.H. (2017). Phase separation drives heterochromatin domain formation. Nature *547*, 241-245.

Subramanian, A., Tamayo, P., Mootha, V.K., Mukherjee, S., Ebert, B.L., Gillette, M.A., Paulovich, A., Pomeroy, S.L., Golub, T.R., Lander, E.S., *et al.* (2005). Gene set enrichment analysis: a knowledge-based approach for interpreting genome-wide expression profiles. Proceedings of the National Academy of Sciences of the United States of America *102*, 15545-15550.

Sugahara, K., and Schwartz, N.B. (1979). Defect in 3'-phosphoadenosine 5'-phosphosulfate formation in brachymorphic mice. Proc Natl Acad Sci U S A *76*, 6615-6618.

Suiko, M., Kurogi, K., Hashiguchi, T., Sakakibara, Y., and Liu, M.C. (2017). Updated perspectives on the cytosolic sulfotransferases (SULTs) and SULT-mediated sulfation. Biosci Biotechnol Biochem *81*, 63-72.

Superti-Furga, A., Hastbacka, J., Wilcox, W.R., Cohn, D.H., van der Harten, H.J., Rossi, A., Blau, N., Rimoin, D.L., Steinmann, B., Lander, E.S., *et al.* (1996). Achondrogenesis type IB is caused by mutations in the diastrophic dysplasia sulphate transporter gene. Nat Genet *12*, 100-102.

Takahashi, H., Kopriva, S., Giordano, M., Saito, K., and Hell, R. (2011). Sulfur assimilation in photosynthetic organisms: molecular functions and regulations of transporters and assimilatory enzymes. Annu Rev Plant Biol *62*, 157-184.

Taylor, M., Qu, A., Anderson, E.R., Matsubara, T., Martin, A., Gonzalez, F.J., and Shah, Y.M. (2011a). Hypoxia-inducible factor-2alpha mediates the adaptive increase of intestinal ferroportin during iron deficiency in mice. Gastroenterology *140*, 2044-2055.

Taylor, M., Qu, A., Anderson, E.R., Matsubara, T., Martin, A., Gonzalez, F.J., and Shah, Y.M. (2011b). Hypoxia-Inducible Factor-2α Mediates the Adaptive Increase of Intestinal Ferroportin During Iron Deficiency in Mice. In Gastroenterology, pp. 2044-2055.

Tennant, J., Stansfield, M., Yamaji, S., Srai, S.K., and Sharp, P. (2002). Effects of copper on the expression of metal transporters in human intestinal Caco-2 cells. FEBS letters *527*, 239-244.

Tessarz, P., Santos-Rosa, H., Robson, S.C., Sylvestersen, K.B., Nelson, C.J., Nielsen, M.L., and Kouzarides, T. (2014). Glutamine methylation in histone H2A is an RNA-polymerase-I-dedicated modification. Nature *505*, 564-568.

Thiele, H., Sakano, M., Kitagawa, H., Sugahara, K., Rajab, A., Hohne, W., Ritter, H., Leschik, G., Nurnberg, P., and Mundlos, S. (2004). Loss of chondroitin 6-O-sulfotransferase-1 function results in severe human chondrodysplasia with progressive spinal involvement. Proc Natl Acad Sci U S A *101*, 10155-10160.

Tiku, V., and Antebi, A. (2018). Nucleolar Function in Lifespan Regulation. Trends Cell Biol *28*, 662-672.

Tiku, V., Jain, C., Raz, Y., Nakamura, S., Heestand, B., Liu, W., Spath, M., Suchiman, H.E.D., Muller, R.U., Slagboom, P.E., *et al.* (2017). Small nucleoli are a cellular hallmark of longevity. Nat Commun *8*, 16083.

Toledano, E., Ogryzko, V., Danchin, A., Ladant, D., and Mechold, U. (2012). 3'-5' phosphoadenosine phosphate is an inhibitor of PARP-1 and a potential mediator of the lithium-dependent inhibition of PARP-1 in vivo. The Biochemical journal *443*, 485-490.

Troen, A.M., Lutgens, E., Smith, D.E., Rosenberg, I.H., and Selhub, J. (2003). The atherogenic effect of excess methionine intake. Proc Natl Acad Sci U S A *100*, 15089-15094.

van den Boom, J., Heider, D., Martin, S.R., Pastore, A., and Mueller, J.W. (2012). 3'-Phosphoadenosine 5'-phosphosulfate (PAPS) synthases, naturally fragile enzymes specifically stabilized by nucleotide binding. The Journal of biological chemistry *287*, 17645-17655.

Vanoaica, L., Darshan, D., Richman, L., Schumann, K., and Kuhn, L.C. (2010). Intestinal ferritin H is required for an accurate control of iron absorption. Cell Metab *12*, 273-282.

Venkatachalam, K.V., Akita, H., and Strott, C.A. (1998). Molecular cloning, expression, and characterization of human bifunctional 3'-phosphoadenosine 5'-phosphosulfate synthase and its functional domains. The Journal of biological chemistry *273*, 19311-19320.

Vissers, L.E., Lausch, E., Unger, S., Campos-Xavier, A.B., Gilissen, C., Rossi, A., Del Rosario, M., Venselaar, H., Knoll, U., Nampoothiri, S., *et al.* (2011). Chondrodysplasia and abnormal joint development associated with mutations in IMPAD1, encoding the Golgi-resident nucleotide phosphatase, gPAPP. Am J Hum Genet *88*, 608-615.

Wagner, F.F., Bishop, J.A., Gale, J.P., Shi, X., Walk, M., Ketterman, J., Patnaik, D., Barker, D., Walpita, D., Campbell, A.J., *et al.* (2016). Inhibitors of Glycogen Synthase Kinase 3 with Exquisite Kinome-Wide Selectivity and Their Functional Effects. ACS Chem Biol *11*, 1952-1963.

Wallace, E.M., Rizzi, J.P., Han, G., Wehn, P.M., Cao, Z., Du, X., Cheng, T., Czerwinski, R.M., Dixon, D.D., Goggin, B.S., *et al.* (2016). A Small-Molecule Antagonist of HIF2alpha Is Efficacious in Preclinical Models of Renal Cell Carcinoma. Cancer Res *76*, 5491-5500.

Wang, G.L., and Semenza, G.L. (1993). Characterization of hypoxia-inducible factor 1 and regulation of DNA binding activity by hypoxia. The Journal of biological chemistry *268*, 21513-21518.

Wang, L., Gao, Y., Zheng, X., Liu, C., Dong, S., Li, R., Zhang, G., Wei, Y., Qu, H., Li, Y., *et al.* (2019). Histone Modifications Regulate Chromatin Compartmentalization by Contributing to a Phase Separation Mechanism. Molecular cell *76*, 646-659.e646.

Ward, R.J., Zucca, F.A., Duyn, J.H., Crichton, R.R., and Zecca, L. (2014). The role of iron in brain ageing and neurodegenerative disorders. The Lancet Neurology *13*, 1045-1060.

Wigerup, C., Pahlman, S., and Bexell, D. (2016). Therapeutic targeting of hypoxia and hypoxia-inducible factors in cancer. Pharmacology & therapeutics *164*, 152-169.

Wilkinson, N., and Pantopoulos, K. (2013). IRP1 regulates erythropoiesis and systemic iron homeostasis by controlling HIF2alpha mRNA translation. Blood *122*, 1658-1668.

Wilmes, G.M., Bergkessel, M., Bandyopadhyay, S., Shales, M., Braberg, H., Cagney, G., Collins, S.R., Whitworth, G.B., Kress, T.L., Weissman, J.S., *et al.* (2008). A genetic interaction

map of RNA-processing factors reveals links between Sem1/Dss1-containing complexes and mRNA export and splicing. Molecular cell *32*, 735-746.

Wu, D., Potluri, N., Lu, J., Kim, Y., and Rastinejad, F. (2015). Structural integration in hypoxia-inducible factors. Nature *524*, 303-308.

Wu, D., Su, X., Lu, J., Li, S., Hood, B.L., Vasile, S., Potluri, N., Diao, X., Kim, Y., Khorasanizadeh, S., *et al.* (2019a). Bidirectional modulation of HIF-2 activity through chemical ligands. Nat Chem Biol *15*, 367-376.

Wu, D., Su, X., Lu, J., Li, S., Hood, B.L., Vasile, S., Potluri, N., Diao, X., Kim, Y., Khorasanizadeh, S., *et al.* (2019b). Bidirectional modulation of HIF-2 activity through chemical ligands. Nat Chem Biol.

Xu, Z.H., Otterness, D.M., Freimuth, R.R., Carlini, E.J., Wood, T.C., Mitchell, S., Moon, E., Kim, U.J., Xu, J.P., Siciliano, M.J., *et al.* (2000). Human 3'-phosphoadenosine 5'-phosphosulfate synthetase 1 (PAPSS1) and PAPSS2: gene cloning, characterization and chromosomal localization. Biochem Biophys Res Commun *268*, 437-444.

Yanagisawa, K., Sakakibara, Y., Suiko, M., Takami, Y., Nakayama, T., Nakajima, H., Takayanagi, K., Natori, Y., and Liu, M.C. (1998). cDNA cloning, expression, and characterization of the human bifunctional ATP sulfurylase/adenosine 5'-phosphosulfate kinase enzyme. Biosci Biotechnol Biochem *62*, 1037-1040.

Yang, F., Lum, J.B., McGill, J.R., Moore, C.M., Naylor, S.L., van Bragt, P.H., Baldwin, W.D., and Bowman, B.H. (1984). Human transferrin: cDNA characterization and chromosomal localization. Proc Natl Acad Sci U S A *81*, 2752-2756.

Yoo, H., Triandafillou, C., and Drummond, D.A. (2019). Cellular sensing by phase separation: Using the process, not just the products. The Journal of biological chemistry *294*, 7151-7159.

York, J.D., Ponder, J.W., and Majerus, P.W. (1995). Definition of a metal-dependent/Li(+)-inhibited phosphomonoesterase protein family based upon a conserved three-dimensional core structure. Proc Natl Acad Sci U S A *92*, 5149-5153.

Yoshizawa, T., Mizumoto, S., Takahashi, Y., Shimada, S., Sugahara, K., Nakayama, J., Takeda, S., Nomura, Y., Nitahara-Kasahara, Y., Okada, T., *et al.* (2018). Vascular abnormalities in the placenta of Chst14-/- fetuses: implications in the pathophysiology of perinatal lethality of the murine model and vascular lesions in human CHST14/D4ST1 deficiency. Glycobiology *28*, 80-89.

Zhang, F., Phiel, C.J., Spece, L., Gurvich, N., and Klein, P.S. (2003). Inhibitory phosphorylation of glycogen synthase kinase-3 (GSK-3) in response to lithium. Evidence for autoregulation of GSK-3. The Journal of biological chemistry *278*, 33067-33077.

Zhang, Y., Conti, M.A., Malide, D., Dong, F., Wang, A., Shmist, Y.A., Liu, C., Zerfas, P., Daniels, M.P., Chan, C.C., *et al.* (2012a). Mouse models of MYH9-related disease: mutations in nonmuscle myosin II-A. Blood *119*, 238-250.

Zhang, Z., Zhang, F., An, P., Guo, X., Shen, Y., Tao, Y., Wu, Q., Zhang, Y., Yu, Y., Ning, B., *et al.* (2011). Ferroportin1 deficiency in mouse macrophages impairs iron homeostasis and inflammatory responses. Blood *118*, 1912-1922.

Zhang, Z., Zhang, F., Guo, X., An, P., Tao, Y., and Wang, F. (2012b). Ferroportin1 in hepatocytes and macrophages is required for the efficient mobilization of body iron stores in mice. Hepatology (Baltimore, Md) *56*, 961-971.

Zhao, N., Zhang, A.S., and Enns, C.A. (2013). Iron regulation by hepcidin. J Clin Invest *123*, 2337-2343.

Zhao, S., Guo, Y., Sheng, Q., and Shyr, Y. (2014). Advanced heat map and clustering analysis using heatmap3. Biomed Res Int *2014*, 986048.

Zhao, Y., and Garcia, B.A. (2015). Comprehensive Catalog of Currently Documented Histone Modifications. Cold Spring Harbor perspectives in biology *7*, a025064.

Zimmer, M., Ebert, B.L., Neil, C., Brenner, K., Papaioannou, I., Melas, A., Tolliday, N., Lamb, J., Pantopoulos, K., Golub, T., *et al.* (2008). Small-molecule inhibitors of HIF-2a translation link its 5'UTR iron-responsive element to oxygen sensing. Molecular cell *32*, 838-848.